University of Potsdam,
Institute of Earth- and Environmental Science

Alfred Wegener Institute
Helmholtz Center for Polar and Marine Research
Potsdam

Master Thesis

Physical processes of lakes in the continuous permafrost zone of northern Siberia - observations and modeling (Lena River Delta, Siberia)

Written by:

Christoph Georgi, student number: 750434

Supervisor:

Prof. Dr. Axel Bronstert
PD Dr. Julia Boike

Potsdam, February 15, 2018

Disclaimer

I hereby declare that I have written the present thesis independently, without assistance from external parties and without use of other resources than those indicated. The ideas taken directly or indirectly from external sources (including electronic sources) are duly acknowledged in the text.

The material, either in full or in part, has not been previously submitted for grading at this or any other academic institution.

Christoph Georgi

Potsdam, February 15, 2018

Erklärung

Hiermit erkläre ich, dass ich die vorliegende Arbeit selbständig, ohne fremde Hilfe und ohne Benutzung anderer als der angegebenen Hilfsmittel angefertigt habe. Die aus fremden Quellen (einschließlich elektronischer Quellen) direkt oder indirekt übernommenen Gedanken sind ausnahmslos als solche kenntlich gemacht. Die Arbeit ist in gleicher oder ähnlicher Form oder auszugsweise im Rahmen einer anderen Prüfung noch nicht vorgelegt worden.

Ferner erkläre ich, dass die Arbeit noch nicht in einem anderen Studiengang als Prüfungsleistung verwendet wurde.

Christoph Georgi

Potsdam, den 15. Februar 2017

Contents

List of Tables

List of Figures

Zusammenfassung

Thermokarstseen sind typische Landschaftseinheiten in nördlichen Permafrost Ökosystemen. Diese unterliegen und beeinflussen den thermischen Austausch zwischen Atmosphäre und Boden. Das Ziel dieser Arbeit ist, den physiografischen Charakter und die entscheidenden thermischen Prozesse von Seen zu beschreiben, sowie Möglichkeiten und Grenzen für die Nutzung des Süßwasserseenmodels FLake zu untersuchen.

Der modellierte See liegt auf der Insel Samoylov im Lena Delta (Sibirien) und ist Teil einer überwiegend seenreichen Permafrostlandschaft, die signifikant durch Thermokarstprozesse beeinflusst ist. Meteorologische Daten werden genutzt, um die Seetemperaturen und ihre Dynamik zu modellieren. Diese Daten beinhalten eingehende kurz- und langwellige Strahlung, Lufttemperatur, Wasserdampfdruck und Windgeschwindigkeit von einer nahegelegenden Station, die 2002 errichtet wurde. Zur Validierung werden mittels Temperaturketten direkt gemessene Wassertemperaturen genutzt. Alle Daten wurden auf den Zeitraum vom Juli 2009 bis Juli 2011 aggregiert und auf stundliche Werte interpoliert. Das Modell FLake vom IGB berechnet daraus unter anderem Wassertemperaturen, auf Basis begründetet angemommener Parameter. In einem weiteren Schritt werden einige dieser Parameter mittels Monte Carlo Simulation in plausiblen Grenzen variiert und resultierende Güteparameter analysiert.

Die Übereinstimmung zwischen Modellergebnissen und direkten Messungen erweisen sich als genrell gut. Die besten Monte Carlo Durchläufe resultieren in einem $RMSE$ von unter 1 K und einem R^2 über 0.9 für eisfreie Zeiten im Sommer während sich höhere Abweichungen während eisbedeckter Zeiten zeigen. Das kann durch unter anderem durch die Eigenschaft von FLake erklärt werden, dass keine Strahlung durch das Eis zum erwärmen des Wasserkörpers geleitet wird.

Um die Charakteristiken des Modells genauer zu untersuchen, werden Monte Carlo Simulationen etabliert, die in der Folge eine klare Abhängigkeit von Wassertiefe und Extinktionskoeffizient bestätigen. Um mögliche Probleme mit flachen und eisreichen Seen zu vermeiden, wurden die Optimierungszeiträume in eisfreie und eisbedeckte Perioden aufgeteilt.

Abstract

Thermokarst lakes are typical features of the northern permafrost ecosystems, which highly affect the thermal exchange between the atmosphere and the subsurface. The objective of this work is to describe the physiographic character and the crucial thermal processes of the lakes and to explore possibilities and limitations of the application of the freshwater lake model FLake to these specific water bodies.

The particular lake modeled within this study is located on Samoylov island in the Lena river delta (Siberia) and embedded in the predominant lake-rich permafrost landscape, which is significantly influenced by thermokarst processes. Meteorological data are used to model lake temperature dynamics. This contains radiation (incoming short and long wave), air temperature, vapor pressure of water and wind speed from a nearby meteorological station build up in 2002. Directly measured lake temperatures in different depths are used for validation. All variables are cropped to the same period (July 2009 to August 2011) and interpolated to hourly values. The model FLake from IGB calculated water temperatures from meteorological data, based on parameters from an educated guess. Following, some of these parameters are varied via Monte Carlo simulation and resulting measured of fit are analysed.

Agreement between the FLake model output and lake temperature measurements is generally good. Best Monte Carlo runs show a $RMSE$ below 1 K and R^2 above 0.9 during the ice-free months in summer while larger deviations occur during the ice-covered period. This might be explained with the effects of solar radiation penetrating through the ice and leading to a heating of the water below, which is not represented in FLake.

To access the specific characteristics of the model a Monte Carlo simulation was set up. It shows a clear interdependence between the extinction coefficient and the lake depth. To avoid possible problems of FLake according shallow and ice-rich lakes, this setup was split into ice-free and ice-full seasons.

Abbreviations

%	percent
BP	before present
CH_4	methan
CO_2	carbon dioxide
°C	degree Celsius
d	day
e	euler number
e_a	actual water vapor pressure
e_s	saturated water vapor pressure
fig.	figure
h	hour
IGB	Leibniz-Institut für Gewässerökologie und Binnenfischerei
K	kelvin
ka	thousand years
LW	long wave
MCS	Monte Carlo simulation
m	meter
mbar	millibar
min	minute
R	language and environment for statistical computing and graphics
R^2	coefficient of determination
rad	radiation
RH	relative humidity
RMSE	root-mean-square-error
s	second
sec.	section
SD	standard deviation
SW	short wave
T	temperature
v	velocity
W	watt

1. Introduction

The interest in physical properties of lakes concerns all areas of natural sciences. According to the world's climate, they can be understood as indicators for larger scale changes. But also on local scale the influence of lakes and climate can be bilateral. The main driver of these effects are heat and water fluxes whose understanding is crucial for further investigation when it comes to all applied disciplines as hydrology, ecology or climatology.

Permafrost areas occupy about 25% of the world's landmass surface while being typical features for the northern hemisphere (Brown et al., 1997). Thermokarst lakes in permafrost landscapes, respectively lakes with a large permanently unfrozen zone below, cover huge areas of arctic regions (Grosse et al., 2013). Heat and water fluxes affect their surroundings, the sediment below and the atmosphere. A typical and important factor to understand the characteristics of arctic lakes is their characteristic to freeze. This leads to completely different fluxes and therefore behavior according the environment. Due to larger heat input and storage of water bodies in comparison to land, lakes are crucial features of thermokarst (Grosse et al., 2013).

Long and short term measurement of water temperatures in lakes is important for modeling subsurface thermal regime to access thermokarst processes, but also for models concerning ecological and physical dynamics. Recent simulations show a rapid degradation of permafrost below waterbodies for the future (Langer et al., 2016). A better understanding might lead to more assured forecasts about their development and general aspects of lake influencing their surroundings. More precise scenarios will help researchers and decision makers to develop sustainable solutions to deal with changing landscapes.

This work aims to quantify thermal dynamics of lakes in the Siberian north. Not many in-detail and in-situ measurements attempts for arctic lakes have been established. Comparable work for lakes in permafrost regimes has been done on Tibetan lakes by Kirillin et al. (2017) but with a focus on surface temperature and mixing depth. FLake demonstrated good performance to describe thermal properties of these lakes. (Thiery et al., 2014) used directly measured data and compared modeleing results of seven different models, but looking at larger lakes in Africa. Though all models reproduced water temperatures, FLake showed by far the fastest computation speed. This is especially useful for multiple simulation runs. Till

now no work has been done with Monte Carlo simulations to access parameter uncertainty in this specific model.

The objectives of this work are to describe the thermal patterns and processes, to explore possibilities and limitations of the application of FLake to these specific water bodies and to give advises for further measurements and modeling. To access this monitoring observatories have been established in the central part of the Lena River Delta on Samoylov island. This site includes meteorological stations and in-situ lake temperature recording.

Presumptions:

- FLake will perform well during summer month and mediocre during winter
- Crucial parameters are depth and extinction coefficient
- FLake might give insights about the thermal properties of the sediment below

FLake is chosen according to following criteria. The model has to (1) be widely used,(2) have shown skill in simulating thermal properties, (3) need low computation time and (4) be available for free.

The ensuing chapter contains a site description that gives the reader a overview of the site the investigated lake is located. This includes knowledge about the emergence of the Lena Delta as well as information about the lake an its direct surroundings. Subsequent, "Data and methods" is about the instruments used and the derived data. It describes briefly the model FLake but also all input data, parameters and output generated. In the next step the idea and methodology of the Monte Carlo simulation and parameter derivation is summarized. The following part contains detailed results of the measurement and simulation. Some aspects of measured and modeled temperatures are examined as well as parameter distribution gathered by the simulation set. To close this work the results and the chosen approaches are discussed on the last paper. This also includes a summary and conclusion for future research needs.

This work is based on a publication by Boike et al. (2015) and includes deeper modeling aspects respectively Monte Carlo simulations and split model setups for ice-less and ice on periods. The results of this publication showed that the extinction coefficient beside of water depth is a main factor in the thermal regime. Therefore Secchi depth measurements were established in July 2015 for validation purposes and taken into account with this work.

2. Site description

(taken from Boike et al. (2015))

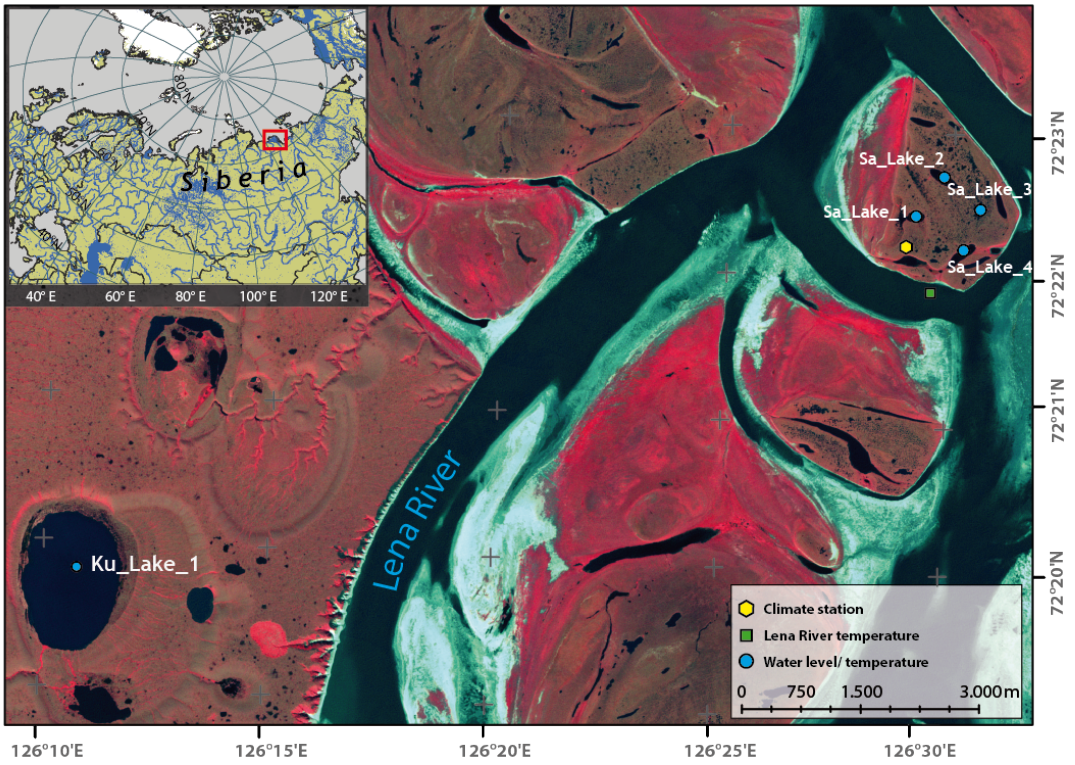

Figure 1: Location of the study site in the Lena River Delta of eastern Siberia; site is within the zone of continuous permafrost on the islands of Samoylov (Sa_Lake_1). The climate station providing data for the model setup is directly next to that. Inset map shows the location of the Lena River Delta in northern Eurasia and the distribution of lakes (Global lakes and wetland map; Lehner and Döll (2004)).

The Lena River Delta in northern Yakutia is one of the largest deltas in the Arctic and has one of the largest catchment areas (2 430 000 km^2) in the whole of Eurasia (Costard and Gautier, 2007). The Lena River discharges about 525 km^3 of water through the delta into the Arctic Ocean every year, with an average annual discharge rate of 16 800 m^3 $s^{-}1$ (Gordeev and Sidorov, 1993). This discharge rate has been reported to be increasing (Fedorova et al., 2015; Rawlins et al., 2009). As it passes through its estuarine area, the main flow of the Lena River splits into numerous arms and transverse branches to form the most extensive delta in the Russian Arctic, covering 25 000 km2 and including about 1500 islands and 60 000 lakes.

Continuous cold permafrost (with a mean annual temperature of - 10°C at 10m depth) underlies the study area to between about 400 and 600m below the surface.

Since observations started in 2006, the permafrost at 10.7m depth has warmed by > 1.5°C (Boike et al. (2013); `http://gtnpdatabase.org/boreholes/view/53/`).

The main features of the annual energy balance for these sites with continuous permafrost in the subsurface typically include low net radiation, higher atmospheric latent heat flux than sensible heat flux, and a large proportion of soil heat flux (Boike et al., 2008; Langer et al., 2011a,b). Previous publications have reported that shallow ($<$ 1m deep) ponds freeze completely in winter, but that the timing of freezeback can vary by up to 2 months between years, depending on the surface energy balance (Langer et al., 2011b, 2015).

The study area is located on the islands of Samoylov, within the central part of the Lena River Delta (see fig. 1). Samoylov Island (72°22' N, 126°28' E) lies within one of the main river channels in the southern part of the delta and is relatively young, with an age of between 4 and 2 ka BP (Schwambornet al., 2002), which is also the estimated maximum age of the investigated lakes on the island. In contrast, Kurungnakh Island forms part of the third terrace of the Lena Delta and is an erosional remnant of a late- Pleistocene accumulation plain. It consists of fluvial sands overlain by Yedoma-type ice complex deposits, which accumulated between 100 and 50 ka BP and since 50 ka BP, respectively, and a Holocene cover (8 to 3 ka BP) (Schwambornet al., 2002; Wetterich et al., 2008). Large thermokarst lakes and basins are major components of the ice-rich permafrost landscape of Kurungnakh Island; they have formed since 13 to 12 ka BP (Morgenstern et al., 2011, 2013).

The lakes presented in this paper are of thermokarst origin which is common for the lowland tundra permafrost areas of Northeast Siberia. These areas were not ice-covered during the latest glacial period (70 000–10 000 years ago) and are characterized by high to moderate ground ice content and thick sediment cover. Arctic lowlands with similar landscape characteristics and lake distributions can be found in central and eastern Siberia, interior and northern Alaska as well as northwest Canada (Grosse et al., 2013).

The landscape on both of these islands, and in the delta as a whole, has generally been shaped by water through erosion and sedimentation (Fedorova et al., 2015), and by thermokarst processes (Morgenstern et al., 2013). The proportion of the total land surface of the delta covered by surface water can amount to more than 25 percent (Muster et al., 2012). Up to 50 percent of the total surface water area in permafrost landscapes is attributed to small lakes and ponds with surface areas of less than $105m^2$, which have the potential to grow into large thermokarst lakes

(Muster et al., 2012). Water budget modeling for the tundra landscape has shown a small positive balance since 1953, which has been confirmed by satellite observations (since 1964) of the surface areas of water bodies (Boike et al., 2013). (...)

Small ponds and lakes emit more CO_2 and CH_4 per square meter than the surrounding tundra, and greenhouse gas production continues during winter in those lakes that do not freeze to the bottom (Langer et al., 2015). Modeling studies have demonstrated that an unfrozen layer of lake sediment is maintained throughout the year beneath thermokarst lakes (Yi et al., 2014). During high spring floods some of the lakes on the first terrace are flooded with Lena River water. Observations in 2014 on Samoylov Island, for example, confirmed the flooding of a large part of the first terrace on the island, including most of the lakes.

Additional detailed information concerning the climate, permafrost, land cover, vegetation, and soil characteristics of these islands in the Lena River Delta can be found in Boike et al. (2013) and Morgenstern et al. (2013).

3. Data and Methods

3.1. Field instrumentation and ground surveys of water temperatures

The site on Samoylov Island comprises four lakes where temperature and water level sensors were installed (HOBO Temp Pro v2, HOBO U20, Onset, $-0.2\,°C$ across a temperature range from 0 to $70\,°C$, and $-0.4\,°C$ across a temperature range from -40 to $0\,°C$). First setups were established in July 2009 and read out a year later with two other subsequent years of measurements. After this period not every lake was examined again leading to gaps of one year or even more. In 2015 the complete setup was removed.

Temperature and water level sensors were placed directly above the sediment while temperature sensors were put at 2m intervals up to 2m below the water surface (Fig. 2). The temperature sensors were suspended in the water column from a buoy and anchored in the sediment below. The sensor at the bottom of the lake (just above the sediment) was labelled as "0 m", the sensor 2m above the sediment as "2 m", and so on. The uppermost sensors were usually about 2m below the water surface since we were concerned about the formation of ice and the potential drift of sensors with the shifting of ice cover.

The data quality is quite diverse as some sensors were frozen (see fig. 5) or the exact location of the instruments could not be found again. Due to hyological influences from the Lena River the water level might change indirectly or the lake might be overflooded which lead to a input of colder water.

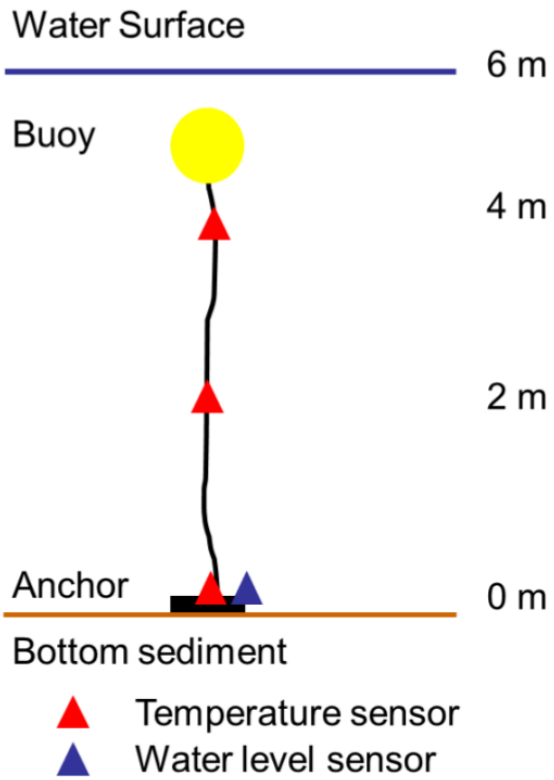

Figure 2: Schematic diagram showing the positions of sensors within the water column. To prevent freezing of the buoy within the ice cover (maximum 2m thick), sensors were deployed 2m below the water surface in most lakes. The water level sensor was located just above the bottom sensor. (from Boike et al., 2015)

3.2. Extinction coefficient

Secchi measurements were established in July 2015 on all monitored lakes on Samoylov island. For this measurement the Secchi disk is sunk until the black and white areas of its surface fade due to the light absorbing particles. To estimate the extinction coefficient needed for modeling, the following equation (Poole and Atkins, 1929) is used:

$$\alpha_1 = -log(0.25) * h_s^{-1} \tag{1}$$

where the value of 0.25 represents the fraction of the incoming radiation remaining as the Secchi disk disappears. This approach does not take into account fractions about mineral and organic content, as measurements of this were not made. FLake offers the possibility to assume different parameters for different optical bands, but in this case just the standard option for the optical band was used.

Also other approaches are taken into account (Thiery et al., 2014):

$$\alpha_1 = 2 * h_s^{-1} \tag{2}$$

$$\alpha_1 = 1.7 * h_s^{-1} \tag{3}$$

$$\alpha_1 = 1.3 * h_s^{-1} \tag{4}$$

$$\alpha_1 = 1.36 * h_s^{-0.806} \tag{5}$$

3.3. Modeling lake thermodynamics via FLake

3.3.1. Model description

FLake is developed for use as a lake parameterization module in numerical weather prediction (also in climate modeling and other environmental applications). The model is capable of predicting the vertical temperature structure and mixing conditions in lakes of various depth on the time scales from a few hours to many years.

It is a bulk model, based on a two-layer parametric representation of the temperature profile. The structure of the stratified layer between the upper mixed layer and the basin bottom, the lake thermocline, is described using the concept of self-similarity (assumed shape) of the temperature-depth curve. The same concept is used to describe the temperature structure of the thermally active upper layer of bottom sediments and of the ice and snow cover.

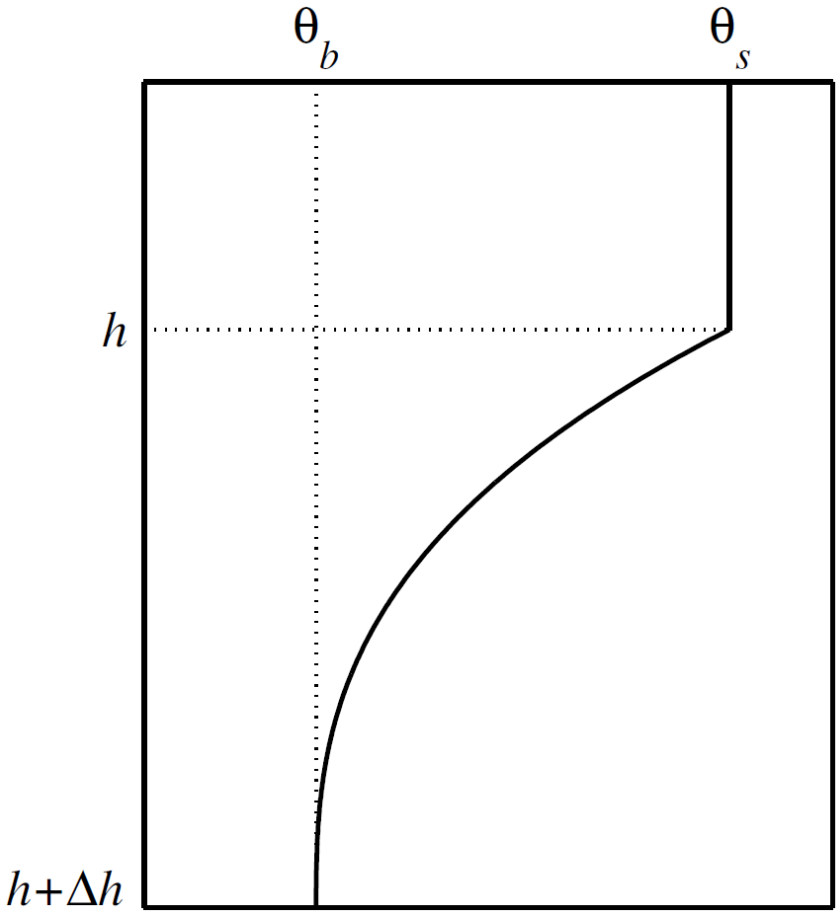

Figure 3: Schematic representation of the water temperature profile. The upper mixed layer is mixed while the thermocline is below, with mixed layer temperature θ_s, temperature at the bottom of the thermocline θ_b, mixed layer depth h and Δh the depth of the thermocline. (from Mirinov, 2000)

This work uses a linux binary of FLake compiled by gfortran (package/version: **gcc-7.1.1**) using incoming long wave radiation instead of cloudiness which is used in the standard version of FLake. For easy parameter variation and model analysis with Monte Carlo simulations it is wrapped by R modeling environment (version: **3.4.1**).

FLake was chosen due to its fast calculation (Thiery et al., 2014) free availability. It was tested well and shows good performance for a variety of lakes (Thiery et al., 2014; Kirillin et al., 2017). Most applications of FLake are based on remote sensing studies, partially on global scale, but also on single lake modeling.

3.3.2. Input data, parameters and output data

FLake needs the following input data as a regular time series:

- short wave radiation (Wm^{-2})
- air temperature (°C)
- water vapor pressure ($mbar$)
- wind speed (ms^{-1})
- long wave radiation (Wm^{-2})

The meterological data was used from Samoylov weather station nearby the lake (72°22.196' N, 126°28.850' E). This station was set up in 2002 and changed in 2009 and 2010. The data used involves a combined air temperature and relative humidity sensor (Vaisala HMP45C and Rotronic MP340-001-CS3), 4-way radiation (Kipp & Zonen CNR1 and Huxeflux NR01) and wind speed (Young 05103-5). No data gaps were present at the relevant times. All parameters were measured directly except water vapor pressure. This was derived via air temperature and relative humidity by Magnus formula combined with the fraction of actual and saturated water vapor pressure respectively relative humidity (Lawrence, 2005):

$$RH = \frac{e_a}{e_s} \tag{6}$$

and

$$e_s = 610.78\ e^{17.27*T/(237.3+T)} \tag{7}$$

combined to

$$e_a = RH * (610.78\ e^{17.27*T/(237.3+T)}) \tag{8}$$

resulting to the actual water vapor pressure e_a in Pascal which is divided by 100 to get mbar which FLake needs.

This time series data is chosen by best quality with a frequency of one hour. The chosen model time range is from July 2009 to July 2011 to have two consecutive and complete years. A longer period was not possible due to insufficient water temperature data. An overview of this processed data can be found in figure 4.

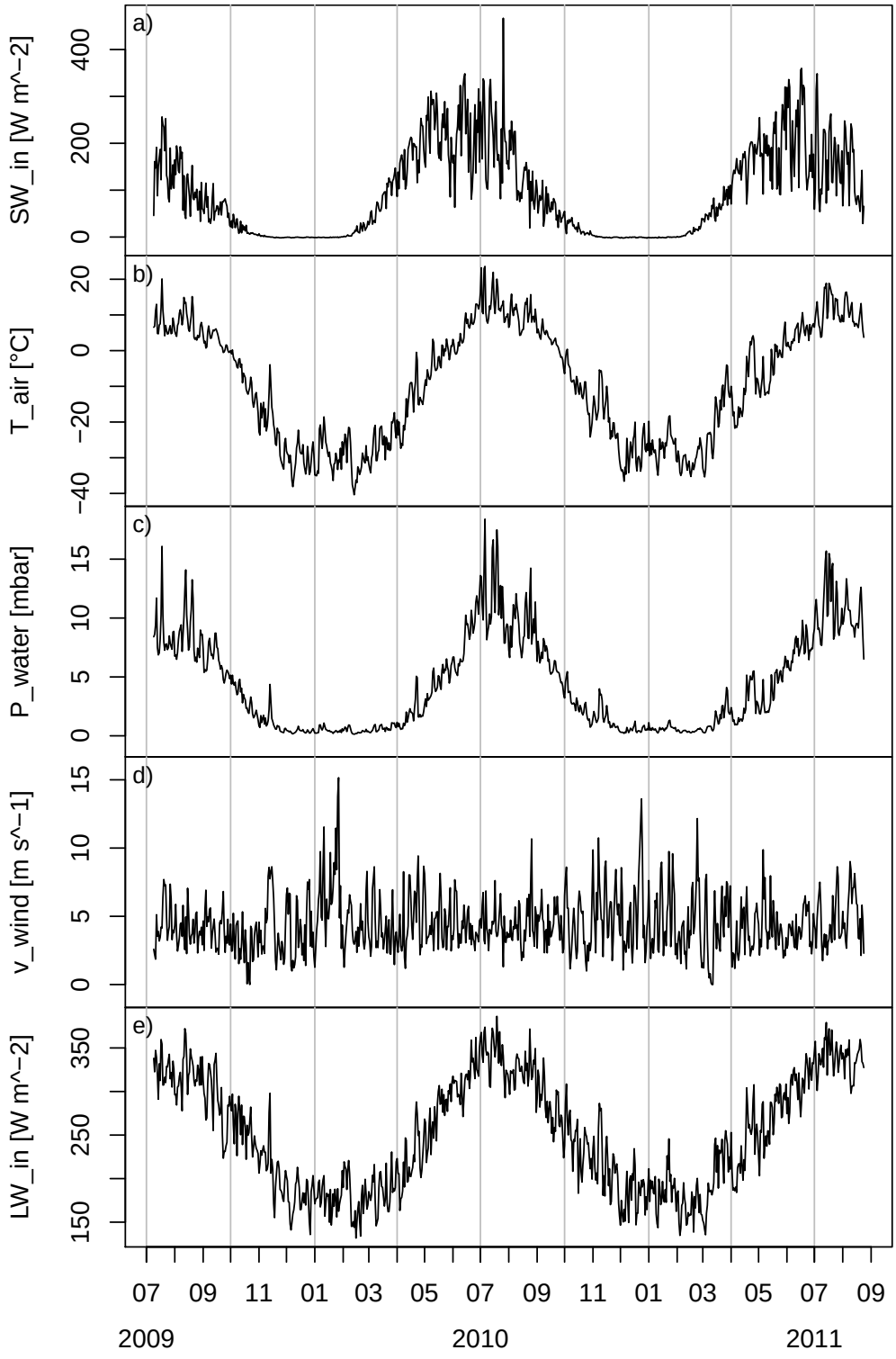

Figure 4: Plots of all input data for FLake from July 9th 2009 to August 24th 2011 (cropped to July 9th 2011 later); **a)** incoming short wave radioation $[Wm^{-2}]$, **b)** air temperature at $2m$ [°C], **c)** partial pressure of water vapour $[mbar]$, **d)** wind speed at $2m$ $[ms^{-1}]$, **e)** incoming long wave radioation $[Wm^{-2}]$

To set up the model the following parameters are the most important, a complete list is attached in the apendix (see tab. 4):

- depth of water column (m)
- wind fetch (m)
- depth of the thermally active sediment layer & temperature at the base (m & °C)
- extinction coefficient ([−])
- additional ice-water heat flux (Wm^{-2})

FLakes output includes a vast variety of variables:

- lake temperatures (bottom, surface, mean) (°C)
- sensible & latent heat fluxes (W)
- longwave radiative flux from water & atmosphere (W)
- mixed layer depth & stratification shape parameter (m & [-])
- active sediement layer temperatures & shape parameter (m & [-])
- snow thickness & temperature (m & °C)
- ice thickness & temperature (m & °C)

The model is set up that these are on the same time grid as the input data. For the validation process bottom and mean temperatures are used as no capable measurements of another variable (like surface temperature, heat fluxes, etc.) are available. A full list and graphs of the output are shown in appendix D.

3.4. Educated guess

First of all, an educated guess about all parameters is made. These values are based on expert opinions regarding past expeditions and optical fitting to the warming and cooling period where FLake performes best according heating and cooling processes (private communication J. Boike & G. Kirillin). An overview of these parameters and their derivation is found in table 1 while the full list of parameters taken into account is in the appendix (see tab. 4).

Table 1: The six main parameters identified during the modeling process, their values as well as derivation.

parameter	value	estimated how
depth of water column (m)	5.5	based on water pressure measurements from the lowest sensor
extinction coefficient ($-$)	0.55	optical fit for the open water cooling season
depth of the thermally active sediment layer (m)	6	based on measurements and prior modeling
temperature at the base (°C)	4	based on measurements and prior modeling
ice-water heat flux (Wm^{-2})	0	artificial, no assumption
wind fetch (m)	5	FLake manual

3.5. Optimization via Monte Carlo simulation

To gain the best fit and insights about FLake model dynamics a Monte Carlo simulation is set up. Six crucial parameters (depth, extinction coefficient, depth thermal active sediment layer, temperature at bottom of thermal active sediment layer, ice-water flux, wind fetch) are varied among plausible ranges, see table 2.

Table 2: Variation range of six main parameters.

parameter	minimum value	maximum value
depth of water column (m)	3	9
extinction coefficient ($-$)	0.3	0.9
depth of the thermally active sediment layer (m)	5	50
temperature at the base (°C)	-15	15
ice-water heat flux (Wm^{-2})	-3	3
wind fetch (m)	0.01	10

The parameter ice-water flux is an artificial parameter not taken into account in the whole modeling process, but just for general analysis of FLake behavior. Later in the modeling process optimization is split into winter (ice-on) and summer (ice-off) season to access the performance of FLakes in isolated times of the year and to analyze the crucial processes during that time. For each run the measures was calculated either for ice-on or ice-off periods.

To access the dependence of the parameters water depth and extinction coefficient these are varied over a regular grid. The resulting measures for each possible

combination give an overview of their interaction. This is set up separately with parameter ranges slightly different than in Monte Carlo sampling. The water depth ranges from 4 to $8m$ with steps of $0.1m$ while the extinction coefficient goes from 0.3 to 0.8 using steps of 0.025. This results in 861 different combinations and measures.

For model performance verification the measures root mean squared error ($RMSE$) and the coefficient of determination (R^2) are used, depending a weighting is intended or not. The statistical parameters were defined as follows:

$$RMSE = \sqrt{\frac{1}{n}\sum (y_i - \hat{y}_i)^2} \tag{9}$$

$$R^2 = \frac{\sum_{i=1}^{n}(\hat{y}_i - \overline{y})^2}{\sum_{i=1}^{n}(y_i - \overline{y})^2} \tag{10}$$

Where n is the total number of values, y_i observed value at i and $\hat{y}_i$ computed value at point i.

The closer $RMSE$ to zero and R^2 to unity, the better the performance is. Resulting values of R^2will be remarkably high because predictor and response variable do have the same form, respectively °C.

4. Results

4.1. Lake thermal dynamics based on observations

The temperature record begins in early summer 2009 and raises till mid of June (Fig. 5). When highest temperatures are occurring stratification is developing partially. As the lake is warming in early summer or cooling in fall the water column is completely mixed, which means low temperature gradients of about 0.2°C m^{-1}. When reaching 0°C at the end of fall ice cover formation starts. No specific measurements of ice thickness were made but experience from former expeditions revealed values of about 1 to $2m$. Freezing point temperatures only occur at the start of ice formation. The water body reheats shortly after due to sediment heating. This effect gets weaker as the winter goes on and the sediment cools from the water causing a lower water-sediment gradient.

Under ice warming starts in march as well as thawing of snow cover at about may to June. Both are induced by rising short wave radiation. Ice break up comes along with complete mixing as a free water body can be mixed by sheer forces of wind.

All years show typical temperature records. During ice-free periods water heats and cools depending of the energy input by radiation. During this time heat is also transferred into the bottom sediment. After ice built-up the sediment reheats the water column with typical thermal stratification. Due to missing energy import by radiation the water column starts cooling again after several weeks. When radiation starts again the water body is warming due to transmission through the ice until the whole water column reaches an equal temperature. This state usually involves ice breakup.

In June 2010 some weeks prior to ice breakup during under ice warming a small input spike of colder water occurs. This can be explained by hydrological influence of Lena river which overflows parts of Samoylov island.

The data quality is generally good, but after the first months 6m sensors fails. In the third consecutive year the lowest sensor also fails and the uppermost is freezing.

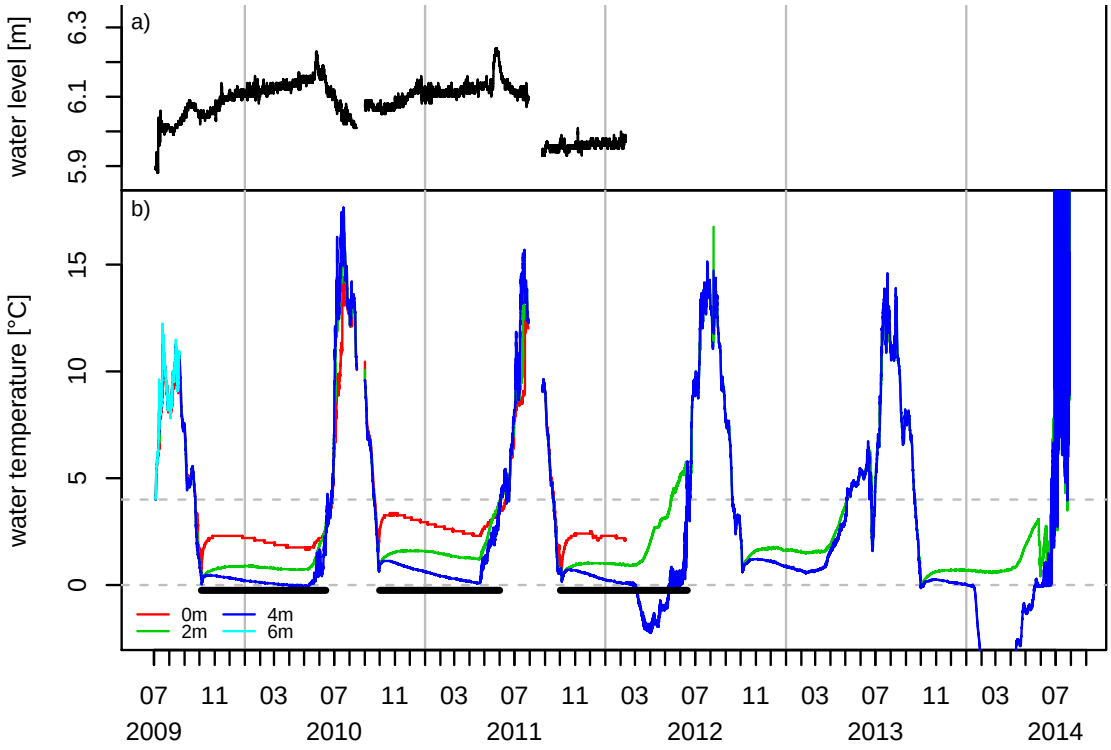

Figure 5: Hourly water level and temperature values for Sa_Lake_1, July 2009 to July 2014. **a)** Depth of bottom lake sensor as an indicator of water level changes; **b)** water temperatures for 0m, 2m, 4m and 6m depth, ice cover is indicated by thick black lines. For orientation grey lines show 0 and 4°C. From February 2014 temperatures exceed plausible ranges.

4.2. Modeled seasonal lake thermal dynamics

Based on the data the best time frame for modeling lasts from from July 2009 to July 2011. during those two year no freezing sensors appears which makes it capable for modeling and validation. The parameters used for the first model set up are chosen due to an educated guess based on knowledge of the site, exploratory modeling attempts and measurements (see sec. 3.2) All values used can be found in table 1. The initial values for modeling are measured water temperatures. The mean temperature represents the mean of all sensors taking to account the vertical fractions while the bottom water temperature is represented by the lowest sensor.

FLake meets the general shape of the mean and bottom very well during the summer. The first three months observed and modeled mean temperatures match with a derivation of 1 K till the ice built-up starts in October. Bottom temperatures have a slightly higher error. From ice built-up on the values differ more with a higher modeled temperature at the bottom and lower temperature for the whole water column while the shape of the curve fitting almost. With the starting ice break-

up the model converges to measured values but being a little to high till summer. Dates of ice-breakup are close to those observed while heating but still some days to early. Mixing and cooling processes follow the data measured. FLake and its parameterization match almost all spikes with a slight tendency to overestimate mean temperatures.

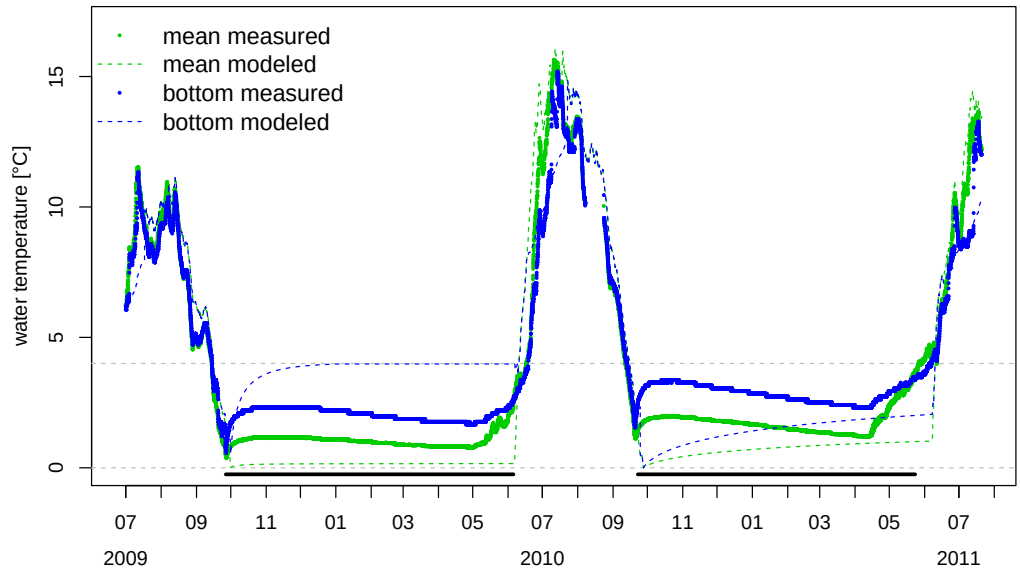

Figure 6: Hourly water temperatures for measured (dotted/bold) and modeled (dashed line) water temperatures from July 2009 to July 2011. Green colour stands for mean, blue for bottom temperatures. Ice cover is indicated by thick black lines. For orientation grey lines show 0 and 4°C.

4.3. Monte Carlo simulation

To estimate the necassary number of Monte Carlo samples a stability analysis is set up. The standard deviation of mean temperature RMSE exceeds oscillation after $200 - 300$ runs and reaches a stability of about $0.24K$ from 500 runs on (see fig. 7a). Almost the same behavior is given for the 5% and 95% percentiles as well as the mean values (see fig. 7b). To get a higher density of parameter space 1000 runs in total are performed.

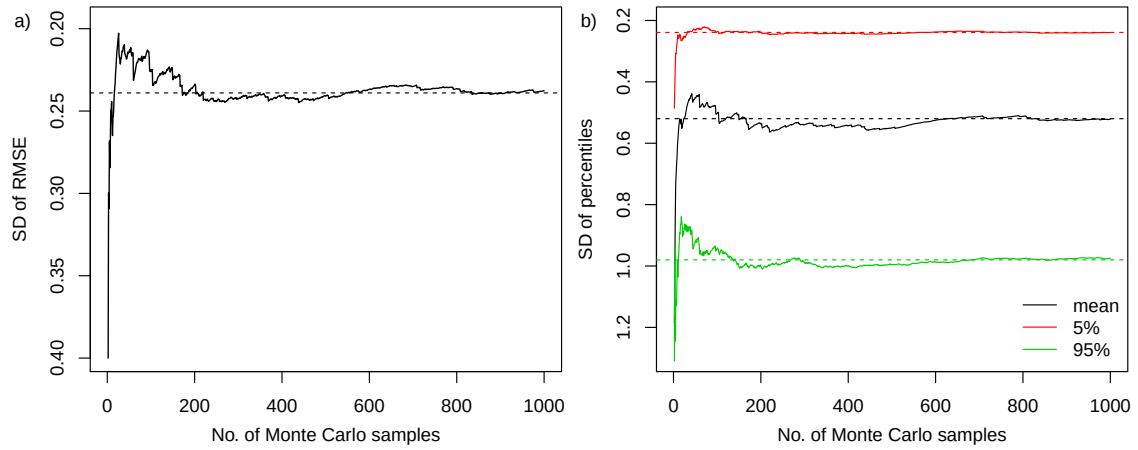

Figure 7: Stability of the Monte Carlo simulation, **a)** progression of the standard deviation of RMSE, **b)** progression of standard deviation of percentiles for mean temperatures of each run

No parameter shows clear ranges of best fits (see fig. 8). RMSE values have a range from 0.93 to $2.23K$, a mean of about $1.37K$ while 50% of all values are in the range between 1.17 and $1.51K$. Values for R^2 range from 0.84 to .96 with a overall mean of 0.93 and 50% between 0.915 and $0.94K$.

The point clouds for every parameter are broadly distributed over the whole range. Just the depth of the water column has a banana shape with an optimum about 5.5 to $7.5m$ while highest RMSE values tend to occur at lowest water depths from about $4.5m$. The extinction coefficient has lowest RMSE at about 0.3 to $0.4K$ with worst runs slightly grouping at higher coefficients. Both sedimental parameters as well as wind fetch have no distinct areas of clustering. Best values of the artificial ice-water flux group betweeen -3 to $0W$, but also the worst runs are located in that range.

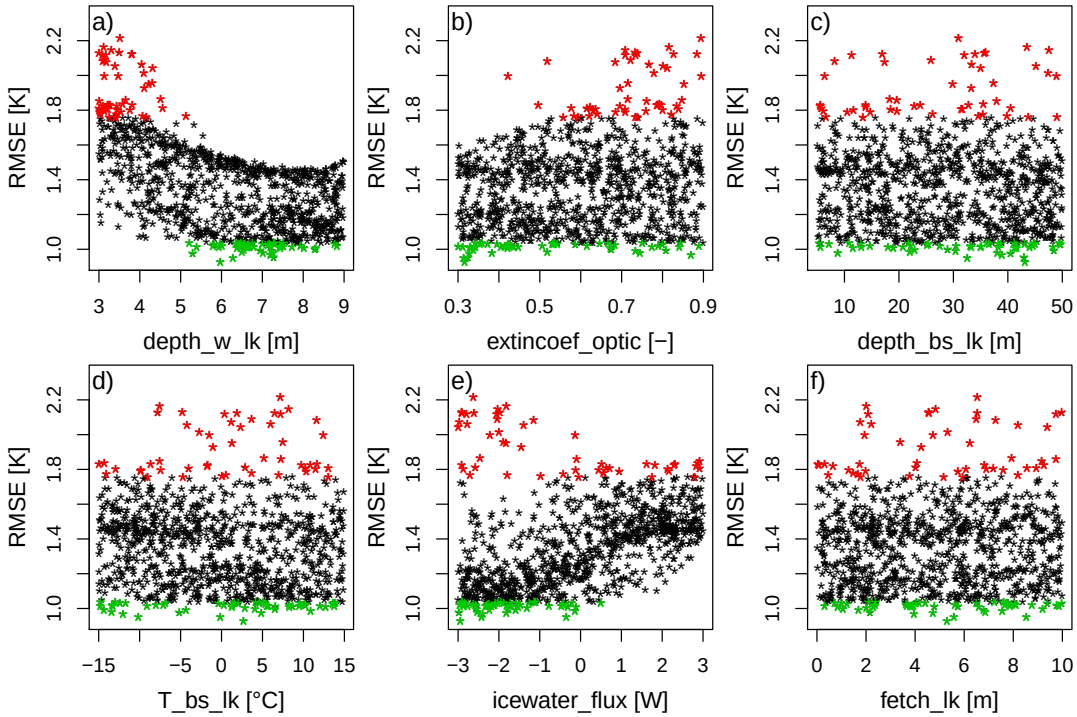

Figure 8: RMSE for the six varied parameters, lower values indicate better fit. **a)** depth of water column (m), **b)** extinction coefficient ($-$), **c)** depth of the thermally active sediment layer, (m) **d)** temperature at the base of the sediment layer (°C), **e)** ice-water heat flux (Wm^{-2}), **f)** wind fetch (m)

The modeled mean water temperatures of the 5% and 1% best parameters sets according the RMSE are shown in figure 9, giving an overview of the width of best temperatures modeled. Results are a little bit closer to the data compared to the prior educated guess. But again, during summer months the best runs meet the data or overestimate the temperature slightly. The data is frequently in the range of the 5% (62% of data) respectively 1% (45% of data) best runs while largest deviations occur during warming and cooling periods for summer months. Best fits are narrow during summer months while widening during ice-on periods in both years. Most and largest deviations during the ice-free season occur while the water body cools. In general, temperature spikes occur at the same dates. The shape of modeled and measured temperature differ more during ice-on season. While the models indicate a steady increasing temperature, measured data first rises, falls after a delay and increases again with some spiked at the end of that period.

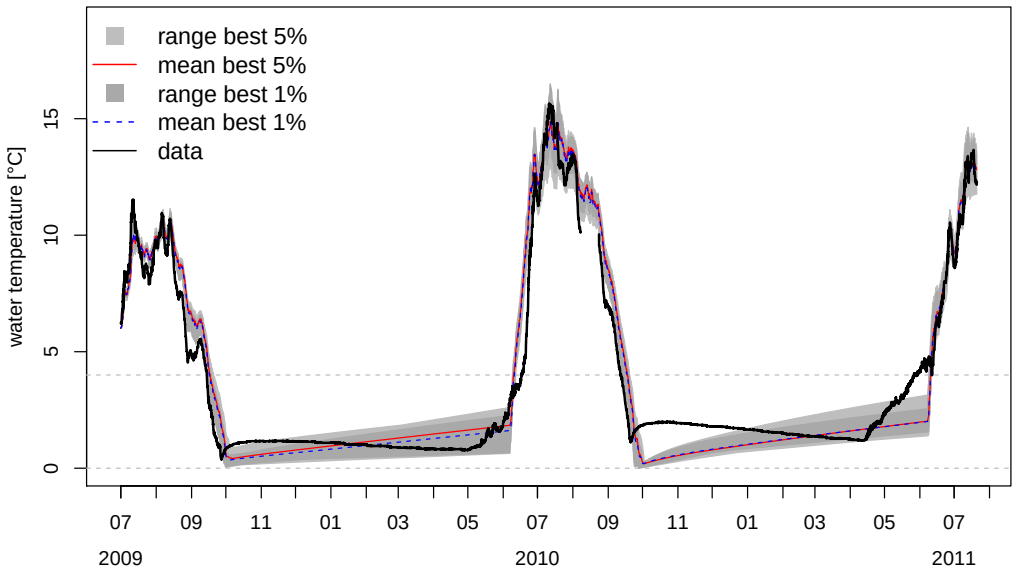

Figure 9: The best 1% & 5 % models according RMSE (lighter gray area), the mean of it (red line), the best 1 % models according RMSE (darker gray area), their total mean (dashed blue line) and the data (black line)

Furthermore model optimization is split into two different seasons and therefore parameter sets. The shapes of the new retrieved plots for the ice off period are more distinct (see fig. 10). Clearest scatter plot shapes are the depth and the extinction coefficient. Optimal water depth groups at 5.5 to $7m$ and worst RMSE tend to be caused for depths below $4m$. The extinction coefficient has it lowest RMSE values between $0.3 - 0.4$ and worst values at the other end of the scale. Again, the sedimental parameters have no big influence as they are widely distributed. The artificial ice-water flux is not taken into account as it has no effects during the ice off period. Also wind fetch is not considered due to no relevance for the mean temperature.

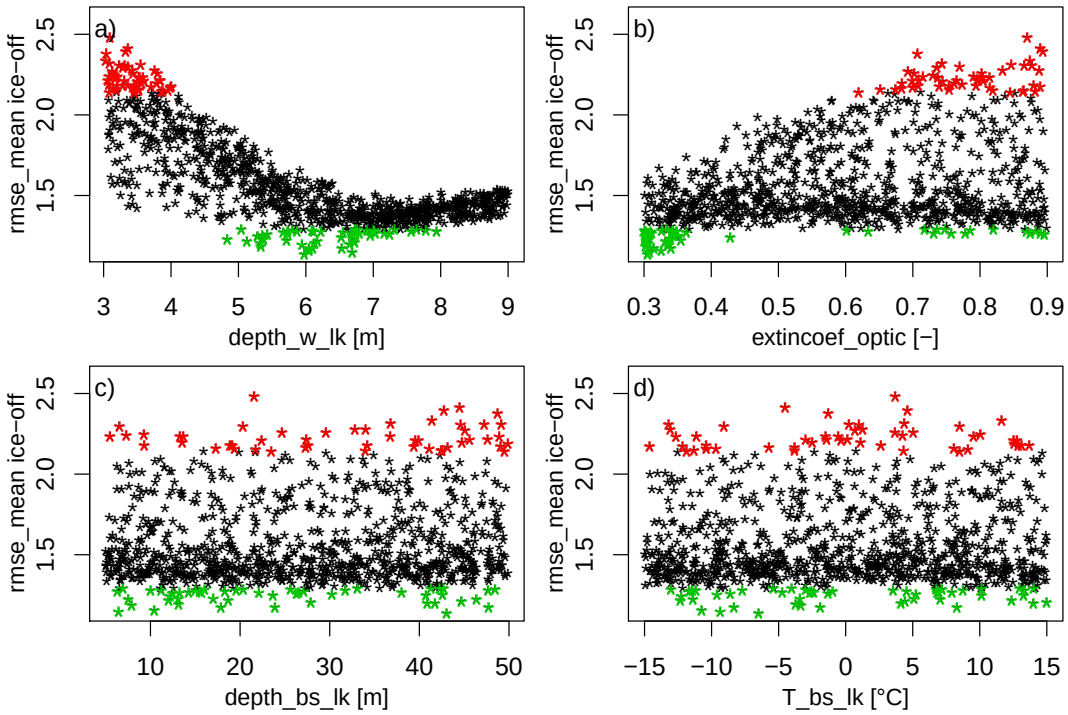

Figure 10: RMSE for the six varied parameters optimized just for the ice-off period, lower values indicate better fit. Red marked points indicate 5% worst fits, green 5% best fits.

All parameters for the ice-on period (see fig. 11) are spread more widely over the whole parameter space. For water depth and extinction coefficient values seem vaguely to group around the values used in the educated guess. Due to FLakes assumption of radiation not transmitting through ice the extinction coefficient has no significance.

Both sediment parameters optima changed. The depth of the thermally active layer is shifted to higher values and is mainly distributed between 30 and 50m. Despite some values are below that range. For the temperature at the bottom of the sediment layer most best fit values moved to the range of -4 to $+12$°C.

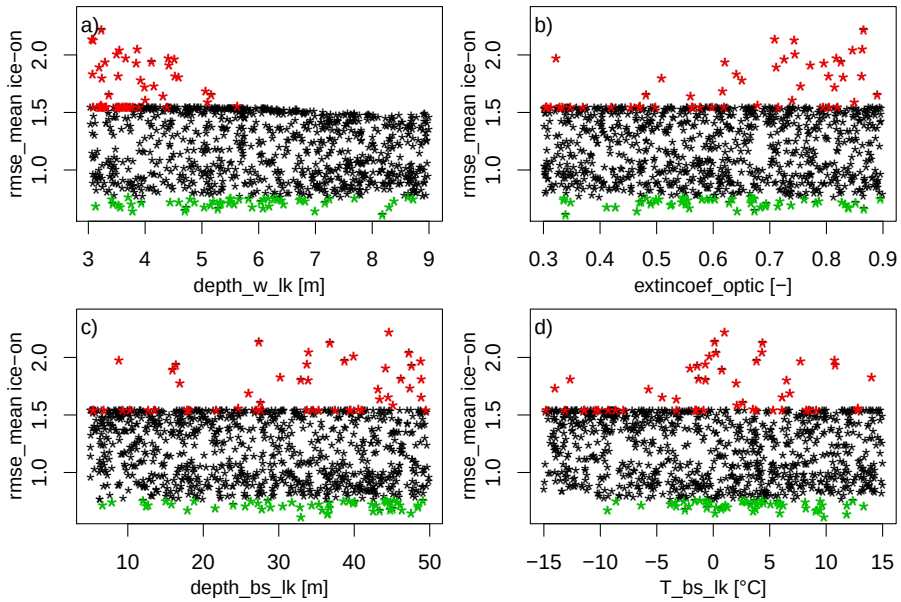

Figure 11: RMSE for the six varied parameters optimized just for the ice-on period, lower values indicate better fit. Red marked points indicate 5% worst fits, green 5% best fits.

To access a possible dependence between depth and extinctions coefficient a surface plot is made for ice-off period (see fig. 12). This time R^2 will also be considered due to its higher weighting of larger errors. Both measured show a definite optimum around a water depth of about $6m$ and for the extinction of 0.3. At this small area RMSE is about $1.1K$ and R^2 at about 0.91.

In general worst parameter combination include parameter values at the boundaries of the Monte Carlo sampling, expecially for water depth and a combination of very high extinction and low depth.

The RMSE plot suggest an increasing water depth to $7m$ in combination with increasing extinction coefficient to the maximum of 0.8 RMSE values below 1.4. Values for R^2 of about 0.9 occur for depths between 0.9 and extinction coefficients up to 0.7.

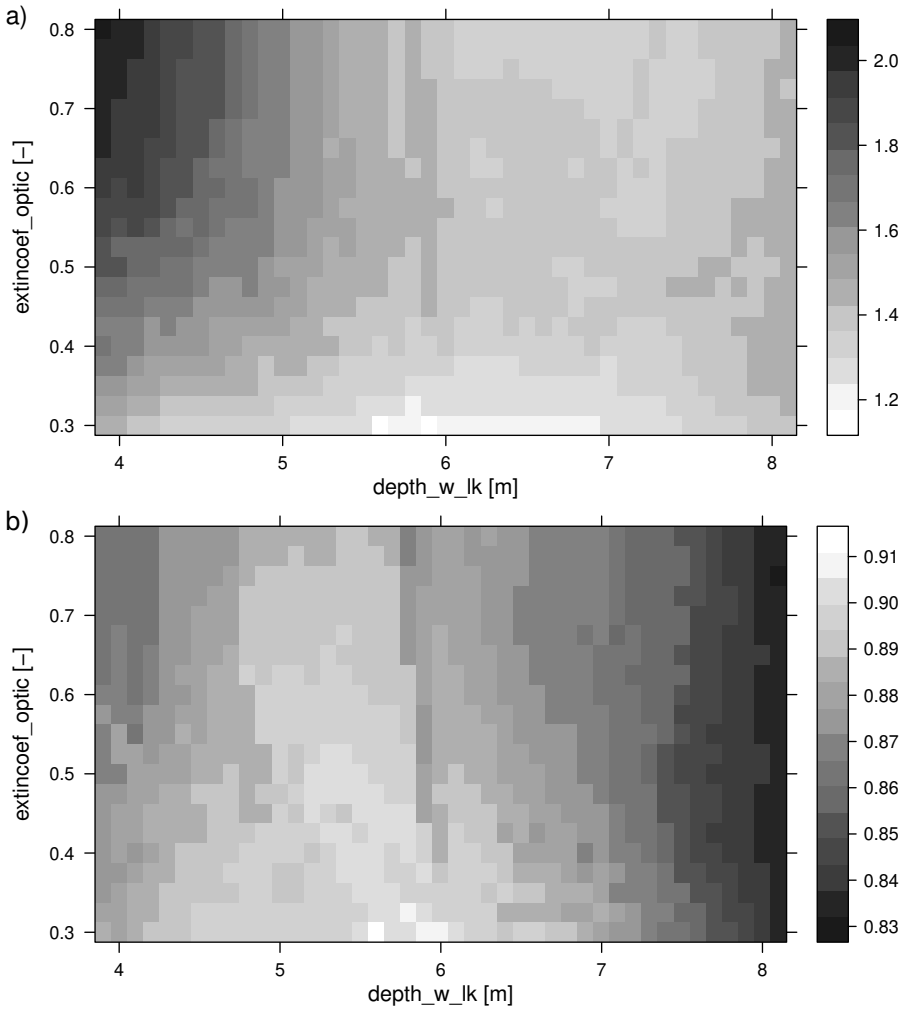

Figure 12: Variation of RMSE for water depth and extinction coefficient over a regular grid, just for ice-off period. **a)** RMSE - lighter color indicates lower values and better fit, **b)** R^2 - darker color indicates higher values and better fit

Modeled mean water temperatures of the 5% and 1% best parameters sets according the RMSE and only for ice-off period are shown in figure 13. The resulting temperatures are close to measured data with maximum derivations of $1K$. Most and largest deviations occur again during cooling and heating of the water body. As before temperature spikes of data and models occur at the same dates.

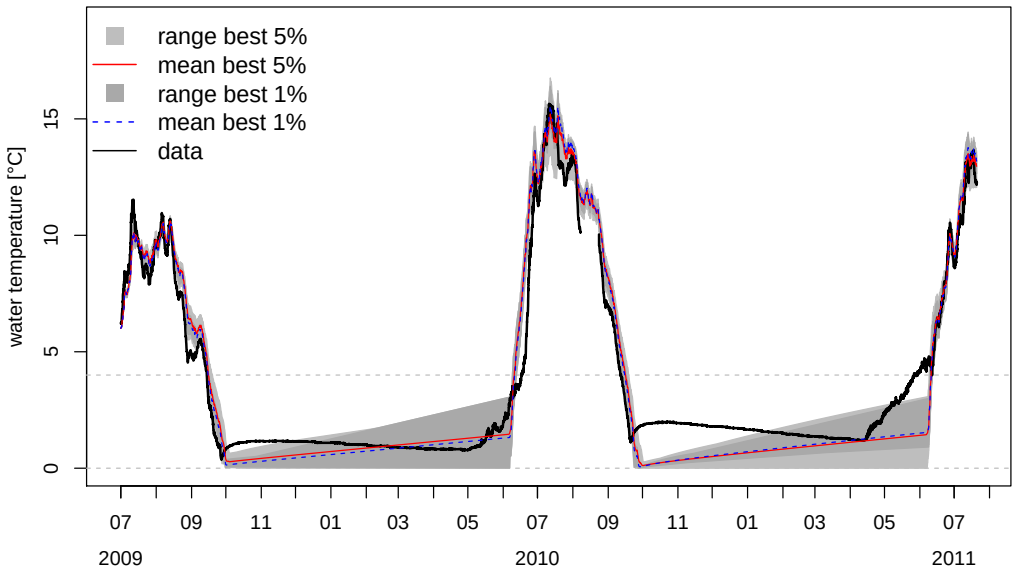

Figure 13: The best 1% & 5 % models for ice-off period according RMSE (lighter gray area), the mean of it (red line), the best 1 % models according RMSE (darker gray area), their total mean (dashed blue line) and the data (black line)

4.4. Secchi depth and extinction coefficient

Secchi measurements for Sa_Lake_1 were between 3 and 6.3 m (see tab. 3). This results to extinction coefficients of 0.22 to 0.6 based on equation (1). Measurement from different lakes of Samoylov island (also tab. 3) showed lower values of the Secchi depth, between 2.0 and 3.2 m resulting in extinction coefficients of 0.43 to 1.1.

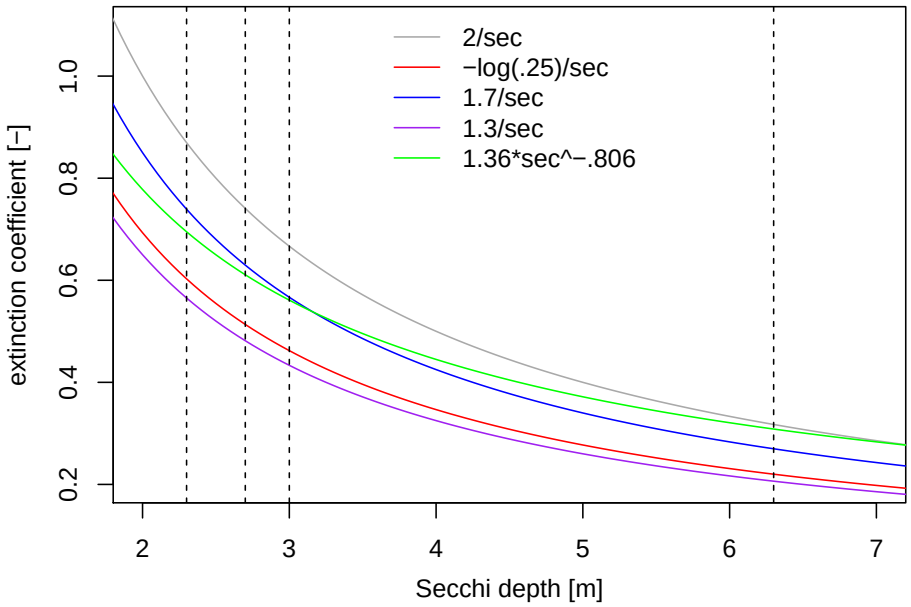

Figure 14: Resulting Secchi depth for 4 in-situ measurements (dashed lines) and 5 different calculation methods

5. Discussion

5.1. Lake level and temperature measurements

The lake water level is quite constant ($5.9 - 6.2m$) over the measurement modeling period (see fig. 5). Changing lake depth can be caused by a real change of the water level induced by hydrological changes or also by sensor location drift. This may lead to these small abbrevations respectively errors. To address this issue a different mounting approach for the temperature chain should be developed.

The drop in water level and scarce overall data in the third and following years of might cause problems in modeling and is therefore not used. Freezing of the $4m$ sensor in the third year might indicate the buoys position might have changed drastically which causes temperature records that may not be comparable to previous data.

In general, a longer time series of this temperatures would lead to more certainty if this influence from Lena river might have bigger effects to the lake. But freezing sensors among the in total five year record lead to a shorter period possible to model.

The logger readout is only possible in ice-free periods and was done during cooling times, which caused missing data. This point of time is important for fitting the right thermal parameters of the water body. This work suggest longer data logging periods to ensure (1) a constant location of the sensor and (2) non-interrupted data series. Unfortunately due to adverse conditions due to heavy ice-builtup and distance from stations this problem is hard to tackle.

Failing top sensors are a problem, as an more certain knowledge of the whole water columns temperature would improve validity of the work. Additionally, most work done with FLake is based on surface temperature (Thiery et al., 2014; Kirillin et al., 2017) Furthermore, from a reliable surface temperature applications using water surface temperature from remote sensing would benefit as this data is a typical product.

5.2. Modeled seasonal lake thermal dynamics

The biggest deviations occur during ice-on periods with 2 to $3K$ due to the poor handling of ice in the FLake scheme as no radiation is forwarded into the water column. An obvious under-ice heating process happens from may on till ice-breakup. This process is well known especially during melting processes in spring as snow and ice become clearer (Jonas et al., 2002). Also the shape of temperature curves do not fit well. While FLake shows a constant heating effect, the measured values rise first due to reheating but then lows again. This interaction of sediment and water temperatures cannot be reproduced. The reason might be that the concept of self similarity is not capable for long ice periods as the temperature gradient from sediment to water is positive during ice-on (see fig. 19b)). But this is not the focus of FLake, as its scheme is built for simplicity according assumptions and parameters. A more detailled look to thermal properties of the sediment is possible with CryoGrid 3 (Langer et al., 2016; Westermann et al., 2016) as its scheme is based on multiple layers of snow, ice, water and sediment connected via finite differences.

5.3. Monte-Carlo simulations

Stability analysis suggest that after about $500 - 600$ Monte Carlo sample this setup produces stable and reproducible results. Therefore the chosen 1000 is a sufficient choice and more runs will not yield better results.

Values for R^2, even for the worst fits, are quite high compared to other models. The narrow plausible parameter range likely causes results that are close to the data, as well as among each other. This suggest that even a rough educated guess can cause reasonable results, depending on the intended use.The resulting RMSE in the range from about 1 to $2K$ is plausible as most deviations are not far greater than this.

First Monte Carlo simulation delivers mediocre results. As nearly all parameters show a wide spread for their optimal zone. Even water depth and extinction coefficient which were assumed to important for the summer period show no clear optimum. The same applies for the bottom temperature and depth of the thermally active sediment. Just the tending negative heat flux from water to ice (respectively positive from ice to water) indicates, that during ice-on periods an additional heat input is needed to fit the data. This is consistent with the missing routing of en-

ergy through the ice in FLake. Additional analysis of this behavior and attempts to overcome this were not made as the ice-water flux is just a constant over the whole period while energy input is based on the variable of solar radiation. For easy model operation this is a important issue that could only be solved properly by implementing radiation routing through the ice to the water column. The bypass of this problem with fixed ice-water flux does not meet processes in reality as snow cover and ice transmissivity lead to highly variable input instead of a simple parameter. Wind fetch has also no distinct values for good fits. As this parameter is only important for stratification depth therefore not relevant for the total energy stored in the water column respectively the mean temperature. Better parameter estimations are not possible as the Monte Carlo simulation produced the best sets. To improve the fit, the model setup or the model itself should be changed. A reasoable step is to split modeling periods as done in this work.

As with the educated guess parameters the temperature of ice-on periods cannot be reproduced optimal for the whole annual cycle. The temperature is in plausible range but the shape of the curve and therefore underlying thermal processes are not represented correctly. This might also affect the start and ending of ice-free periods where most derivations occur. This lake clearly has two states with very different thermal regimes FLake is not able to handle at once. Still, for long term modeling, larger spatial scale approaches or lower detail analysis one model for multiple years is appropriate. But for a detailed view of the FLake and its performance a separate treatment is reasonable. To eliminate the dependence of ice-on/ice-off periods and to possibly gain more insight of both states are considered for their own.

Separate parameter estimations for both conditions lead to higher information about each state and minimizes the errors, especially for the summer season (see fig. 13). The optimum of the extinction coefficient lowers and narrows, but still fits to previous assumptions and is plausible comparing to the educated guess. Considering Secchi depth measurements these values are very low but still plausible (see fig. 14). Both sediment parameters have almost no influence on the goodness of fit. This approves the presumption from educated guess that FLake is not very capable to describe the sediment condistion in detail. Another explanation might be that the sediment is not crucial part on modeling summer temperatures still being relevant for long term trends as in reality heat input of summer strongly affects winter thermal regime. This gets more relevant considering longer time scales due to talik formation, like in the study of Langer et al. (2016).

Referring to ice-on parameters no clear insights are possible. Obviously the

RMSE is clustering at slightly above $1.5K$ which might be caused by huge number of runs with mean temperatures of 0° C through the whole period. Yet tending higher values of thermally active sediment layer depth above $30m$ and temperatures at the bottom of that sediment between -4 and $+9$°C could be an indicator for a deep talik. A high sediment temperature might also be an adaption of FLake and the Monte Carlo simulation to paraphrase the under-ice cooling expecially during end of the ice-on season. But as FLake does not meet the general curve shape both interpretations might be to vague. This again strongly sugggest to dismiss FLake for sediment analysis.

5.4. Secchi depth and extinction coefficient

The estimated extinction coefficient is lower than the measured. This may be due to mixing conditions and therefore particle distribution among the water column. Also the measurement itself or windy conditions might cause a higher measured extinction than in reality. In fact, the extinction coefficient is variable during the year as sediment and algae distribution have seasonal circles resulting in resulting temperature deviation of up to 8K in (Zolfaghari et al., 2017). FLake assumes it constant over the whole year. Also there might be an variation between the years. Also the measurements were made a possible microbiotical active an therefore turbid dates in July. Another explanation may be the different sensitivity of organic and mineral particles and therefore heat transfer into the system (Babin et al., 2003).

6. Summary and conclusion

This work aimed to establish a proper model setup with FLake for a specific lake on Samoylov island and to fit gathered data. FLake seems generally capable of modeling shallow water bodies in the circumartic region thus some adjustments may have to be made. Typical physical processes can be described as well as reproduced and were validated by this work.

As modeled temperatures follow the seasonal circle, especially during ice-free season, FLake is adequate for ice free or barely ice covered lakes, even shallow ones. The different lake states depending on ice cover lead to restrains that remain, even after splitting the model setup. A Monte Carlo simulation can produce good and plausible parameter ranges for water depth and the extinction coefficient. To access sedimental parameters, FLake showed oneself as not capable to deliver good estimation. For a detailed analysis other models like CryoGrid 3 are suggested.

FLakes fast computation speed of about one second for two years on casual computer proved oneself useful for Monte Carlo simulations. This offers more possibilities for longer time series, more parameter variation and bigger ranges.

Still, resulting modeling parameters derived from this work are plausible. Even the ranges assumed produce reasonable results so these parameters can be used in further works about comparaable shallow arctic lakes. This applies for remote sensing uses or other works with very sparse data.

Results can be improved by having steady data series of meteorological data, water temperature and level. Further advantages might be achieved with continuous measurements of the extinction coefficient or at least multiple measurements during the ice-free season.

The most crucial problem is the treat of ice which is not well represented in the model. As no energy will be passed through ice a radiation induced warming of the water body is not occuring in the model. Secondly, the ice layer is just built on top while not being subtracted from the water column causing different energy budgets. This leads to a inaccurate behavior during the ice-on period and therefore different parameters. This makes FLake use best with lakes $>$ 6m depth and preferably short times of ice cover. Recent trends in FLake development address the issue of snow cover (Thiery et al., 2017), but not the transmission of radiation through ice.

References

Babin, M., Morel, A., Fournier-Sicre, V. , Fell F. and Stramski D., *Light scattering properties of marine particles in coastal and open ocean waters as related to the particle mass concentration*, Limnol. Oceanogr., 2002 (48), pp 843-859

Boike, J., Wille, C., and Abnizova, A. *Climatology and summer energy and water balance of polygonal tundra in theLena River Delta, Siberia*, J. Geophys. Res., 2008 (113), G03025

Boike, J., Kattenstroth, B., Abramova, K., Bornemann, N., Chetverova, A., Fedorova, I., Fröb, K., Grigoriev, M., Grüber, M., Kutzbach, L., Langer, M., Minke, M., Muster, S., Piel, K., Pfeiffer, E.-M., Stoof, G., Westermann, S., Wischnewski, K., Wille, C. and Hubberten, H.-W. *Baseline characteristics of climate, permafrost and land cover from a new permafrost observatory in the Lena River Delta, Siberia (1998–2011)*, Biogeosciences, 2013 (10), pp 2105-2128.

Boike, J., Georgi, C., Kirilin, G., Muster, S., Abramova, K., Fedorova, I., Chetverova, A., Grigoriev, M., Bornemann, N. and Langer, M. *Thermal processes of thermokarst lakes in the continuous permafrost zone of northern Siberia - observations and modeling (Lena River Delta, Siberia)*, Biogeosciences, 2015 (12), pp 5941-5965.

Brown, R. *Relationships between suspended solids, turbidity, light attenuation, and algal productivity*, Lake Reserv. Manage., 1984, pp 198-205.

Brown, J.B., Ferrians, O.J., Heginbottom, J.A. and Melnikov, E.S. *Circum-arctic map of permafrost and ground-ice conditions*, U.S. Geol. Surv., Map CP-45, scale 1:10,000,000.

Costard, F. and Gautier, E. *The Lena River: Hydromorphodynamic Features in a Deep Permafrost Zone*, Geomorphology and Management, 2007, pp 225–233

Fedorova, I., Chetverova, A., Bolshiyanov, D., Makarov, A., Boike, J., Heim, B., Morgenstern, A., Overduin, P. P., Wegner, C., Kashina, V., Eulenburg, A., Dobrotina, E. and Sidorina, I. *Lena Delta hydrology and geochemistry: long-term hydrological data and recent field observations*, Biogeosciences, 2015 (12), pp 345–363

Gordeev, V. V. and Sidorov, I. S. *Concentrations of major elements and their outflow into the Laptev Sea by the Lena River*, Chem., 1993 (43), pp 33–45

Grosse, G., B. Jones, and C. Arp *Thermokarst lake, drainage, and drained basins*, Treatise on Geomorphology, edited by: Giardino, R. and Harbor, J., Glacial and Periglacial Geomorphology, 2013 (29), pp 325-353

Jonas, T., Terzhevik, A. Y., Mironov D. V. and Wüst, A. *Radiatively driven convection in an ice-covered lake investigated by using temperature microstructure technique* Journal of Geophysical Research, 2002 (108), pp 14-1-18

Kirillin, G., Wen, L. and Shatwell, T. *Seasonal thermal regime and climatic trends in lakes of the Tibetan highlands*, Hydrol. Earth Syst. Sci., 2017 (21), pp 1895-1909

Langer, M., Westermann, S., Muster, S., Piel, K., and Boike, J. *The surface energy balance of a polygonal tundra site in northern Siberia – Part 1: Spring to fall*, The Cryosphere, 2011 (5), pp 151-171

Langer, M., Westermann, S., Muster, S., Piel, K., and Boike, J. *The surface energy balance of a polygonal tundra site in northern Siberia – Part 2: Winter*, The Cryosphere, 2011 (5), pp 509-524

Langer, M., Westermann, S., Heikenfeld, M., Dorn, W., and Boike, J. *Satellite-based modeling of permafrost temperatures in a tundra lowland landscape*, Remote Sens. Environ., 2013 (135), pp 12-24

Langer, M.,Westermann, S.,Walter Anthony, K.,Wischnewski, K. and Boike, J. *Frozen ponds: production and storage of methane during the Arctic winter in a lowland tundra landscape in northern Siberia, Lena River delta*, Biogeosciences, 2015 (12), pp 977-990

Langer, M., S. Westermann, J. Boike, G. Kirillin, G. Grosse, S. Peng, and G. Krinner *Rapid degradation of permafrost underneath waterbodies in tundra landscapes—Toward a representation of thermokarst in land surface models* J. Geophys. Res. Earth Surf., 2016 (121), pp 2446-2470

Lawrence, M. G.: *The Relationship between Relative Humidity and the Dewpoint Temperature in Moist Air*, B. Am. Meteorol. Soc., 2005(86), pp 225-233

Lehner, B. and Döll, P. *Development and validation of a global database of lakes, reservoirs and wetlands*, J. Hydrol., 2004 (296), pp 1-22

Mironov, D. V. *Parameterization of lakes in numerical weather prediction. Description of a lake model*, COSMO Technical Report, Deutscher Wetterdienst, Offenbach am Main, Germany, 2008 (11), p 41

Morgenstern, A., Grosse, G., Günther, F., Fedorova, I. and Schirrmeister, L. *Spatial analyses of thermokarst lakes and basins in Yedoma landscapes of the Lena Delta*, The Cryosphere, 2011 (5), pp 849- 867

Morgenstern, A., Ulrich, M., Günther, F., Roessler, S., Fedorova, I. V., Rudaya, N. A., Wetterich, S., Boike, J. and Schirrmeister, L. *Evolution of thermokarst in East Siberian icerich permafrost: A case study*, Geomorphology, 2013 (201), pp 363-379

Muster, S., Langer, M., Heim, B., Westermann, S. and Boike, J. *Subpixel heterogeneity of ice-wedge polygonal tundra: a multi-scale analysis of land cover and evapotranspiration in the Lena River Delta, Siberia*, Tellus B, 2012 (64), 17301

Poole, H. H. and Atkins, W. R. G. *Photo-electric Measurements of Submarine Illumination throughout the Year*, J. Mar. Biol. Assoc. UK. 16, pp 297-324

Rawlins, M. A., Serreze, M. C., Schroeder, R., Zhang, X. and McDonald, K. C. *Diagnosis of the record discharge of Arcticdraining Eurasian rivers in 2007*, Environ. Res. Lett., 2009 (4), pp 1-8

Schwamborn, G., Rachold, V., and Grigoriev, M. N. *Late Quaternary sedimentation history of the Lena Delta*, Quatern. Int., 2002 (89), pp 119-134

Thiery, W., Stepanenko, V. M., Fang, X., Jöhnk, K. D., Li, Z., Martynov, A., Perroud, M., Subin, Z. M., Darchambeau, F.,Mironov, D. and Van Lipzig, N. P. M. *LakeMIP Kivu: evaluating the representation of a large, deep tropical lake by a set of one-dimensional lake models*, Tellus A, 2014 (66), p 21390

Thiery, W., Kirillin, G., Stepanenko, V. and Mironov, D. *Towards FLake2.0* 5th workshop on "Parameterization of Lakes in Numerical Weather Prediction and Climate Modelling", 16-19 October 2017

Westermann, S., Langer, M., Boike, J., Heikenfeld, M., Peter, M., Etzelmüller, B. and Krinner, B. *Simulating the thermal regime and thaw processes of ice-rich permafrost ground with the land-surface model CryoGrid 3*, Geosci. Model Dev., 2016 (9), pp 523-546,

Wetterich, S., Schirrmeister, L., Meyer, H., Andreas, F. A. and Mackensen, A. *Arctic freshwater ostracods from moder periglacial environments in the Lena River Delta (Siberian Arctic, Russia): geochemical applications for palaeoenvironmental reconstructions*, J. Paleolimnol., 2008 (39), pp 427-449,

Yi, S., Wischnewski, K., Langer, M., Muster, S. and Boike, J. *Freeze/thaw processes in complex permafrost landscapes of northern Siberia simulated using the TEM*

ecosystem model: impact of thermokarst ponds and lakes, Geosci. Model Dev., 2014 (7), pp 1671–1689

Zolfaghari, K., Duguay, C. R., and Kheyrollah Pour, H. *Satellite-derived light extinction coefficient and its impact on thermal structure simulations in a 1-D lake model*, Hydrol. Earth Syst. Sci., 2017 (21), pp 377-391

A. Lake bathymetry

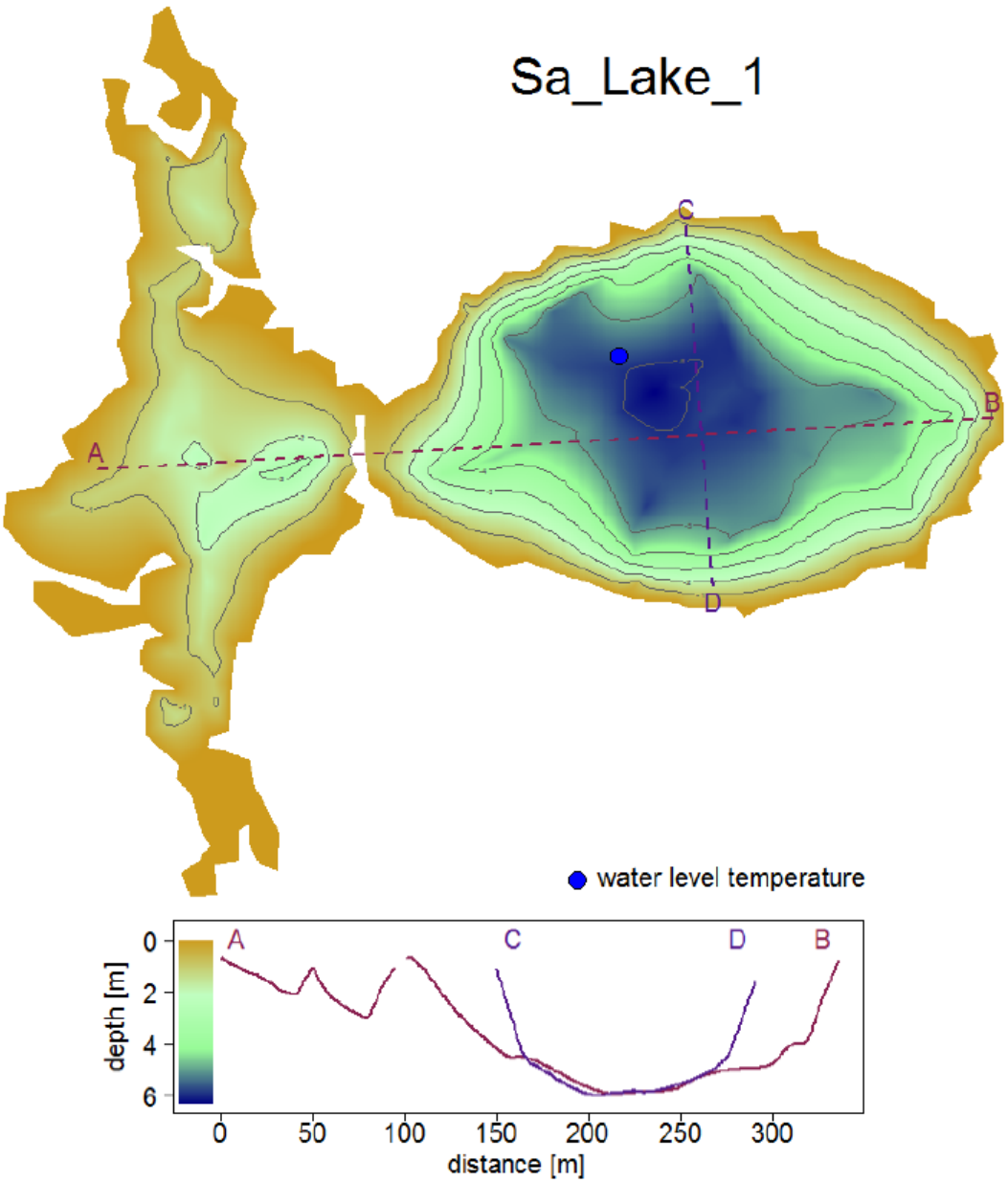

Figure 15: Bathymetry and cross sections of fish lake. Blue dot represents temperature chain position.

B. Secchi measurements

Table 3: Secchi measurements from field book of Lena expedition in July 2015

lake	date	Secchi depth	conditions
Sa_Lake_4	11th July 2015	2.3 m	cloudy, windy
Sa_Lake_1	11th July 2015	6.3 m	cloudy, windy
Sa_Lake_4	13th July 2015	2.9 m	no information
Sa_Lake_1	14th July 2015	3 m	cloudy, windy
Sa_Lake_2	17th July 2015	2.2 m	cloudy, rainy
Sa_Lake_3	20th July 2015	2 m	cloudy, rainy, cloudy
Sa_Lake_4	21th July 2015	2.7 m	cloudy, rainy

C. FLake parameters

Table 4: List of all parameters used in FLake model

parameter	value	unit	description
del_time_lk	3600	[s]	model time step
time_step_number	18639	[-]	total number time steps
save_interval_n	1	[-]	saving interval in time steps
T_wML_in	6	[°C]	mixed-layer temperature
T_bot_in	6	[°C]	temperature at the water-bottom sediment interface
h_ML_in	1	[m]	thickness of the mixed-layer
z_wind_m_1	2	[m]	where wind speed is measured
depth_w_lk	5.5	[m]	lake depth
extincoef_optic	0.55	[-]	extinction coefficients
fetch_lk	.1	[m]	typical wind fetch
depth_bs_lk	6	[m]	depth of the thermally active layer of the bottom sediments
T_bs_lk	4	[°C]	temperature at the outer edge of the thermally active layer of bottom sediments
latitude_lk	72	[°]	geographical latitude
icewater_flux	0	$[Wm^{-2}]$	additional heat flux from ice to water
nband_optic	1	[-]	number of wave-length bands
frac_optic	1	[-]	fractions of total radiation flux

D. FLake output

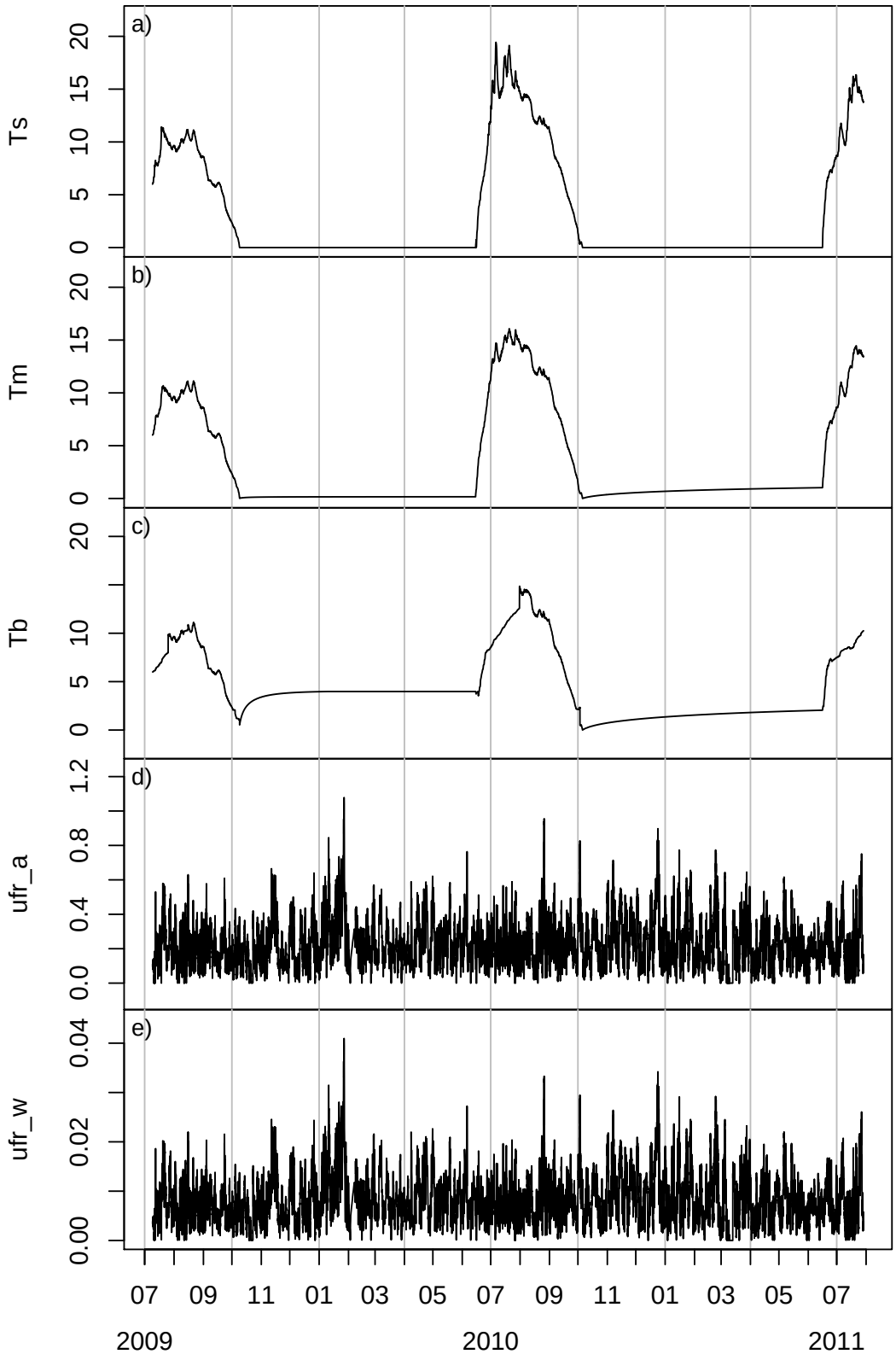

Figure 16: FLake output, **a)** surface temperature (°C), **b)** mean water temperature (°C), **c)** bottom temperature (°C), **d)** friction velocity in air (m/s), **e)** friction velocity in surface water (m/s)

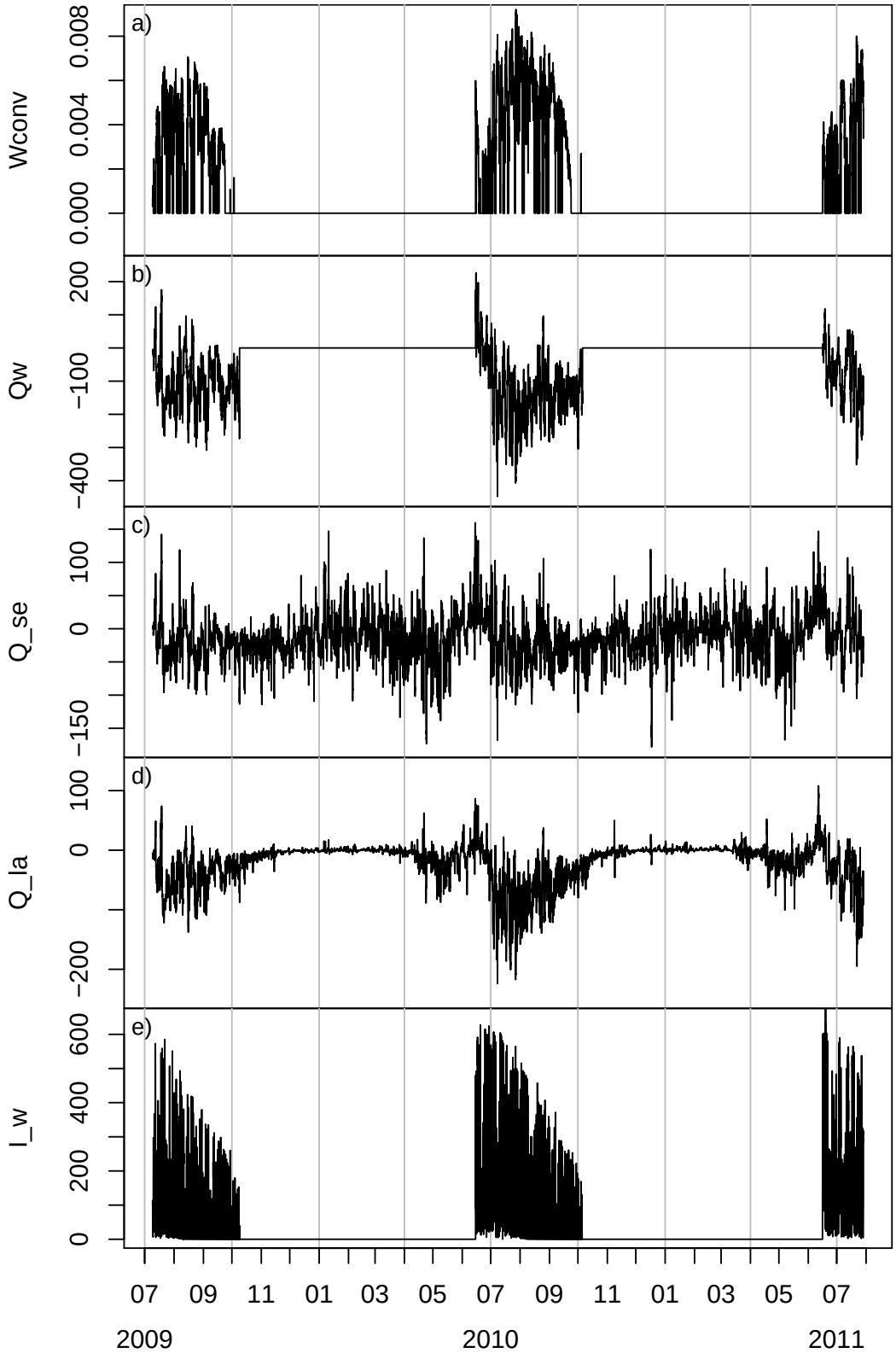

Figure 17: FLake output, **a)** convective velocity scale (m/s), **b)** QW????, **c)** Sensible surface heat flux (W/m2), **d)** latent surface heat flux (W/m2), **e)** short-wave radiation (W/m2)

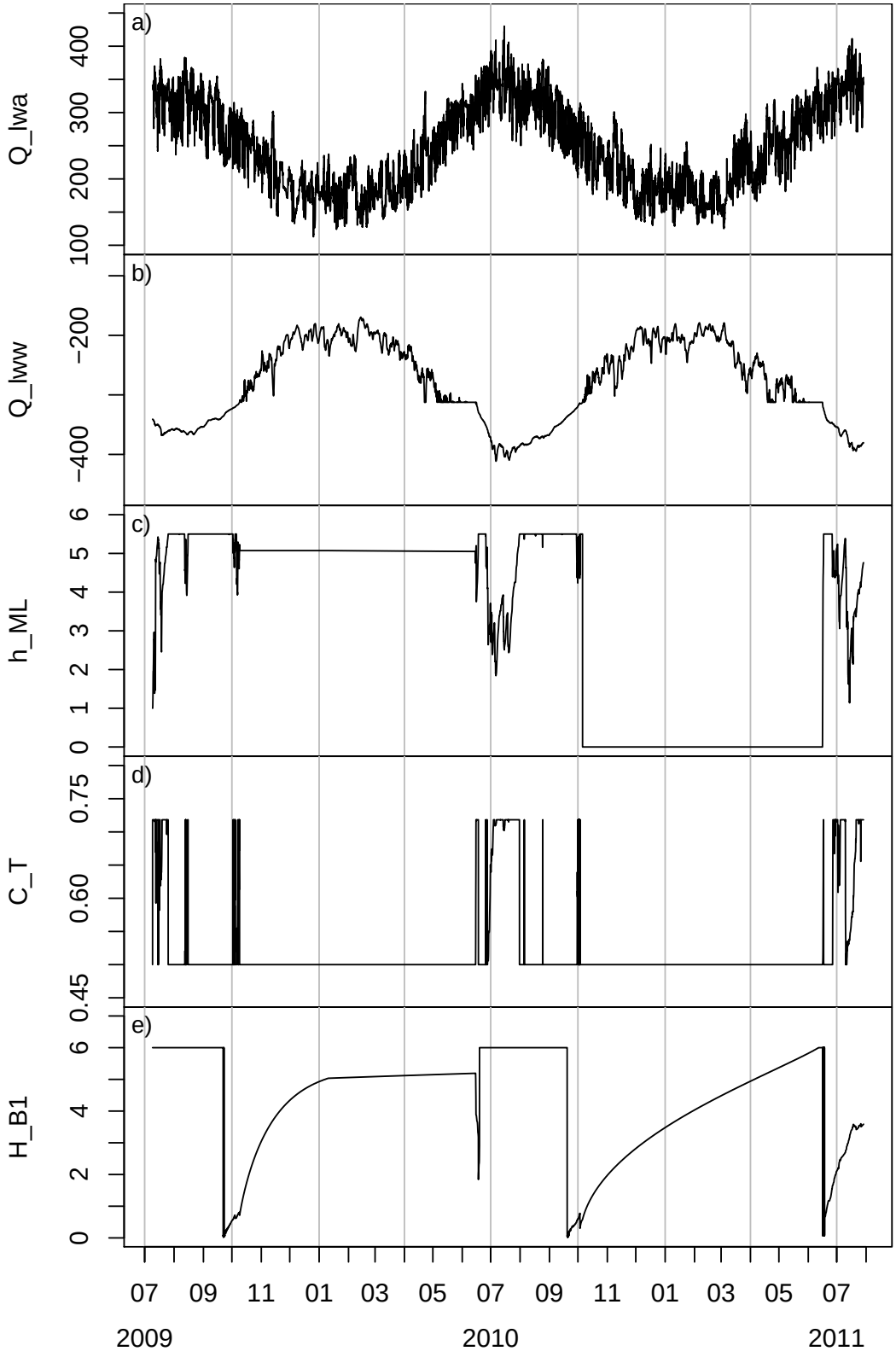

Figure 18: FLake output, **a)** long-wave radiative flux from the atmosphere (W/m2), **b)** long-wave radiative flux from the water (W/m2), **c)** mixed layer depth (m), **d)** stratification shape factor (-), **e)** depth of the thermal wave penetration in sediments (m)

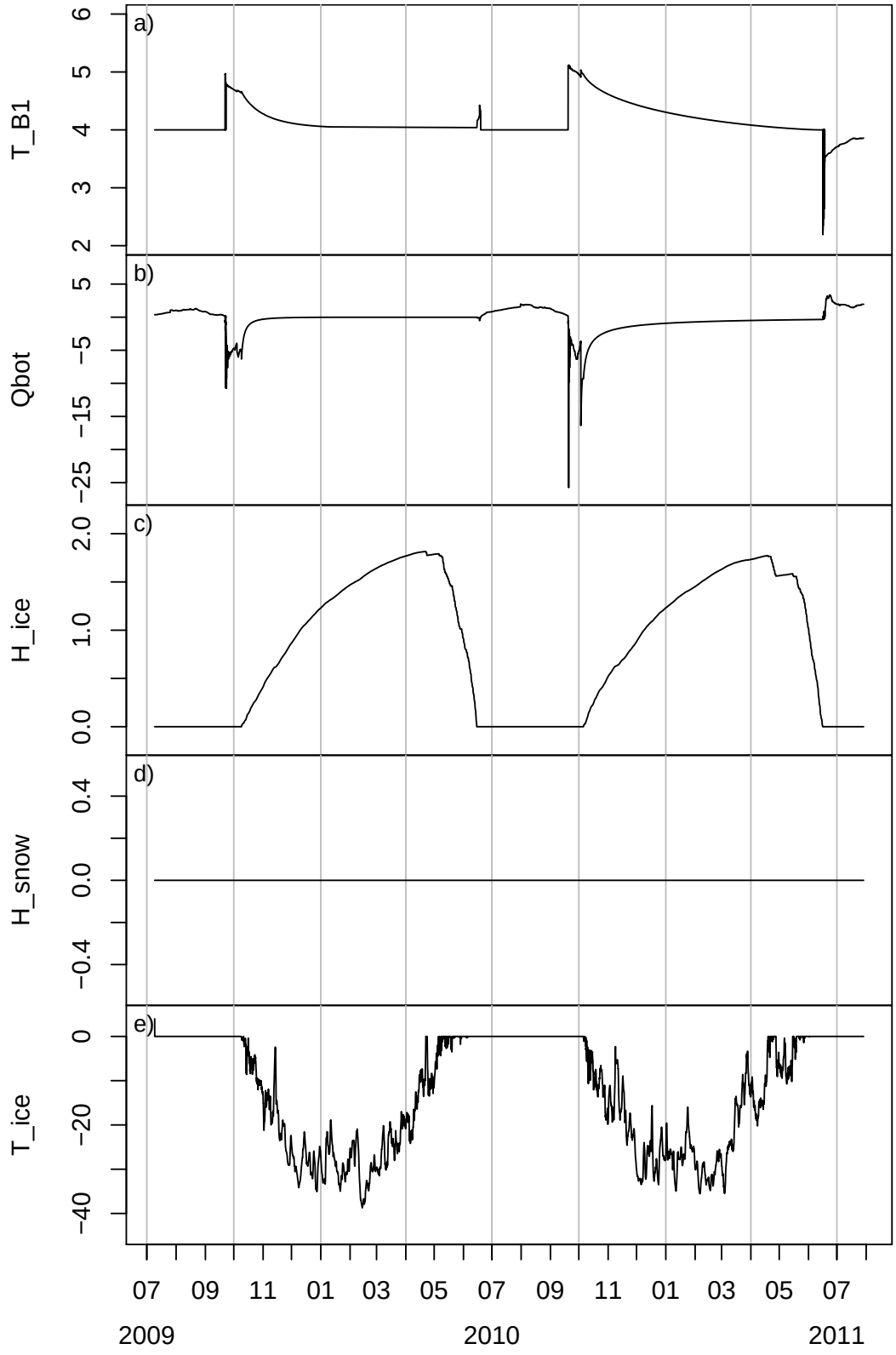

Figure 19: FLake output, **a)** temperature at the crest of the thermal wave in sediments (oC), **b)** heat flux across the water-sediments boundary (W/m2), **c)** ice thickness (m), **d)** snow thickness (m), **e)** ice temperature (°C)

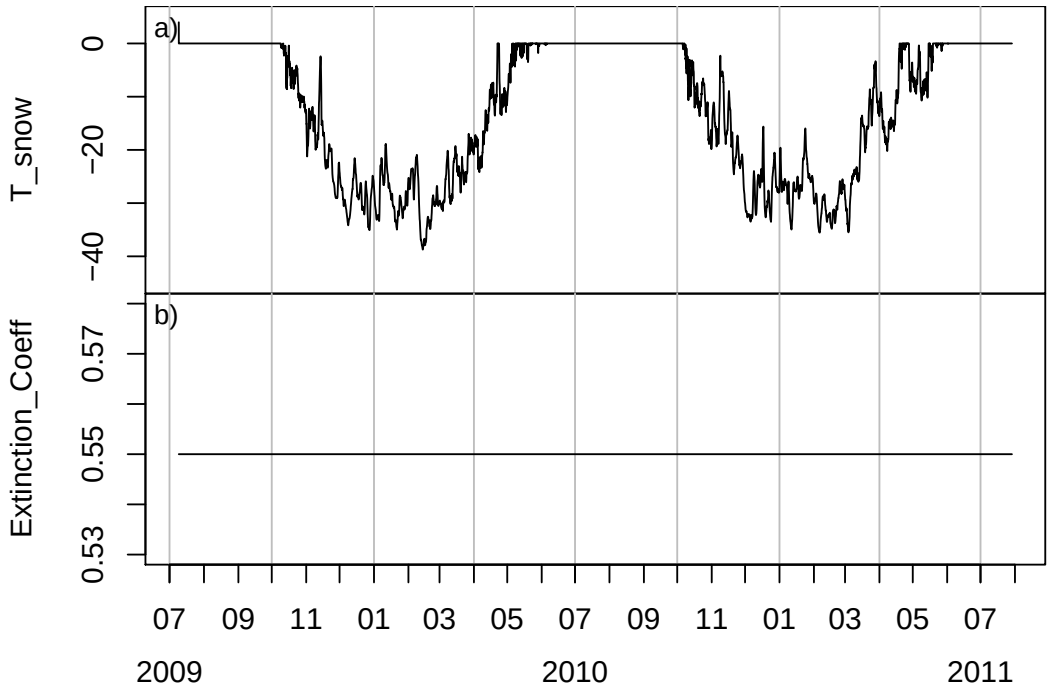

Figure 20: FLake output, **a)** ice temperature (°C), **b)** extinction coefficient (-)

Biogeosciences, 12, 5941–5965, 2015
www.biogeosciences.net/12/5941/2015/
doi:10.5194/bg-12-5941-2015

Biogeosciences Open Access

Thermal processes of thermokarst lakes in the continuous permafrost zone of northern Siberia – observations and modeling (Lena River Delta, Siberia)

J. Boike[1], C. Georgi[1], G. Kirilin[2], S. Muster[1], K. Abramova[3], I. Fedorova[4,5,6], A. Chetverova[4,5], M. Grigoriev[7], N. Bornemann[1], and M. Langer[1,8]

[1]Alfred Wegener Institute Helmholtz Center for Polar and Marine Research, Telegrafenberg A43, 14473 Potsdam, Germany
[2]Leibniz-Institute of Freshwater Ecology and Inland Fisheries (IGB), Mueggelseedamm 310, 12587 Berlin, Germany
[3]Lena Delta Nature Reserve, Ak. Fedorova 28, 678400 Tiksi, Sakha Republic, Russia
[4]Institute of Earth Science, Saint-Petersburg State University, 10th line of Vasiljevsky Island, 33–35, 199178 Saint-Petersburg, Russia
[5]Arctic and Antarctic Research Institute, 38, Beringa Str., St. Petersburg, 199397, Russia
[6]Kazan Federal University, 18, Kremlyovskaya str., Kazan, Russia
[7]Melnikov Permafrost Institute, Siberian Branch, Russian Academy of Sciences, Yakutsk, Russia
[8]Laboratoire de Glaciologie et Géophysique de l'Environnement (LGGE), 38402 St Martin d'Hères, CEDEX, France

Correspondence to: J. Boike (julia.boike@awi.de)

Received: 16 April 2015 – Published in Biogeosciences Discuss.: 30 April 2015
Revised: 1 October 2015 – Accepted: 2 October 2015 – Published: 19 October 2015

Abstract. Thermokarst lakes are typical features of the northern permafrost ecosystems, and play an important role in the thermal exchange between atmosphere and subsurface. The objective of this study is to describe the main thermal processes of the lakes and to quantify the heat exchange with the underlying sediments. The thermal regimes of five lakes located within the continuous permafrost zone of northern Siberia (Lena River Delta) were investigated using hourly water temperature and water level records covering a 3-year period (2009–2012), together with bathymetric survey data. The lakes included thermokarst lakes located on Holocene river terraces that may be connected to Lena River water during spring flooding, and a thermokarst lake located on deposits of the Pleistocene Ice Complex. Lakes were covered by ice up to 2 m thick that persisted for more than 7 months of the year, from October until about mid-June. Lake-bottom temperatures increased at the start of the ice-covered period due to upward-directed heat flux from the underlying thawed sediment. Prior to ice break-up, solar radiation effectively warmed the water beneath the ice cover and induced convective mixing. Ice break-up started at the beginning of June and lasted until the middle or end of June. Mixing occurred within the entire water column from the start of ice break-up and continued during the ice-free periods, as confirmed by the Wedderburn numbers, a quantitative measure of the balance between wind mixing and stratification that is important for describing the biogeochemical cycles of lakes. The lake thermal regime was modeled numerically using the FLake model. The model demonstrated good agreement with observations with regard to the mean lake temperature, with a good reproduction of the summer stratification during the ice-free period, but poor agreement during the ice-covered period. Modeled sensitivity to lake depth demonstrated that lakes in this climatic zone with mean depths > 5 m develop continuous stratification in summer for at least 1 month. The modeled vertical heat flux across the bottom sediment tends towards an annual mean of zero, with maximum downward fluxes of about 5 W m^{-2} in summer and with heat released back into the water column at a rate of less than 1 W m^{-2} during the ice-covered period.

The lakes are shown to be efficient heat absorbers and effectively distribute the heat through mixing. Monthly bottom water temperatures during the ice-free period range up to 15 °C and are therefore higher than the associated monthly

Published by Copernicus Publications on behalf of the European Geosciences Union.

air or ground temperatures in the surrounding frozen permafrost landscape. The investigated lakes remain unfrozen at depth, with mean annual lake-bottom temperatures of between 2.7 and 4 °C.

1 Introduction

Lakes can be interpreted as sensitive climatic indicators that respond to a range of different influences affecting the world's climate. They can also exert an important influence on the local, regional, and global climate and hydrology by regulating heat and water fluxes, but their thermal dynamic represented in RCMs and GCMs is rather simple, and does not include all physical processes that are necessary for reproducing atmosphere–lake interaction (Walsh et al., 1998; Martynov et al., 2012). Lakes are often typical features of Northern Hemisphere ecosystems (Fig. 1). In permafrost areas, which occupy about 25 % of the world's landmass, lakes influence not only the thermal regime of the surrounding and underlying permafrost, but also the atmospheric heat and water fluxes, due to their large thermal heat reservoirs and heat capacities. The winter heat flux into the atmosphere through the ice cover from deep lakes that remain unfrozen at depth is several times greater than that from the surrounding tundra (Jeffries et al., 1999). Even smaller polygonal water bodies (thermokarst ponds), which freeze to the bottom every winter, have heat fluxes that are an order of magnitude greater than those from the surrounding permafrost (Langer et al., 2011b). The large thermal heat reservoir in lakes prevents the sediment beneath those lakes with a water depth greater than about 2 or 3 m from freezing, thus allowing a talik to develop (Lachenbruch, 1962). However, few data exist on the thermal conditions of lakes in north and central Yakutia, or the taliks beneath them (Grigoriev, 1960, 1966; Are, 1974; Pavlov et al., 1981). These unfrozen layers of lake sediment can enhance mobilization of the carbon reservoir by enabling year-round microbial decomposition in otherwise frozen surroundings, and water bodies can thus be hotspots for CO_2 and CH_4 emissions (Langer et al., 2015; Schneider von Deimling et al., 2015; Walter et al., 2006; Abnizova et al., 2012; Laurion et al., 2010). Water bodies are also important because they provide habitats for zooplankton, fish, and migratory birds (Alerstam et al., 2001), and are a source of drinking water for northern communities, of water for irrigation, and of water for industry, exploration, and ice-road construction in winter (Vincent et al., 2013).

Measuring the water temperatures in lakes over both short and long terms is therefore important, not only for modeling the development of the subsurface thermal regime, but also for understanding and modeling ecological and physical dynamics. Few investigations have, however, been carried out into the physical and thermal characteristics of Arctic water bodies, especially over the long term, and there is a particular shortage of data from northern Siberia. A notable exception is the long term biological, physical and chemical lake study initiated in 1975 at the Toolik Lake Long Term Ecological Research (LTER) site in Alaska. The lakes studied are located on the North Slope of Alaska, in the foothills of the Brooks Range, and are classified as low Arctic lakes (Hobbie and Kling, 2014). Toolik Lake and most of the other lakes in this area are "kettle lakes" that formed as a result of glaciation; their lake morphometries (surface areas, depths) are a result of the glaciation history and the age of the landscape. Water depths can range up to 25 m, as is the case in Toolik Lake (Hobbie and Kling, 2014). The thermal stratification varies considerably between lakes (depending on the lake's morphometry), as well as between years (Luecke et al., 2014). Also in northern Alaska, Arp et al. (2010) made use of an original method that combined short-term (for example, over 1 year) measured lake surface temperatures (from depths of 0.5 and 1.0 m) with meteorological and remote-sensing data on lake surface temperatures and ice thicknesses. The latter variables were compared with measured temperatures and ice thicknesses, and with modeled results (Arp et al., 2010). The advantage of this approach is that, following successful calibration, a monitoring network can be established that is based purely on remote-sensing data. Monitoring in some of these lakes on the Alaskan Coastal Plain has continued since 2010 as part of the new Circum-Arctic Lakes Observation Network (CALON) initiative (http://www.arcticlakes.org/calon-lakes.html; Hinkel et al., 2012). An initial series of data for vertical temperature profiles from the summer of 2010 has been provided for a number of lakes, together with time series of hourly temperature data, in order to demonstrate the seasonal and temporal variability (Hinkel et al., 2012).

Sporadic measurements of lake temperatures have been obtained in conjunction with limnological studies (for example, by Keatley et al., 2007, or Pienitz et al., 1997), paleolimnological investigations (such as in the 172 m deep El'gygytgyn Lake of northeastern Siberia, a meteoritic impact crater; Nolan and Brigham-Grette, 2006), and physical experiments (such as dye tracing under the ice cover in a small Arctic lake; Welch and Bergmann, 1985). Vincent et al. (2008) measured temperatures and salinity in a high Arctic, 125 m deep, perennially ice-covered lake on Ellesmere Island in Nunavut, Canada. The authors then successfully modeled the lake's temperature regime using a one-dimensional heat diffusion equation and including heat transfer by radiation through ice and water. For lakes within the Mackenzie Delta (Northwest Territories of Canada), Burn (2002, 2005) demonstrated that the temperatures in the deep central pool of a thermokarst lake on Richards Island remained positive throughout the winter, with a mean annual temperature of 3.5 °C, whereas freezing occurred in the shallow littoral terrace of the lake (mean annual temperature −3.7 °C).

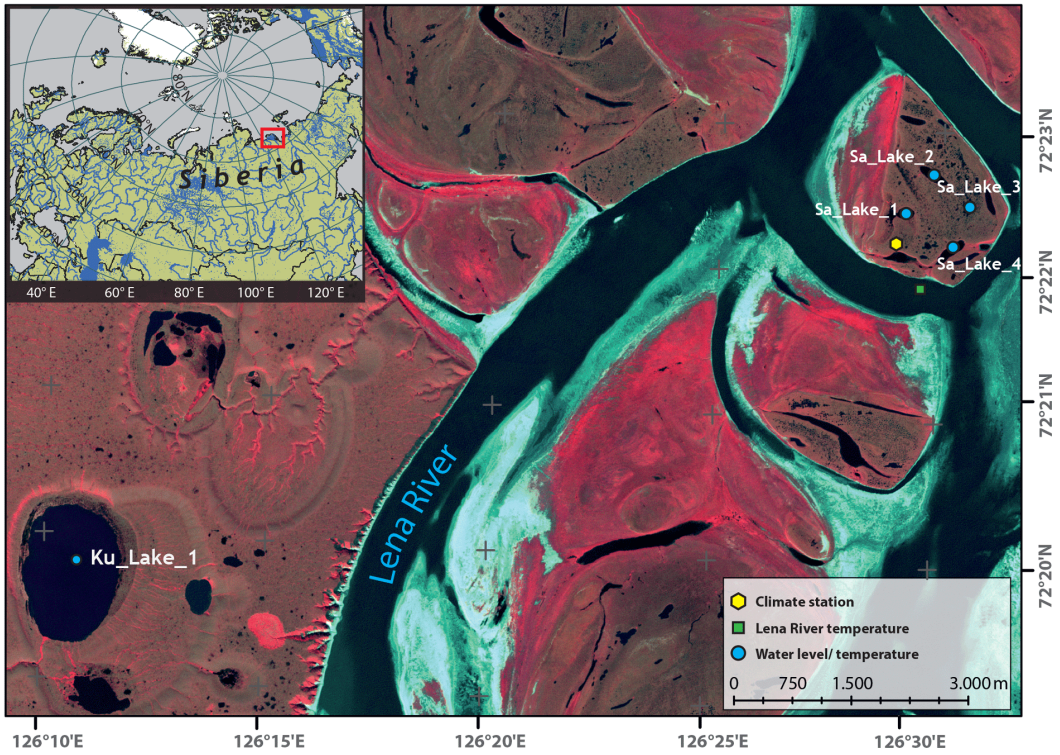

Figure 1. Location of the study sites in the Lena River Delta of eastern Siberia; sites are within the zone of continuous permafrost on the islands of Kurungnakh (Ku_Lake_1), and Samoylov (Sa_Lakes_1-4). The inset map shows the location of the Lena River Delta in northern Eurasia and the distribution of lakes (Global lakes and wetland map; Lehner and Döll, 2004).

This paper aims to quantify the seasonal thermal dynamics of lakes in the Eurasian north, where monitoring observatories have recently been established in the central part of the Lena River Delta. Our objectives are (i) to describe the thermal patterns and processes in both thermokarst lakes and "perched" lakes (which can have seasonal connections to river water), and (ii) to make use of measured data to validate the freshwater model FLake, as well as estimate water sediment heat exchange. FLake offers a good compromise between computational efficiency and physical reality, and has been coupled to several regional and global climate models (Thiery et al., 2014; Martynov et al., 2010). FLake has been used in various one-dimensional modeling studies, for a wide range of lakes, including tropical lakes, and in lake model intercomparison projects (LakeMIP; Thiery et al., 2014; Stepanenko et al., 2010). However, it has not been used for Arctic lakes and this study tests the ability of FLake to reproduce the temperature regimes of thermokarst lakes in northern Siberia.

2 Site description

The Lena River Delta in northern Yakutia is one of the largest deltas in the Arctic and has one of the largest catchment areas (2 430 000 km^2) in the whole of Eurasia (Costard and Gautier, 2007). The Lena River discharges about 525 km^3 of water through the delta into the Arctic Ocean every year, with an average annual discharge rate of 16 800 m^3 s^{-1} (Gordeev and Sidorov, 1993). This discharge rate has been reported to be increasing (Fedorova et al., 2015; Rawlins et al., 2009). As it passes through its estuarine area, the main flow of the Lena River splits into numerous arms and transverse branches to form the most extensive delta in the Russian Arctic, covering 25 000 km^2 and including about 1500 islands and 60 000 lakes.

Continuous cold permafrost (with a mean annual temperature of −10 °C at 10 m depth) underlies the study area to between about 400 and 600 m below the surface. Since observations started in 2006, the permafrost at 10.7 m depth has warmed by > 1.5 °C (Boike et al., 2013; http://gtnpdatabase.org/boreholes/view/53/).

The main features of the annual energy balance for these sites with continuous permafrost in the subsurface typically include low net radiation, higher atmospheric latent heat flux than sensible heat flux, and a large proportion of soil heat flux (Boike et al., 2008; Langer et al., 2011a, b). Previous publications have reported that shallow (< 1 m deep) ponds freeze completely in winter, but that the timing of freeze-back can vary by up to 2 months between years, depending on the surface energy balance (Langer et al., 2011b, 2015).

The study areas are located on the islands of Samoylov and Kurungnakh, within the central part of the Lena River Delta (Fig. 1). Samoylov Island (72°22′ N, 126°28′ E) lies within one of the main river channels in the southern part of the delta and is relatively young, with an age of between 4 and 2 ka BP (Schwamborn et al., 2002), which is also the estimated maximum age of the investigated lakes on the island. In contrast, Kurungnakh Island forms part of the third terrace of the Lena Delta and is an erosional remnant of a late-Pleistocene accumulation plain. It consists of fluvial sands overlain by Yedoma-type ice complex deposits, which accumulated between 100 and 50 ka BP and since 50 ka BP, respectively, and a Holocene cover (8 to 3 ka BP) (Schwamborn et al., 2002; Wetterich et al., 2008). Large thermokarst lakes and basins are major components of the ice-rich permafrost landscape of Kurungnakh Island; they have formed since 13 to 12 ka BP (Morgenstern et al., 2011, 2013).

The lakes presented in this paper are of thermokarst origin which is common for the lowland tundra permafrost areas of Northeast Siberia. These areas were not ice-covered during the latest glacial period (70 000–10 000 years ago) and are characterized by high to moderate ground ice content and thick sediment cover. Arctic lowlands with similar landscape characteristics and lake distributions can be found in central and eastern Siberia, interior and northern Alaska as well as northwest Canada (Grosse et al., 2013).

The landscape on both of these islands, and in the delta as a whole, has generally been shaped by water through erosion and sedimentation (Fedorova et al., 2015), and by thermokarst processes (Morgenstern et al., 2013). The proportion of the total land surface of the delta covered by surface water can amount to more than 25 % (Muster et al., 2012). Up to 50 % of the total surface water area in permafrost landscapes is attributed to small lakes and ponds with surface areas of less than 10^5 m^2, which have the potential to grow into large thermokarst lakes (Muster et al., 2012). Water budget modeling for the tundra landscape has shown a small positive balance since 1953, which has been confirmed by satellite observations (since 1964) of the surface areas of water bodies (Boike et al., 2013). The chemical and isotopic signals from the water in lakes on Samoylov Island generally indicate low levels of mineralization (Table 1). The stable isotopic ratios indicate that the thermokarst lake water is sourced mainly from thawed ground ice mixed with precipitation and the water in shallow ponds is sourced mainly from summer precipitation (Abnizova et al., 2012).

Small ponds and lakes emit more CO_2 and CH_4 per square meter than the surrounding tundra, and greenhouse gas production continues during winter in those lakes that do not freeze to the bottom (Langer et al., 2015). Modeling studies have demonstrated that an unfrozen layer of lake sediment is maintained throughout the year beneath thermokarst lakes (Yi et al., 2014). During high spring floods some of the lakes on the first terrace are flooded with Lena River water. Observations in 2014 on Samoylov Island, for example, confirmed the flooding of a large part of the first terrace on the island, including most of the lakes.

Additional detailed information concerning the climate, permafrost, land cover, vegetation, and soil characteristics of these islands in the Lena River Delta can be found in Boike et al. (2013) and Morgenstern et al. (2013).

3 Methods

3.1 Field instrumentation and ground surveys

In July 2009, water level and temperature sensors (HOBO Temp Pro v2, HOBO U20, Onset, ±0.2 °C across a temperature range from 0 to 70 °C, and ±0.4 °C across a temperature range from −40 to 0 °C) were installed within the water columns of the investigated lakes on Samoylov and Kurungnakh islands. Figure 1 shows the locations of the lakes (labelled Sa_Lake_1–4 for Samoylov and Ku_Lake_1 for Kurungnakh) and the location of the long-term weather station. Gaps in the climate data record (air temperature, radiation, humidity, wind speed and direction, and snow depth) were filled whenever possible with data from temporary climate and eddy covariance stations located in close proximity to the weather station (Boike et al., 2013). Temperature and water depth sensors were placed directly above the sediment-water interface and then temperature sensors at 2 m intervals up to 2 m below the water surface (Fig. 2). The sensors were suspended in the water column from a buoy and anchored in the sediment below. The sensor at the bottom of the lake (just above the sediment) was labelled as "0 m", the sensor 2 m above the sediment as "2 m", and so on. The uppermost sensors were usually about 2 m below the water surface since we were concerned about the formation of ice and the potential drift of sensors with the shifting of ice cover. End-of-winter ice thickness (obtained by drilling) was measured in 2014; it ranged between 1.9 and 2 m in lakes Sa_Lake_1–4 on Samoylov Island. During some winters the uppermost sensors became enclosed within the ice cover (for example, Sa_Lake_1 in 2012), but they were not moved out of position. One sensor was installed in the Lena River during August 2009 (Fig. 1) and recorded data from July 2009 to August 2010 but was lost during the following year.

Sensors were usually retrieved once a year (in August) and then re-launched in approximately the same position. The temperature record was therefore briefly interrupted during the period when the sensors were retrieved and read. The water depth ("sensor depth") recorded by the bottom sensor sometimes changed following retrieval due to a change in the sensor position, although the actual water level of the lake remained the same. For example, for Sa_Lake_4 (a perched lake), sensors that were deployed at a water depth of about 8.5 m in 2009 were reinstalled at a depth of about 9.5 m in August 2010. Water level variations due to water balance changes (when the sensor position had not changed),

Table 1. Physical and chemical characteristics of the studied lakes in the Lena River Delta, Siberia.

	Sa_Lake_1	Sa_Lake_2	Sa_Lake_3	Sa_Lake_4	Ku_Lake_1
Area [m^2]	39 541	39 991	23 066	47 620	1 730 000[a]
Max. depth [m]	6.4	5.7	3.4	11.6	3.6[a]
Mean depth [m]	3	3.1	1.2	4.5	2.4
Volume [m^3]	106 500	103 600	18 800	175 121	3 321 000
Volume/Area [m]	2.7	2.6	0.8	3.7	1.8
Perimeter [m]	1931	1471	1760	1474	5170[a]
Period of data collection	4 Jul 2009 to 7 Aug 2012	10 Jul 2009 to 7 Aug 2012	13 Jul 2009 to 14 Aug 2012	6 Jul 2009 to 6 Aug 2012	24 Jul 2009 to 29 Jul 2010
Location	126.486° E, 72.373° N	126.496° E, 72.378° N	126.511° E, 72.374° N	126.505° E, 72.369° N	126.177° E, 72.328° N
Start of ice cover formation (temp. diff. from bottom to top > 0.1 °C)	5 Oct 2009 1 Oct 2010 2 Oct 2011	1 Oct 2009 28 Sep 2010 5 Oct 2011	4 Oct 2009 30 Sep 2010 26 Sep 2011	4 Oct 2009 28 Sep 2010 4 Oct 2011	4 Oct 2009 2 Oct 2010
Start of ice cover break-up (temp. diff. from bottom to top >0.1 °C)	4 Jul 2009 14 Jun 2010 8 Jun 2011 15 Jun 2012	12 Jul 2009 23 Jun 2010 16 Jun 2011 15 Jun 2012	24 Jun 2009 14 Jun 2010 10 Jun 2011 10 Jun 2012	7 Jul 2009 20 Jun 2010 20 Jun 2011 21 Jun 2012	24 Jul 2009 20 Jun 2010
% ice cover (satellite radar data[b]) 2011	5 Jun 100 % 10 Jun 95 % 16 Jun 85 % 21 Jun ice free	5 Jun 100 % 10 Jun 100 % 16 Jun 90 % 21 Jun ice free	5 Jun 100 % 10 Jun 90 % 16 Jun ice free	5 Jun 95 % 10 Jun 95 % 16 Jun 85 % 21 Jun 50 %	5 Jun 95 % 10 Jun 95 % 16 Jun 90 % 21 Jun 40 % 27 Jun ice free
2012	27 Jun ice free	27 Jun ice free	27 Jun ice free	27 Jun ice free	5 Jun 90 % 27 Jun ice free
Mean annual bottom temperature [°C] (2010–2011)	3.7	3.6	2.7	2.9	4.0
Winter lake water heat budget [MJ m^{-2}]	93	66	44	145	61
Summer lake water heat budget [MJ m^{-2}]	140	206	161	340	112
Annual lake heat budget [MJ m^{-2}] (2010–2011)[c,d]	[233] 838	[272] 877	[205] 810	[485] 1090	[173] 778
Residence time [years][e]	14	14	4	24	9
Electrical conductivity [µS cm^{-1}]	140[f]	127[f]	64[i]	185[f] 59[g] 80[h]	30[i]
pH-value[f]	6.99[f]	6.82[f]	7. 3[i]	6.95[f] 7.36[g] 7.28[h]	7.64[i]

[a] Data provided in Morgenstern et al. (2011, 2013) and doi:10.1594/PANGAEA.848485. [b] Sobiech et al. (2012) & TerraSar-X data (copyright: DLR, 2011) where available with sufficiently high resolution. [c] Numbers in brackets represent the total annual lake water budget (sensible heat), without taking into account the latent heat of ice cover formation. [d] Includes latent heat for the formation of a 2 m ice cover (605 MJ m^{-2}). [e] Residence time $F = V / E$; roughly approximated by the ratio of the lakes's volume (V) divided by the sum of evapotranspiration (E) and runoff R ($F = V / (E - R)$; Schertzer, 1997). Within the study area, the annual evapotranspiration is about ~ 190 mm and runoff is to be negligible within the overall water balance (Boike et al., 2013). [f] Mean value for ice-covered period (April–May 2014). [g] Mean value for the Lena River flood period (May–June 2014). [h] Mean value for summer period (July–August 2014). [i] Mean value for summer period (measured in July 2009).

for example during the summer period, were usually less than 0.5 m.

Data are only available over a 1-year period for the lake on Kurungnakh Island (2009–2010) as the loggers were subsequently displaced, presumably during ice break-up. For the lakes on Samoylov Island, however, we obtained continuous temperature and water level data over a period of 3 years from 2009 to 2012. All data and metadata are provided in the Supplement for this publication and through the PANGAEA website (doi:10.1594/PANGAEA.846525).

Bathymetric surveys were carried out in 2009 and 2010 on all of the investigated thermokarst lakes, using a GPSMAP 178 Cecho sounder, a GPSMAP 421S plotter and a GPS 60 navigator, all from Garmin. The shorelines were mapped either by GPS field survey or by manually digitizing the shoreline from high-resolution aerial images. The accuracy of the echo sounder equipment was about 0.1 m and was regularly checked using manual profiling. Depth measurements were taken along the longest lake axis as well as along a zigzag track in order to cover most of the lake surface and to locate any local "holes" that might exist as a result of thermokarst processes. Surface areas, mean and maximum depths, volumes, and hypsographic (depth/area) curves were calculated for the five lakes investigated using linear distance nearest neighbor interpolation in ArcGIS software (v.10.1) (Table 1). A description of the morphometry, including two-dimensional contour plots and cross-sectional profiles of the lakes can be found in the appendix of this paper (Figs. A1 to A5). Bathymetric records were also obtained for eight additional lakes (Chetverova et al., 2013) but are not included herein since temperature sensors were not installed. Bathymetric data, metadata and morphomet-

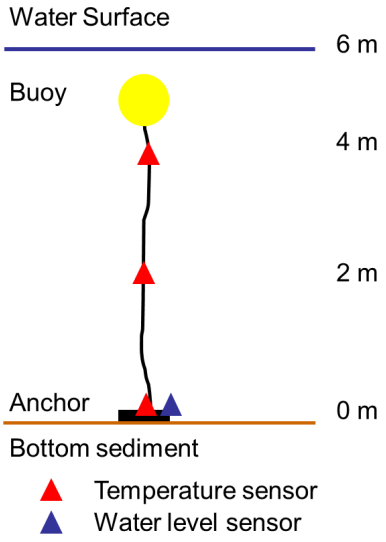

Figure 2. Schematic diagram showing the positions of sensors within the water column. To prevent freezing of the buoy within the ice cover (maximum 2 m thick), sensors were deployed 2 m below the water surface in most lakes. The water level sensor was located just above the bottom sensor, referred to in Figs. 4 and 5 as the "lowest sensor depth".

ric descriptions can be found in the appendix material for this publication, as well as through the PANGAEA website (doi:10.1594/PANGAEA.846525).

3.2 Heat content

The ability of lakes to store and redistribute additional heat at seasonal timescales may affect the heat budget of adjacent permafrost areas at the landscape spatial scale. For this reason, we observe the thermal regime of tundra lakes to make inferences about their effect on heat exchange processes. The heat content of each lake (H_l) was calculated at hourly time steps from the thermal energy stored in a water column from the lake's surface to its maximum depth (z_{max}):

$$H_l = c_w \rho_w \int T(z,t)\mathrm{d}z, \quad (1)$$

where c_w is the specific heat capacity of water, ρ_w is the freshwater density, and T is the temperature. The calculated heat budgets were divided into different time periods, as proposed by Wetzel (2001). The summer heat income is defined as the amount of heat required to raise the temperature of the lake from isothermal conditions at 4 °C to the maximum observed depth-averaged summer temperature (summer heat content). The winter heat income is the amount of heat required to raise the temperature from the minimum temperatures to 4 °C. The annual heat budget is the total amount of heat necessary to raise the water from the minimum temperature to maximum summer temperature. The winter heat income and the annual heat budget must include the latent heat of fusion for the ice cover, especially for high-latitude lakes (Wetzel, 2001). The ice cover thickness was measured during May 2014 and varied slightly from 2 m (Sa_Lake_1, Sa_Lake_2) to 1.9 m (Sa_Lake_4). The ice cover in these lakes melts completely every summer so that freezing and melting energies usually balance out over a year. The timing of spring ice break-up extends from the first ice melt, through moat formation and drifting of the ice cover, to the complete disappearance of ice. It is defined herein as the time at which the temperatures from all sensors indicate isothermal conditions, with temperature differences from the bottom to the top of the water column of < 0.1 °C following the period of stratification that occurs during ice cover, i.e., the time at which the lake water becomes completely mixed. The ice formation in fall is defined by the start of stratification in lake temperatures, i.e., when temperature differences from bottom to top exceed 0.1 °C. The uncertainties in these determined times are estimated to be ±5 days and are based on comparison with (infrequently available) satellite data (Table 1).

3.3 Modeling of lake thermodynamics

FLake is a freshwater lake model (Mironov, 2008) aimed at predicting the vertical thermal structure and mixing conditions in lakes over periods ranging from a few hours to a few years. The model is based on a two-layer parametric representation of the evolving temperature profile in the water column and on the integrated heat and kinetic energy budgets. The upper mixed layer is treated as thermally homogeneous, while the structure of the stratified layer between the upper mixed layer and the bottom of the basin (the lake thermocline) is described using the concept of self-similarity (or assumed shape) of the temperature-depth curve. The same self-similarity concept is used to describe the temperature structure of the thermally active upper layer of bottom sediments (Golosov and Kirillin, 2010) and of the ice (Mironov et al., 2012). It should be noted that no change in water depth as a result of winter ice formation is included in the computation, and the water depth is therefore assumed to be constant. Precipitation is also not included as an input into the model and snow accumulation is therefore not computed. Visual observations confirm that the lakes are usually snow free due to the generally low snowfall (although a few areas with snow and hardened wind crusts occur locally), combined with high wind speeds blowing the snow away.

The following input data and settings were used for the lakes investigated in this study and tested with data for Sa_Lake_1, i.e., a lake depth of 4 m (93 % of this lake has a water depth of not more than 4 m), a water optical light extinction coefficient of 0.5 m^{-1}, a 6 m thickness for the thermally active sediment layer beneath the lake, and a temperature of 4.5 °C at the bottom of the thermally active sediment layer. Due to their very low contents of organic material and low levels of biological productivity the lakes are usually very clear: in shallow lakes (for example, Sa_Lake_3) the

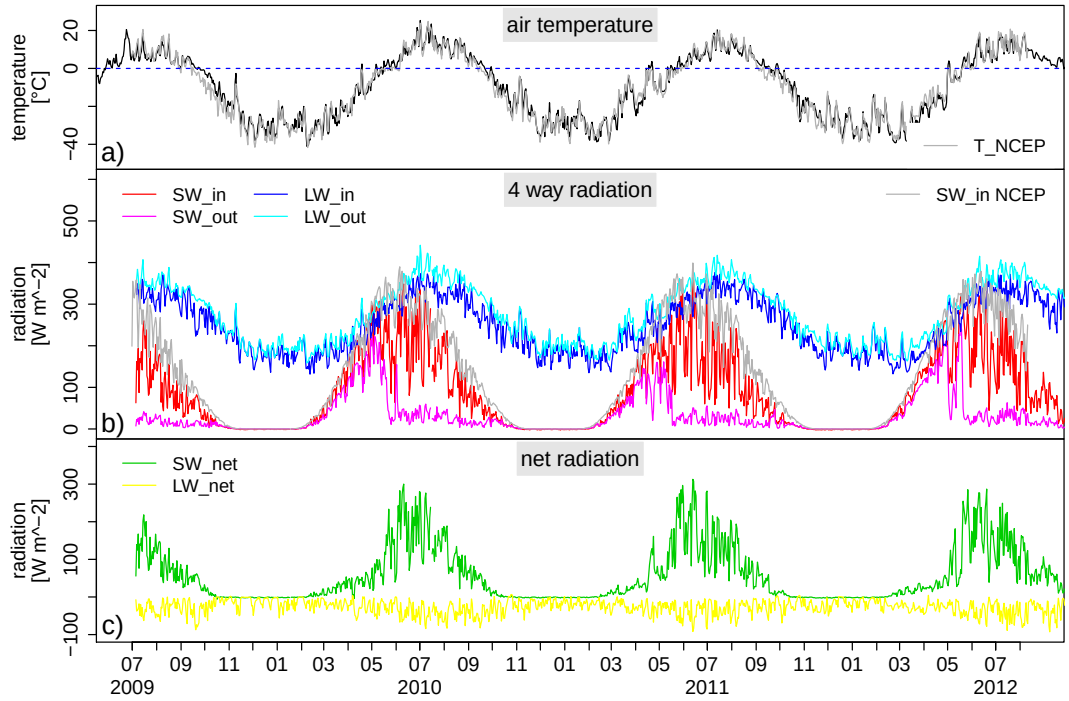

Figure 3. (a) Mean daily air temperature at 2 m above ground level from Samoylov and NCEP; **(b)** radiation balance (Samoylov) and shortwave incoming radiation (NCEP); **(c)** net shortwave and longwave radiation (Samoylov) and radiation balance measured at the Samoylov climate station July 2009 to August 2012.

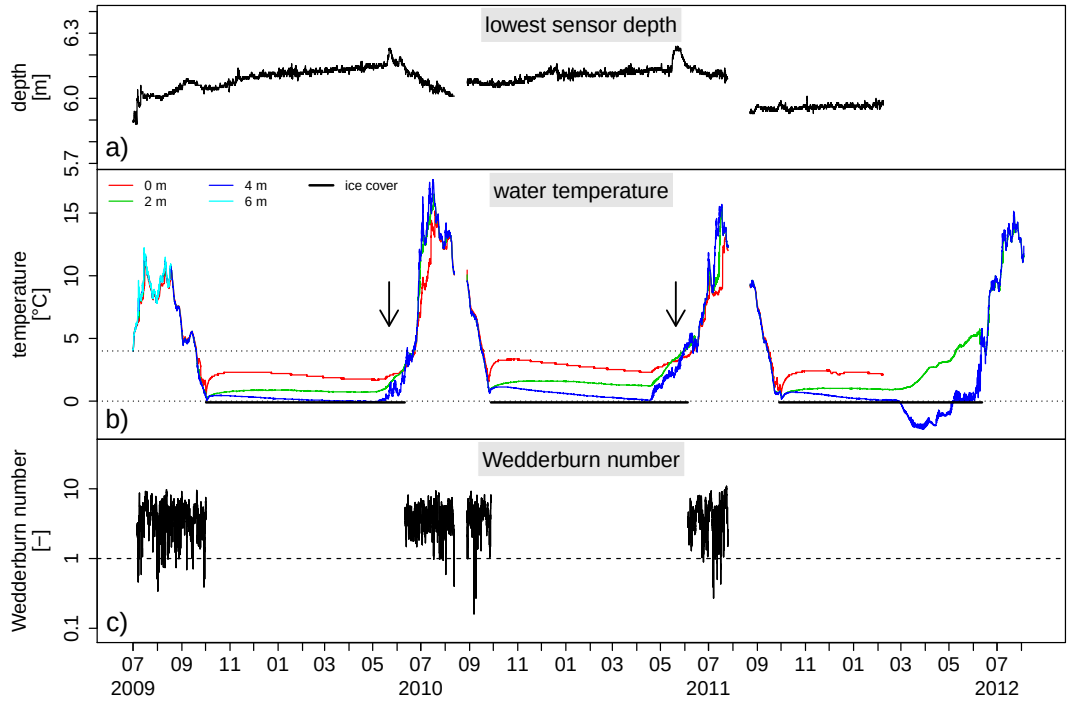

Figure 4. Hourly physical characteristics for Sa_Lake_1, July 2009 to August 2012. **(a)** Depth of bottom lake sensor as an indicator of water level changes; **(b)** water temperatures and ice cover duration; **(c)** Wedderburn number (dimensionless), calculated for the ice-free period only. Arrows indicate the timing of the lake's seasonal flooding by Lena river water.

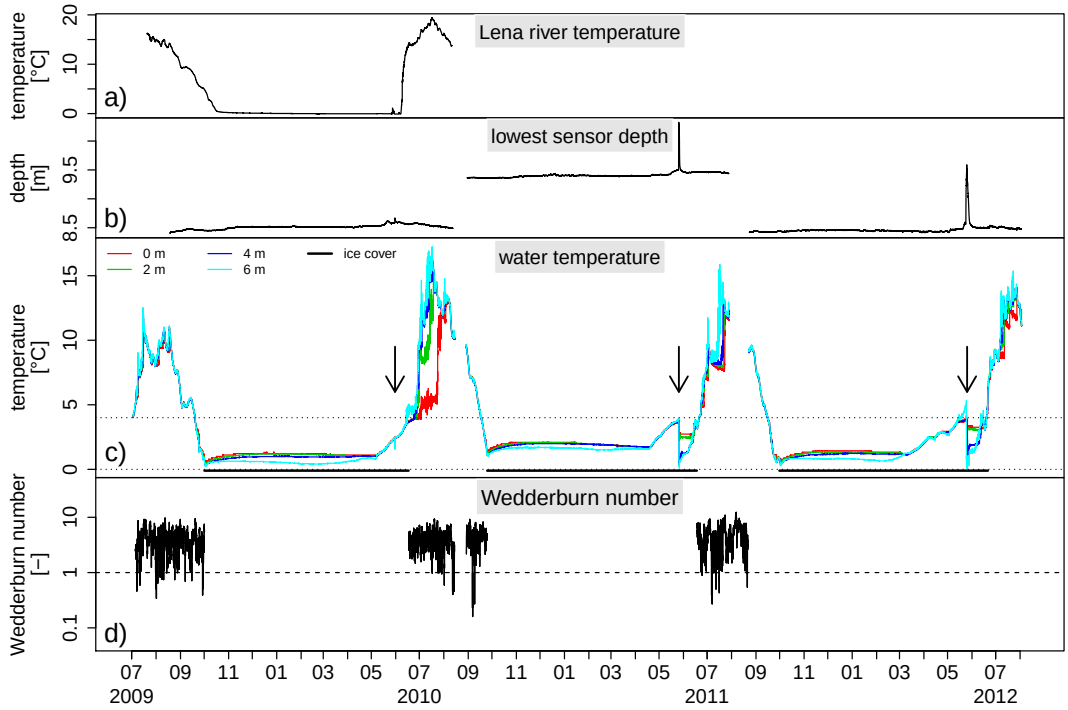

Figure 5. (a) Hourly temperatures for the Lena River from July 2009 to July 2010, and for Sa_Lake_4 (July 2009–August 2012): **(b)** depth of bottom sensor as indicator for water level changes: sharp increase in depth during May 2011 and 2012 indicates flooding with Lena River water; **(c)** water temperatures and ice cover duration; **(d)** Wedderburn number (dimensionless) calculated for the ice-free period. Arrows indicate the timing of the lake's seasonal flooding by Lena river water.

lake bottom is visible even at 2 m water depths. The thermal characteristics of the sediment are based on sediment temperatures measured beneath two lakes in the Lena River Delta (on the Bykovsky Peninsula; Grigoriev, 1993) and are discussed in Sects. 4 and 5. Two temperature profiles were obtained in June 1984 for one shallow (1 m) and one deep (5 m) lake, down to a sediment depth of 16 and 21 m below the lake bed, respectively. These temperature profiles are used as input for the model experiments since the assumption of thermal equilibrium does not necessarily exist for the lakes in the permafrost landscape.

Two meteorological data sets were used to drive the model: (1) hourly data from the on-site weather station (air temperature at 2 m height, wind speed, humidity, and radiation components), and (2) 6-hourly NCEP/NCAR reanalysis data provided by the NOAA/OAR/ESRL PSD, Boulder, Colorado, USA (http://www.esrl.noaa.gov/psd/; Kalnay et al., 1996). The two driving data sets were compared and were found to be in good agreement with each other, having some discrepancies in the short-wave radiation components (Fig. 3). The modeled lake temperatures were nearly identical in both data sets (not shown), indicating that reanalysis data sets perform well for lake modeling in these remote areas, where on-site meteorological information is often limited. For further analysis we used the measured on-site meteorological data set, which can be found in the Supplement for this publication. The FLake model output parameters (water temperatures, ice cover thickness, bottom sediment heat flux) for one of the lakes (Sa_Lake_1) are compared for the time period 9 July 2009 to 29 July 2011 with the measured parameters in Sect. 4. The model was used to:

- validate the one-dimensional modeling approach and qualify the main mechanisms governing features of the lake thermal regime, such as summer stratification, water-sediment heat exchange, and ice melt,
- characterize the water-sediment heat exchange at annual timescales,
- establish a relationship between the morphometry and summer stratification duration.

The "Lake Analyzer" numerical tool (http://lakeanalyzer.gleon.org/; Read et al., 2011) was used to determine the dimensionless Wedderburn number (*Wd*), a quantitative measure of the balance between wind mixing and stratification that is important for describing the biogeochemical cycles of lakes (Spigel and Imberger, 1980). A *Wd* number of 1 indicates a threshold value at which the wind shear brings the thermocline to the lake's surface along the upwind shoreline. For large Wedderburn numbers ($\gg 1$) the buoyancy force is much greater than the wind stress suggesting strong vertical stratification. For small Wedderburn numbers ($\ll 1$) the wind

stress is much greater than the buoyancy force suggesting destruction of the vertical thermal stratification in the lake. On-site weather data from hourly time series of water temperature, wind speed, and bathymetric data were used as model inputs for the calculation of *Wd*.

4 Results

4.1 Lake thermal dynamics based on observations

The following analyses were based on temperature and sensor depth (water depth) data collected over the course of 3 years (2009–2012) from the investigated lakes, covering a range of morphometric characteristics and located on two geomorphologically different terraces (consisting of sediments of the Pleistocene Ice Complex on Kurungnakh and a Holocene flood plain on Samoylov). The seasonal thermal dynamics are only discussed in detail for two of these lakes: Sa_Lake_1 which is a thermokarst lake, and Sa_Lake_4 which is a perched/oxbow lake (Figs. 4 and 5; an animation of the daily temperatures of Sa_Lake_1 is also provided in the Supplement). These lakes were selected as they have the best data records, taking into account the temporal coverage and the total number of sensors in each lake profile. The seasonal temperature dynamics of the other lakes (Sa_Lake_2, Sa_Lake_3, and Ku_Lake_1) are illustrated in the Appendix of this paper (Figs. A6–A8).

4.2 Fall and winter

During fall, cooling and complete mixing occurs at about the end of September resulting in isothermal conditions at 0 °C immediately prior to ice cover formation (Figs. 4 and 5). The ice cover growth can be briefly interrupted due to short-lived warming events during the fall (as was observed, for example, in late September and early October of 2008) but the ice cover then persists from October through to June (Figs. 4b and 5c; Table 1). The water column becomes stratified following the formation of the ice cover and the initial isothermal conditions change so that lake-bottom temperatures are consistently warmer than those higher up in the water column (towards the water/ice interface). This bottom temperature development under ice, which involves rapid warming immediately after ice-cover formation followed by subsequent gradual cooling, takes place in all lakes but the rates of warming and cooling vary (Figs. 4b, 5c, A6–A8). In Sa_Lake_1 the maximum vertical temperature gradient was less than $1\,^{\circ}\mathrm{C\,m^{-1}}$ (with a maximum of $1\,^{\circ}\mathrm{C\,m^{-1}}$) in the winter of 2010/2011 and decreased over the course of the winter (Fig. 4b). In Sa_Lake_4, the maximum temperature gradient was less than $0.2\,^{\circ}\mathrm{C\,m^{-1}}$ and, in contrast, increased over the course of the winter (Fig. 5c). The waters in both lakes remained stratified during the winter, with gradual overall cooling of the stratified profile continuing until the end of winter.

4.3 Spring

The snow cover on the tundra landscape was usually very thin during the winter (< 0.5 m) and had usually thawed by the end of May or early June. Field observations during a number of spring field campaigns showed that the frozen surfaces of the lakes were normally kept snow-free by wind action. It is interesting to note that the under-ice warming of the water column (Figs. 4b, 5c) started as early as the beginning of March (e.g., in 2012), when air temperatures were still well below 0 °C, as a result of strong solar radiation input through the ice. A temperature increase of about 4 °C over the 6-week period prior to ice break-up is equal to an energy input of about $30\,\mathrm{W\,m^{-2}}$. With solar radiation returning after the polar night, the shortwave net radiation on the ice surface is about $50\,\mathrm{W\,m^{-2}}$ in March and increases to about $300\,\mathrm{W\,m^{-2}}$ by the end of May or the beginning of June (Fig. 3b). The net shortwave radiation penetrating to the water column is thus reduced by about 15–20 % as a result of transmission through the ice cover. Radiation can penetrate to great water depths depending on the optical properties of the lake water. Assuming light extinction in the water column to be $0.5\,\mathrm{m^{-1}}$, about 13 % of the radiation penetrating the ice cover (or $\sim 4\,\mathrm{W\,m^{-2}}$) will reach the lake floor beneath 4 m of water. The solar radiative heating of the water (still below its maximum density at 4 °C) and subsequent convective mixing effectively reduced the temperature gradient beneath the ice cover to less than $0.5\,^{\circ}\mathrm{C\,m^{-1}}$ for Sa_Lake_1 and less than $0.1\,^{\circ}\mathrm{C\,m^{-1}}$ for Sa_Lake_4 (Figs. 4b and 5c), this being a well-known mechanism in ice-covered fresh water lakes during spring (Mironov et al., 2002; Kirillin et al., 2012). Continued solar radiation and air temperature warming induce lake ice melt, which can also be accelerated by high wind speeds. For example, in 2009 the ice cover on Sa_Lake_1 was observed to drift, break-up, shrink, and then disappear, over the course of just a few days due to strong, warm winds. Satellite radar observations from 2011 show that the ice cover break-up occurred over a period of about 10 days from the beginning of June, starting with the formation of a moat. On 10 June all lakes had an ice cover with a moat (i.e., an unfrozen ring close to the shoreline); on 21 June, Sa_Lakes 1, 2, and 3 were ice free but the largest and deepest lakes (Ku_Lake_1 and Sa_Lake_4) still had 40–50 % ice cover (Table 1). Complete mixing of the water, as indicated by the first isothermal conditions after the winter stratification (Table 1), had already occurred during the early part of ice break-up (Table 1; Figs. 4b, 5c). The lakes were usually ice free by the middle or end of June (Table 1).

Seasonal flooding by the Lena River was an additional process that had an important effect on the water temperatures in Sa_Lake_4 (which was formed in a former river channel) and Sa_Lake_1. River ice break-up and flooding took place at the end of May in all 3 years, when the lakes were still ice covered (Table 1). Lena River temperatures recorded over a complete year (2009–2010) showed that the river tempera-

tures remained around 0 °C during the winter, warmed up briefly for about 2 days to a peak temperature of 1.1 °C (31 May 2010) and then cooled again to 0 °C before steadily increasing thereafter to reach a maximum of 19.4 °C on 20 July 2010 (Fig. 5a). Radiative under-ice warming and convection in Sa_Lake_4 continued until lake ice break-up in 2010, but this spring under-ice warming was interrupted in both 2011 and 2012 by intense flooding with cold Lena River water, as indicated by both the temperature profiles and the water depth data (Fig. 5b). The water level in this lake rose by about 1 m over the course of a few hours (28–29 May 2011 and 27–28 May 2012), returning to the original level within 4–5 days. Concomitant with water level rise in Sa_Lake_4, the water temperatures fell to 0 °C in the upper sensors (immediately beneath the ice). Lake_Sa_1 was also connected to the river during the flood events, as can be recognized by the slight increase in water depth at the end of May in 2010 and 2011 (no water depth data are available for 2012), but the increase was less than in Sa_Lake_4 (< 10 cm variation; Fig. 4a).

4.4 Summer

During the summer months positive air temperatures and continuous heat input from solar radiation steadily raised the water temperatures of the lakes at all depths, until September. Heat input from net shortwave radiation supplied about 150 W m^{-2} in mid-July (Fig. 3). Maximum air temperatures occurred over very short (daytime) periods, reaching up to more than 25 °C. The highest air temperatures were recorded in July 2010, reaching a maximum of 31.9 °C on 5 July.

All of the lakes experienced short periods of thermal stratification during the summer, which varied both between the lakes and between the summers; the highest temperature gradient reached was about 5 °C m^{-1} in the deepest lake, Sa_Lake_4 (Fig. 5). Maximum water temperatures of around 20 °C were usually reached in mid-July, with up to 22 °C recorded for the shallow lake (Sa_Lake_3). Mean monthly bottom temperatures during periods with no ice cover ranged between 4 and 15 °C (Fig. 6), and can therefore be considerably higher during the summer than their annual means (Table 1).

The monthly bottom temperatures for some lakes were also warmer than the corresponding monthly air temperatures (Fig. 6), confirming that radiation input is an important additional energy source, as well as effective mixing of the lake waters. Starting with colder mean bottom temperature in July, gradual warming creates warmest mean bottom temperatures in the deepest lake (Sa_Lake_4) in August and in the shallowest lake (Sa_Lake_3) in July. For all other lakes, maximum bottom temperatures occur either in July or August, depending on the timing of ice break up and the lake's seasonal energy balance.

The Wedderburn numbers are in agreement with the observed short periods of weak stratification during the ice-free period (Figs. 4c, 5d). Remarkably, *Wd* remain rather

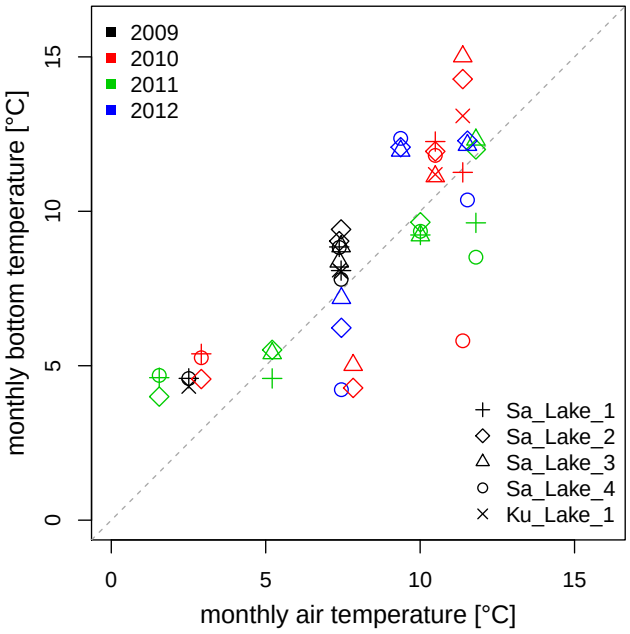

Figure 6. Relationship between mean monthly lake bottom temperatures for all five lakes during the ice-free period and the corresponding mean monthly air temperatures, from July 2009 to August 2012. Data are also provided in the Supplement of this paper.

low throughout the whole summer (between 1 and 8 for Sa_Lake_1 and Sa_Lake_4) and there are even short periods with $Wd < 1$. These *Wd* values indicate that buoyancy and wind stress were almost in equilibrium, suggesting favorable conditions for occasional upwelling of the thermocline along the upwind shorelines of the lakes, which would make an additional contribution to the mixing of water in the lakes and to the heat–mass exchange between the lakes and the atmosphere. During short periods with $Wd < 1$ the wind stress is much greater than the buoyancy, effectively destroying the thermal stratification.

4.5 Lake heat content

The heat content in the investigated lakes at times varied by up to ±50 MJ m^{-2} over just a few days (Fig. 7), with the maximum heat content being reached at the end of July or in early August. The summer heat income of the lakes was of the order of 100 to 400 MJ m^{-2} and had a linear relationship with their depths (see Eq. 1). The winter heat income of the lake water beneath the ice cover varied between 50 and 150 MJ m^{-2}, not including the heat transfer associated with the formation of the ice cover. However, if a 2 m thick ice cover is taken into account (which is especially important for Arctic lakes; Wetzel, 2001), the annual heat budget can reach up to about 1 GJ m^{-2} (Table 1).

Sa_Lake_4, which can be subjected to substantial seasonal flooding during spring, showed a reduction in heat content of about 100 MJ m^{-2} (in 2010 and 2011) within a few hours,

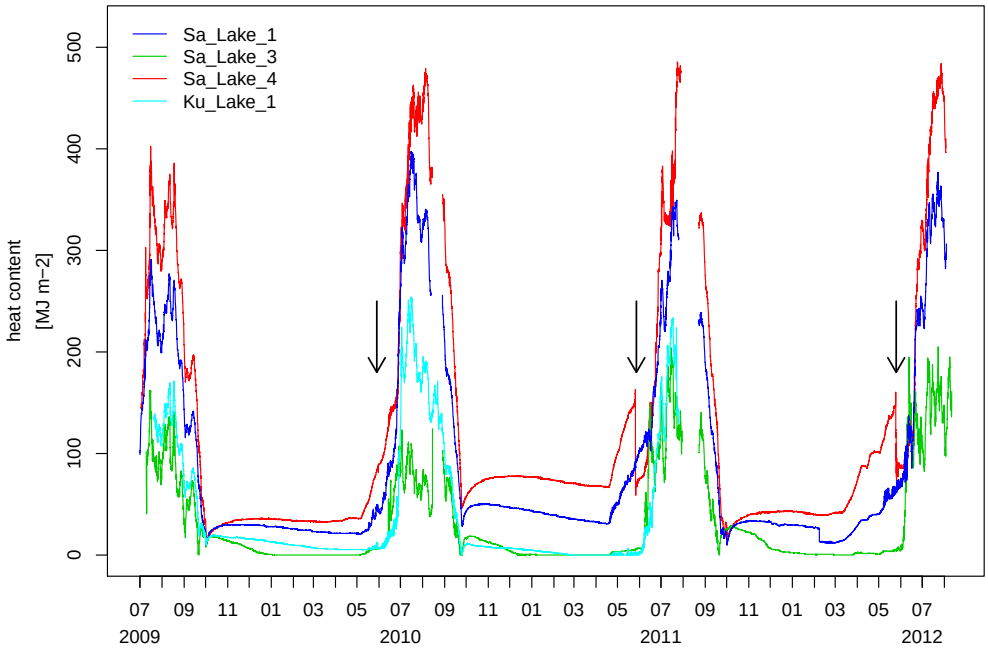

Figure 7. Sensible heat content (calculated using Eq. 1) for four lakes lakes, from July 2009 to August 2012. Arrows indicate the timing of the lake's seasonal flooding by Lena river water.

thus suppressing the ongoing radiative warming of the lake water. Although the Lena River carries a substantial amount of heat into its delta every year ($\sim 0.49 \times 10^{12}$ J s^{-1}; Alekseevsky, 2007) due to very warm summer temperatures, the flooding of the lakes occurs when its temperatures are at their coldest.

4.6 Modeled seasonal lake thermal dynamics

A comparative analysis of the modeling results and observational data has revealed the capabilities of, and flaws in, the use of one-dimensional modeling to reproduce the thermal dynamics of lakes formed on permafrost, as well as providing additional quantitative insights into the major mechanisms governing the seasonal thermal dynamics of Siberian lakes. The FLake model results for the Sa_Lake_1 over a period of 2 years (2009–2011) have been in overall good agreement with on-site observations with regard to seasonal variations in lake temperatures, the mean and maximum temperatures in winter and summer, and the durations of the open water and ice cover seasons (Fig. 8a–c).

To quantify the model performance for thermokarst lakes we applied standard measures (e.g., Thiery et al., 2014) of the model's ability to reproduce the observed mean temperature (T_m), the standard deviation ratio (SD_{model} / SD_{obs}), the centered root mean squared error ($RMSE_c$), and the Pearson correlation coefficient (r). In contrast to other lake model evaluations using surface temperature T_s (for example, from African and west European lakes), we used T_m since no temperature probes were installed at the surface due to the seasonal ice cover. FLake demonstrated good performance with regard to the mean lake temperature. The statistics–Pearson correlation coefficient $r = 0.97$, SD_{model} / SD_{obs} 1.28, $RMSE_c$ 1.49 °C are slightly worse than those reported previously for temperate lakes ($r = 0.988$; Stepanenko et al., 2010) and better than FLake performance on deep tropical lakes ($r = 0.78$, SD_{model} / SD_{obs} 1.25, $RMSE_c$ 0.75 °C; Thiery et al., 2014). The model reproduced summer stratification during the ice-free period ($r = 0.93$, SD_{model} / SD_{obs} 1.25, $RMSE_c$ 1.82 °C). Solar heating of the water below the ice is not included in the model and thus the agreement between model and observations is lower during the ice-covered period ($r = -0.42$, SD_{model} / SD_{obs} 0.37, $RMSE_c$ 0.66 °C). The resulting uncertainties in the ice break up prediction affect also the model performance with regard to the lake heat content at the beginning of the open water period in early summer (Fig. 8). As thermal dynamics under the ice cover are crudely reproduced by the majority of one-dimensional lake models used in coupled climate modeling systems (Stepanenko et al., 2010), estimation of the role played by thermokarst lakes in regional climate requires integration of a cost-effective and physically sound sub-model of winter lake thermodynamics into lake parameterization schemes for climate models (e.g., Oveisy and Boegman, 2014).

4.6.1 Open water period and summer stratification

The duration of the warming and cooling periods, as well as the mean water temperatures during the autumn cooling,

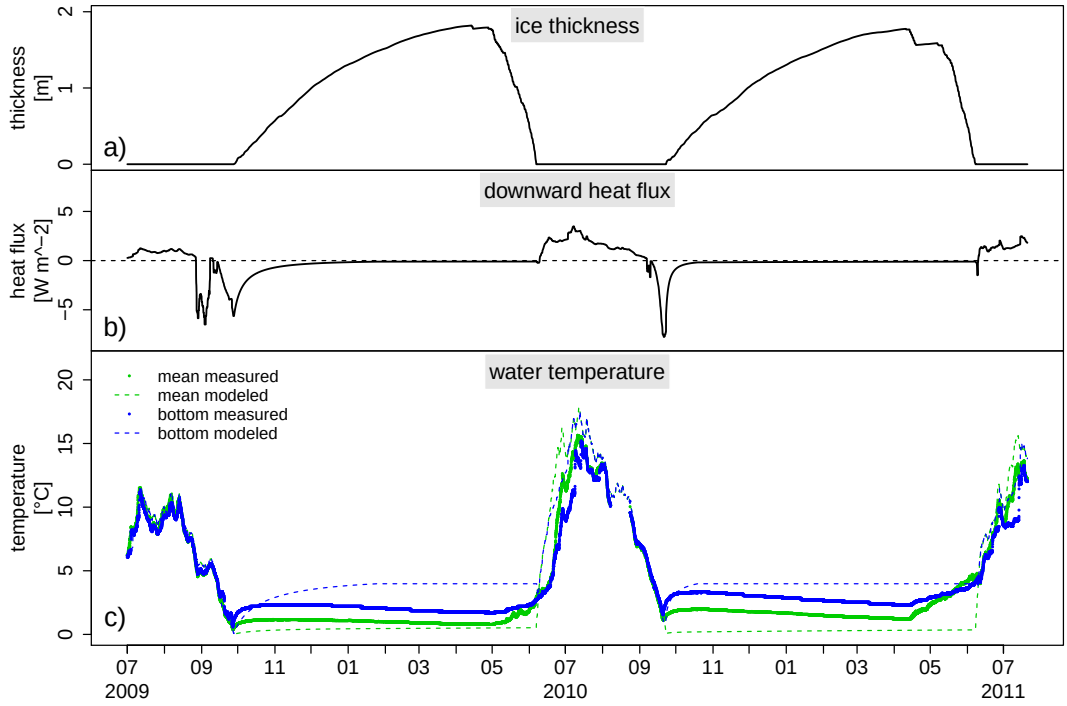

Figure 8. Modeled and measured hourly characteristics for Sa_Lake_1 from August 2009 to August 2011. **(a)** Modeled ice thickness; **(b)** modeled vertical heat flux at the water-sediment boundary: negative fluxes indicate fluxes from the sediment into the water column – a running median filter was used to remove spikes; **(c)** measured (continuous line) and modeled (dashed lines) lake-bottom and mean water temperatures.

are well simulated by the model suggesting that the model adequately captures the net heat storage of the lakes. The model was also able to reproduce the development of weak thermal stratification in summer (i.e., the short periods during which the bottom temperatures differed from the mean temperatures of the lakes in June and July, 2010 and 2011: Fig. 8c). The largest discrepancies in the water temperatures produced by the model occurred during the period of spring warming, with maximum deviations of about 6 °C from the measured mean temperatures (Fig. 8). These deviations can be explained by the ice break-up being modeled too early, with subsequent early warming of the lake. Lake temperatures were consequently consistently overestimated during the warming period in 2010.

4.6.2 Ice duration and thickness, and water temperatures beneath the ice cover

The mean rate of ice growth modeled with FLake was about 0.92 cm day^{-1} for 2010 (minimum 0.021 cm day^{-1}, maximum 8 cm day^{-1}) and 0.89 cm day^{-1} for 2011 (minimum 0.026 cm day^{-1}, maximum 4.6 cm day^{-1}), with the maximum thickness of ice cover remaining below 2 m. The modeled ice thickness of no more than 2 m agrees well with the temperature data from the sensor located 4 m above the sediment (approximately 2 m from the lake surface) in Sa_Lake_1 (Fig. 4b). This sensor did not record any freezing in 2010 or 2011, but in 2012 the sensor froze into the lake ice (Fig. 4b), recording sub-zero temperatures and thus indicating thicker ice (> 2 m) in 2012.

The modeled melting of the ice cover in spring and subsequent warming of lake temperatures is, in general, well reproduced by the model. The measured development of under-ice bottom temperatures (with warming following the onset of ice cover formation, followed by a later winter cooling) is only partly reproduced in the modeled results due to rather simplified parameterization of the under-ice thermodynamics in the FLake model, with a linear vertical temperature profile in the ice-covered water column and no solar radiation penetrating the ice cover.

4.6.3 Thermal properties of the lake sediments and water-sediment heat flux

Heat conduction from a lake's water column to the underlying sediment is a key thermodynamic process for understanding the role of lakes in the permafrost landscape. The Flake model incorporates simulation of seasonal temperature variations within the thermally active sediment layer, based on an assumption of thermal equilibrium in the sediment over longer-than-seasonal timescales (i.e., a constant temperature beneath the seasonally thermally active sediment layer,

ensuring zero mean annual flux across the water-sediment boundary; Golosov and Kirillin, 2010). Since this thermal equilibrium does not necessarily exist in lakes on permafrost, we performed two separate model experiments with different thermal conditions beneath the lakes, based on temperature profiles measured in lake sediments at comparable sites in the Lena River Delta (Grigoriev, 1993; Fig. 9). While the sediment temperature beneath the shallow lake fell to below 0 °C at about 2 m depth and reached −6 °C at 15 m depth, the temperatures beneath the deeper lake indicated an unfrozen layer to about 25 m depth, with a maximum temperature of about 4.5 °C at a depth of about 3 m beneath the lake floor (Fig. 9a, b). The reported temperatures at depth, where seasonal variations were minimal, ranged from −6 °C beneath the 1 m deep lake to 4 °C beneath the 5 m deep lake. Using the measured temperature profile below the 5 m deep lake, the thickness of the sediment layer with appreciable seasonal variations in temperature was estimated to be ∼ 6 m (Fig. 9 b). The FLake modeled heat flux at the lake-sediment boundary for different ground temperatures revealed two characteristic seasonal patterns of lake-permafrost heat exchange: the flux across the frozen sediment beneath the shallow lake was directed downwards during the summer, with a magnitude of up to 4 W m^{-2}, the fast release of heat from the sediment during autumn cooling, and the water-sediment heat flux of ∼ 0 W m^{-2} during the entire ice-covered period (Fig. 9c). This seasonal pattern suggests an annually positive heat budget of the under-lake ground and thawing of the permafrost, which is continuously heated by the lake above. For a lake with deep sediment temperatures approaching 4 °C, the annual mean flux across the sediment tended towards zero, with maximum downward fluxes in summer of 3 W m^{-2}, a maximum of 7 W m^{-2} heat released back into the water column during early freeze back, and a continuous low rate of < 1 W m^{-2} during the ice-covered winter (Fig. 9d). In the absence of any additional information available on the ground temperatures under Sa_Lake_1, the latter case was adopted for the longer model run (Fig. 8b, c), with an "equilibrium state" suggesting little or no permafrost thawing beneath the lake. The maximum modeled heat flux at the sediment-water interface was about 4 W m^{-2} into the sediment (in summer) and about 7 W m^{-2} (to almost zero) from the sediment into the water column during the ice-covered period. The rapidly changing (negative) hourly heat fluxes during the fall cooling period were due to rapid cooling of the water column, which could not be reproduced by the model.

Overall, the calculated energy density for the lake with mean annual water temperature of 3 °C is about 65 MJ m^{-3}, thus more than six times the amount for the permafrost soil of about 10 MJ m^{-3}. Lakes are therefore effective for energy storage compared to the frozen landscape, and the fraction of landscape covered by thermokarst lakes has the potential to significantly affect the land-atmosphere energy exchange.

5 Discussion

Lakes can be considered to represent "hot spots" in the permafrost landscape. This study has demonstrated that the investigated lakes remain unfrozen throughout the winter and have mean bottom water temperatures (between 2.7 to 4.0 °C) that are significantly warmer than the mean annual air temperature (∼ −13 °C) or the permafrost temperature (−9.2 °C at 10.7 m depth). This is in agreement with observations made by Jorgenson et al. (2010) who reported thermokarst lake-bottom temperatures in Alaska that were up to 10 °C warmer than the mean annual air temperatures. Harris (2002) attributed the anomalously high mean annual temperature in a shallow lake in western Canada to convective heat exchange and the absorption of radiation through the water column. Mean annual lake-bottom temperatures in northern Alaska also showed a similar range of values (Arp et al., 2012; CALON), and this range has therefore been used in previous modeling studies to estimate the development of talik (Burn, 2002; Ling and Zhang, 2003). Differences in heat content are related to morphometric parameters, particularly to water depth. Burn (2002) found mean annual lake-bottom temperatures of between 1.5 and 4.8 °C for the deeper pools in tundra lakes on Richards Island (northwestern Canada). Ensom et al. (2012) reported mean annual bottom temperatures of between 3.4 and 5.5 °C from a number of lakes and channels in the Mackenzie Delta (Canada) and computed that 60 % of the lakes maintained taliks.

Mean bottom lake temperatures, which ranged between 2.7 and 4 °C in this study, depend on lake depth and are important for constraining future numerical modeling experiments on talik development. Our study also confirms previous findings that there is a "critical lake depth" (lake depth > winter ice cover thickness) for water to remain unfrozen beneath the ice cover (Arp et al., 2012; Burn, 2002). All lakes in this study had a depth >3 m, which exceeds the maximum ice thickness of about 2 m.

The bottom temperatures in the lakes varied significantly between summer and winter but their annual mean temperatures and temperature dynamics were similar despite the range of morphometric and geomorphological characteristics. The *Wd* numbers indicated that the lakes were all well-mixed during the summer periods, and it can therefore be assumed that both heat and dissolved gases, in particular, oxygen, are effectively transported through the water column. This assumption is supported by the measured oxygen concentrations in these lakes, which ranged between 8 and 10 mg L^{-1}, and the lack of any detected vertical stratification (R. Osudar, personal communication, 2015).

We observed and simulated short stratification periods in summer in the studied lakes (Figs. 4 and 5). These stratification events are probably the major physical factor affecting biogeochemical processes in lakes. In particular, the duration of the thermal stratification in summer affects the concentration and vertical distribution of dissolved oxygen.

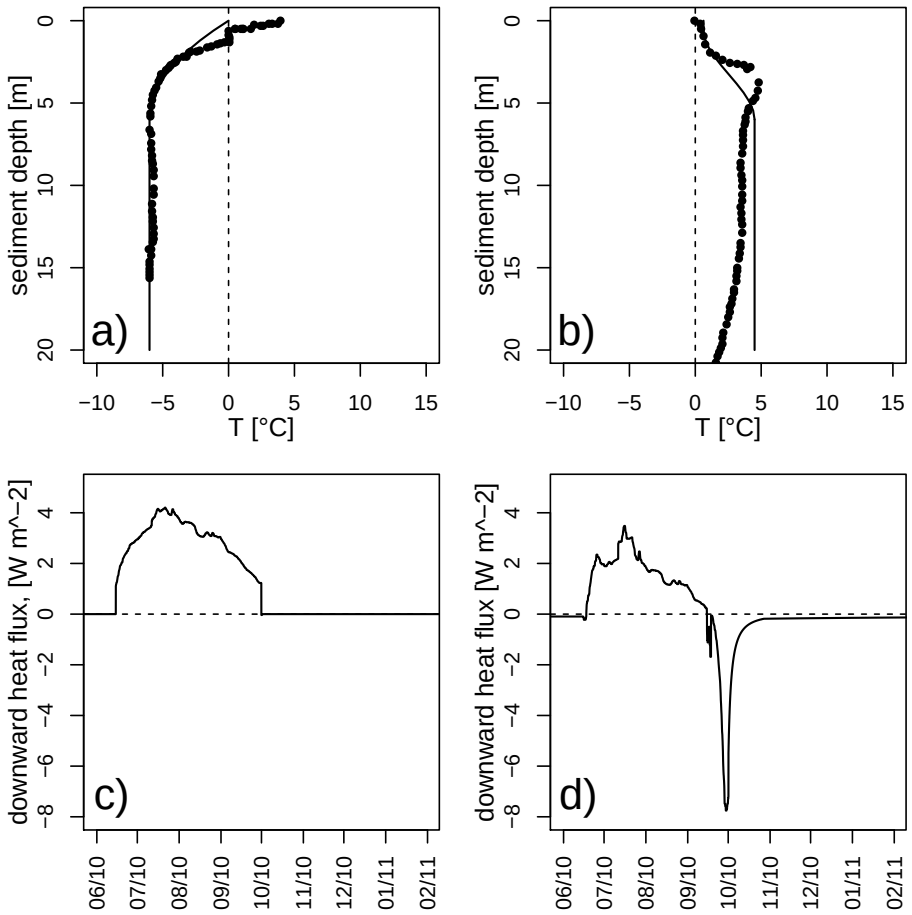

Figure 9. (**a**, **b**) Measured temperature profiles (squares) beneath two lakes (with a) 1 m water depth, and **(b)** 5 m water depth) on the Bykovsky Peninsula, in the southeastern part of the Lena River Delta (Grigoriev, 1993). Temperatures were measured between 9 and 11 June 1984. Modeled sediment temperature profiles (continuous line) are for 10 June 2010 using model parameters described in the Methods section. (**c**, **d**) Modeled daily vertical heat flux at the water-sediment boundary for **(c)** the shallow lake, and **(d)** the deep lake, 2010–2011.

Longer summer stratification provokes deep anoxia and favors methanogenesis in the deep water column and upper sediment (Golosov et al., 2012). Under equal climatic forcing, lake depth is the primary factor determining the duration of summer stratification (the second one being the water transparency, Kirillin, 2010). Sensitivity model runs with the lake depth varying in the range 2–12 m using the same meteorological input data from Samoylov demonstrated that lakes in this climatic zone with mean depths > 5 m should have dimictic stratification regimes, i.e., develop continuous stratification in summer with a duration of 1 month or longer (Fig. 10). This also supports the observation of summer stratification in deeper (> 6 m) Alaskan thermokarst lakes (Sepulveda-Jáuregui et al., 2015). In lakes of about 8 m depth or more, the summer stratification duration significantly increases since high thermal inertia prevents vertical mixing during the autumn cooling in August–September (Fig. 11).

The summer heat budgets of Arctic lakes are much smaller than those of low-latitude lakes. The only previously reported summer heat budget for an Arctic lake (Chandler Lake, Alaska) was 240 MJ m^{-2}, which lies in the same range as the heat budgets in this study (Wetzel, 2001). In contrast, the summer heat budget for a large lake such as Lake Superior on the Canada-USA border is much larger at about 1.3 GJ m^{-2}. In comparison, the annual heat budget of Lake Baikal in Siberia is estimated to be about 2.7 GJ m^{-2} (Wetzel, 2001). The total annual heat budget for all of the investigated lakes (including the latent heat of the ice cover) amounts up to about 1 GJ m^{-2} (Table 1). In view of the large proportion of land covered by water bodies in this landscape (25 %) and the volumes of water that they contain, their energy storage and turnover within the permafrost landscape are of considerable significance. Furthermore, changes in the heat content of lakes occur much more rapidly than changes in the heat content of the surrounding permafrost soils as a result of efficient energy absorption and effective mixing. In contrast, progressive deepening of the seasonally thawing upper layer of permafrost (the active layer) of the polygo-

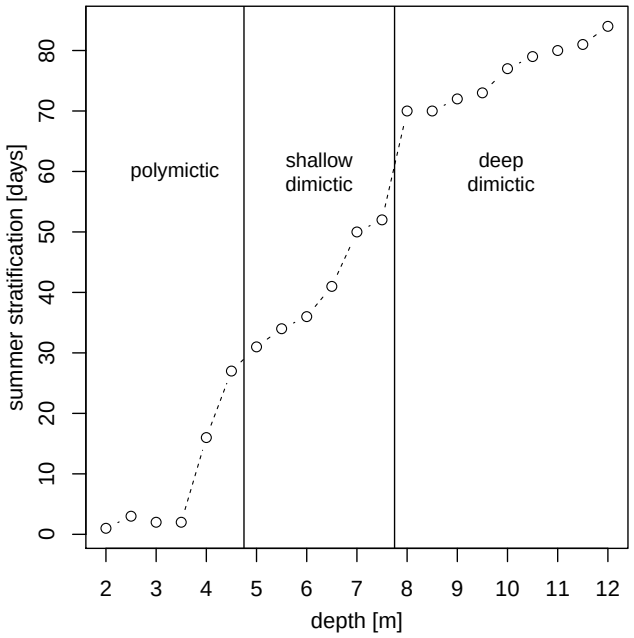

Figure 10. Total number of days with summer stratification in lakes of varying depths modeled with FLake driven by the meteorological data from the Samoylov observatory station for 2010. Existence of stratification was determined by the criterion $(T_s - T_b) > 0.5\,^{\circ}\mathrm{C}$, where T_s and T_b are the modeled temperatures at lake surface and lake bottom, respectively.

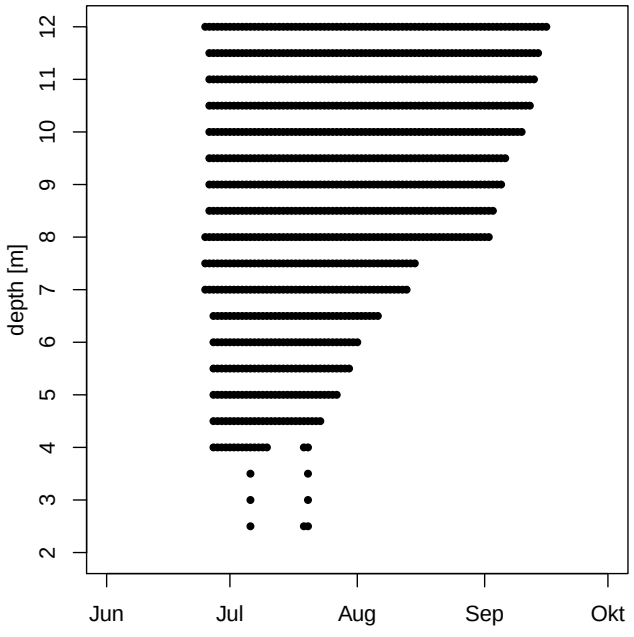

Figure 11. Summer stratification duration in lakes of varying depth (see Fig. 10 for definitions).

nal tundra landscape at this site takes several months and only reaches an average maximum thaw depth of about 0.6 m (Boike et al., 2013; Langer et al., 2013). Lakes also have an important effect on the subsurface thermal conditions beneath the lake and potentially also in the surrounding permafrost. Our results show that, during the summer, heat is continuously transferred from lake water into the bottom sediment. The importance of summer heat gain and its dissipation into the water body and the underlying sediment was first discussed by Vtyurina (1960), using data from a 12 m deep lake in Siberia. Her findings showed heat fluxes directed into the sediments during winter (Fig. 5 in Vtyurina, 1960; also reported in Grosse et al., 2013) which, according to our findings, is an indicator of permafrost thaw. Our modeling results, however, suggest that the temperature increase associated with permafrost thaw eventually results in a net annual heat equilibrium between deeper lakes and the underlying sediments, characterized by a continuous negative heat flux (i.e., heat loss from the sediment into the water column) during the long ice-covered winter and heat gain by the sediment during the open water summer period. The warming of lake-bottom temperatures with the onset of ice cover was initially attributed by Brewer (1958) to heating by shortwave solar radiation and by Mortimer and Mackereth (1958) to the heat release from the lake sediment. Our observed near-bottom temperatures increased beneath the ice cover and the modeling experiments suggested this warming was solely due to heat flow from the sediment, with typical rates of $< 10\,\mathrm{W\,m^{-2}}$. However, the heat flux from the sediment in tundra lakes appears to decay within less than 1 month, which is much faster than in ice-covered lakes of the temperate and boreal climates (cf. Rizk et al., 2014), and is followed by a gradual decrease of the deep water temperatures. The latter is not reproduced by the parameterized sediment module of FLake.

Our numerical modeling of the thermal dynamics of lakes has shown that the basic processes can be accurately reproduced for the summer. However, the model parameters that yielded the best fit for the seasonal heat budget and ice cover duration resulted in less accurate predictions of the bottom temperature under ice. Lake temperatures increase, starting in spring 1–2 months before ice-off, apparently by radiative solar heating. This temperature increase suggests that radiation can make a significant direct contribution to sediment heating in shallow and clear-water thermokarst lakes – a contribution that is usually neglected in lake models. The concept of self-similarity cannot account for the permafrost-talik specific lake processes, such as (i) warming of bottom waters immediately following onset of ice formation and (ii) phase change in the lake's frozen sediment, i.e., annual freeze thaw processes and thawing at the talik-permafrost boundary. While the short period of warming of bottom water during the ice-covered period is due to heat flux from the sediment into the water body, the cooling in winter from mid-winter onwards suggests a loss of heat. This heat loss may occur through conductive heat transfer into both the sediment and the atmosphere. In particular during winter the subsurface heat flux becomes a major component in the surface energy balance due to the lag of incoming short-wave radiation. The

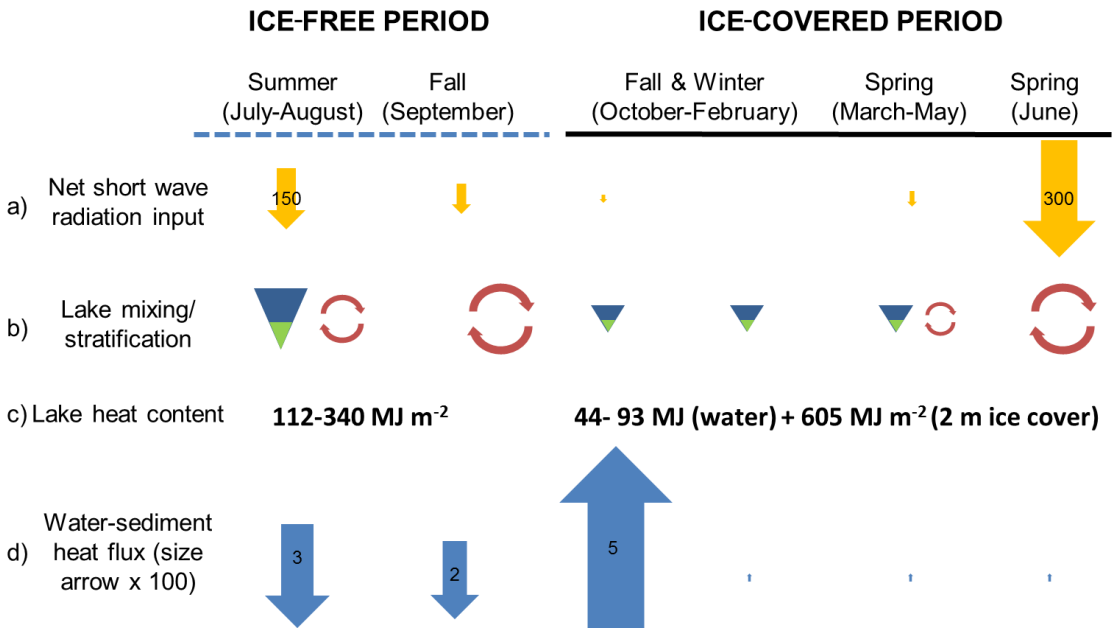

Figure 12. Summary of thermal processes in thermokarst lakes over a 1-year cycle. **(a)** Net short-wave radiation input (measured at the climate station on Samoylov); **(b)** dominant in-lake processes (mixing and stratification) – size of symbol reflects intensity of process; **(c)** lake heat content (divided into summer and winter lake heat content according to Wetzel, 2001); **(d)** average heat fluxes across the lake's water-sediment boundary: downward arrows denote heat flux into the sediment and upward arrows flux out of the sediment into the water column. The size of the arrows and their numbers indicate the relative magnitudes of the fluxes [W m^{-2}]. Note that the sizes of arrows representing bottom heat fluxes have been enlarged by a factor of 100 due the small magnitude of the fluxes.

heat flux from ice-covered water bodies to the atmosphere can be much higher than the heat flux from snow covered soils (for example, shown by Langer et al. (2011b) for ponds and Jeffries et al. (1999) for Alaskan lakes) and can balance up to 90 % of the radiative losses. Further investigations into these processes of warming and subsequent gradual cooling under the ice cover would require a more advanced lake model that is able to take into account deep, continuously frozen sediments and characteristic processes such as thawing.

6 Summary and conclusions

We have measured and modeled the thermal dynamics of lakes in the Lena River Delta of northern Siberia over a 3-year period (2009–2012), with the objective of understanding and quantifying the important thermal processes that operate in this permafrost environment. The investigated lakes were situated in two different geomorphologic settings (sediments of the Pleistocene Ice Complex and on a younger river terrace) with a range of morphometric characteristics. Some of the lakes were seasonally connected to the Lena River through high floods that occurred during spring. Such annual flooding of these lakes by cold river water results in a significant reduction in the ongoing warming (and thus sensible heat storage), depending on the magnitude of the flooding. A schematic summary of our results is provided in Fig. 12.

The lakes were shown to receive substantial energy for warming from net shortwave radiation during the summer. Warming also occurs during the ice cover period in spring, resulting in convective mixing beneath the ice cover. Mixing also occurs following ice break-up, during the summer, and during the fall cooling, resulting in efficient heat transfer to bottom waters and across the sediment-water interface. Numerical modeling suggests that the annual mean net heat flux across the bottom sediment boundary is approximately zero, with positive summer downward fluxes during the ice-free period (4 months) and heat-release back into the water column at much lower rates during the ice-covered period (8 months). Overall, the ice formation and thaw together account for most of the annual variations in a lake's heat content. Furthermore, their timing and durations determine the magnitude and direction of bottom sediment heat fluxes and the timing of water column mixing. Future warming may result in changes to the ice cover but may also produce more pronounced summer stratification, thus potentially reducing the heat input into the sediment layers.

In view of the large area covered by water bodies in permafrost landscapes (25 % of the land surface) and their efficiency at energy absorption and mixing, these water bodies are clearly of considerable importance with respect to energy

storage and turnover, atmospheric fluxes, and sediment heat fluxes in permafrost landscapes.

The investigated thermokarst lakes are representative of Arctic tundra lowlands characterized by thermokarst processes that are common for large regions in central and eastern Siberia, interior and northern Alaska as well as northwest Canada. Despite their importance, however, lakes are not yet included in earth system models. Future work should therefore include lakes in these models and test their sensitivity to possible future changes in climate.

Data availability

The data are available in the Supplement for this paper and through the PANGAEA website (doi:10.1594/PANGAEA.846525).

Appendix A: Morphometry of lakes, hourly lake temperatures and lowest sensor depths data

The topographic slope on the polygonal tundra (first terrace) is very low (< 5°). Aerial images of Sa_Lake_2 and Sa_Lake_3 show submerged polygons beneath the water surface, indicating that these lakes are likely to have been formed by the thawing of ground ice and ice wedges and the subsequent merging of polygonal ponds. The shorelines adjacent to shallow parts of these younger thermokarst lakes (with depths of 0–3 m) are very irregular and feature protrusions of different shapes and sizes (Figs. A1–A4). Where deeper sections (> 3 m) occur close to the shore, the shorelines are smooth and the lakes tend to have an oval shape. The profiles of thermokarst lakes tend to be V-shaped rather than flat-bottomed and the thermokarst lakes investigated were up to 6.4 m deep. The deepest lake on this island, with up to 11.6 m water depth, is Sa_Lake_4. It has an elongated shape and is one of three interconnected lakes that occur in an abandoned channel of the Lena River ("oxbow" or "perched" lakes; Fig. A4). The largest monitored lake in this series of lakes was Ku_Lake_1, located on sediments of the Pleistocene Ice Complex, which have high ice content. This lake is the largest of three residual lakes located within an alas that is more than 20 m deep. This thermokarst basin evolved in two phases (Morgenstern et al., 2013). In the first phase the original large lake covered the entire basin. It drained abruptly through a thermos-erosional valley at about 5.7 ka BP, leaving the > 20 m deep alas with residual lakes. This was then followed by thermokarst processes of varying intensity during the second phase (5.7 ka BP to the present). This lake is an order of magnitude larger in surface area than the other four thermokarst lakes investigated and, in contrast to those lakes on Samoylov Island, has a regular oval shape, occurs within a basin with steep sides and has a smooth, flat shoreline. The maximum water depth is about 3.6 m and the profile is flat-bottomed (Fig. A5).

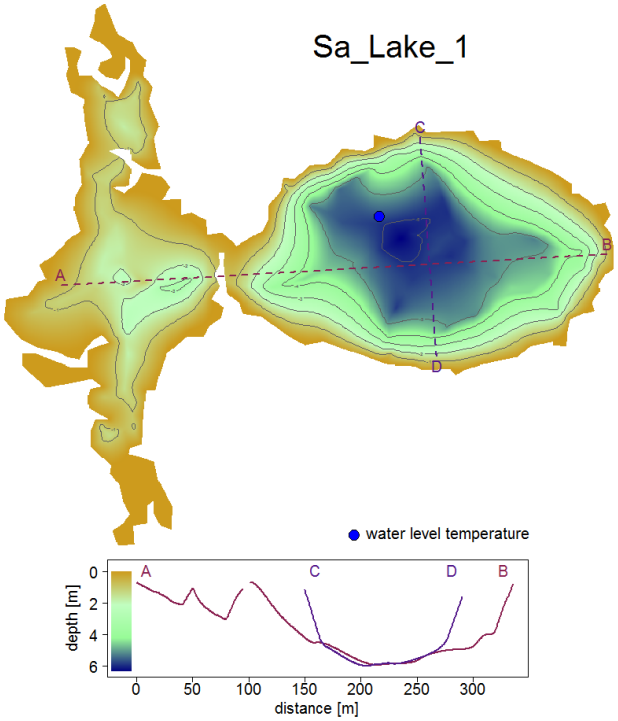

Figure A1. Bathymetry and cross sections of Sa_Lake_1 with location of sensors.

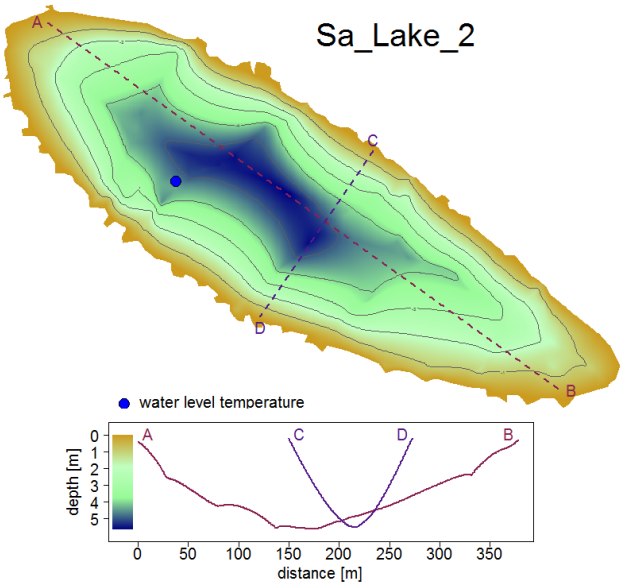

Figure A2. Bathymetry and cross sections of Sa_Lake_2 with location of sensors.

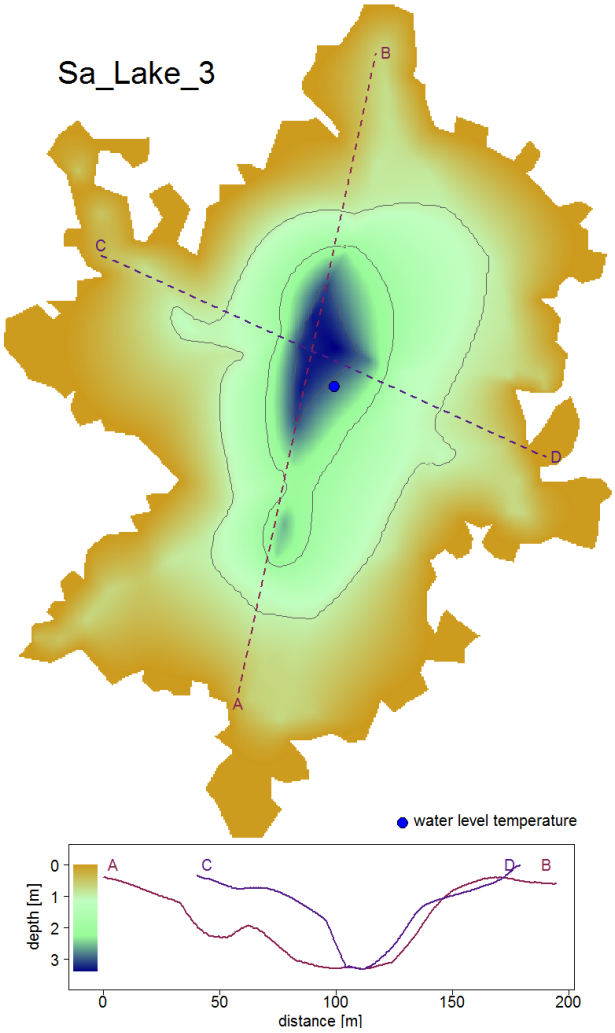

Figure A3. Bathymetry and cross sections of Sa_Lake_3 with location of sensors.

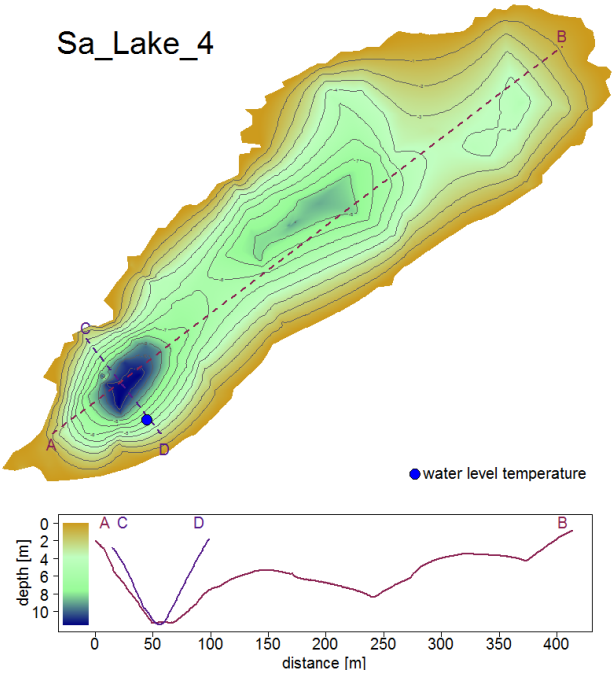

Figure A4. Bathymetry and cross sections of Sa_Lake_4 with location of sensors.

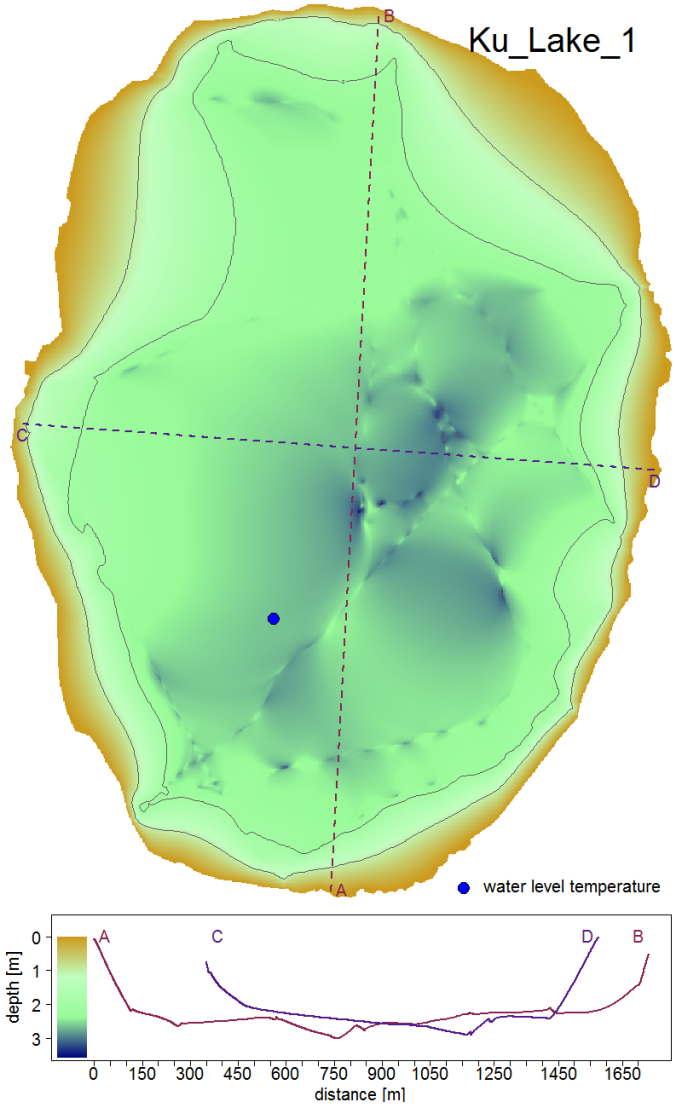

Figure A5. Bathymetry and cross sections of Ku_Lake_1. Data from Morgenstern et al. (2011) and 10.1594/PANGAEA.848485.

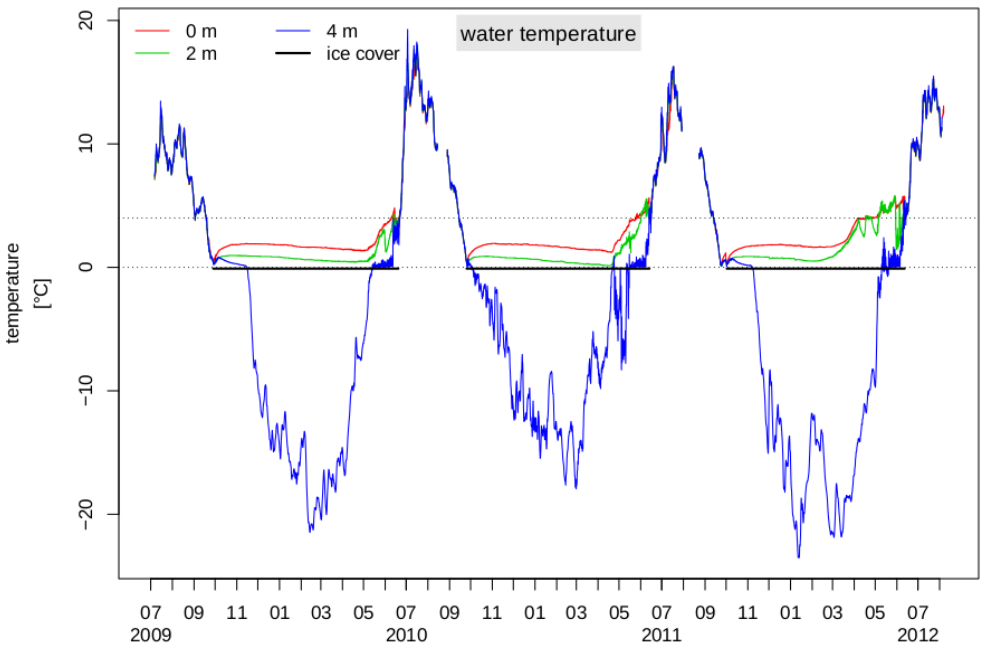

Figure A6. Hourly lake temperatures for Sa_Lake_2, from July 2009 to August 2012. Thick black lines indicate ice-covered periods.

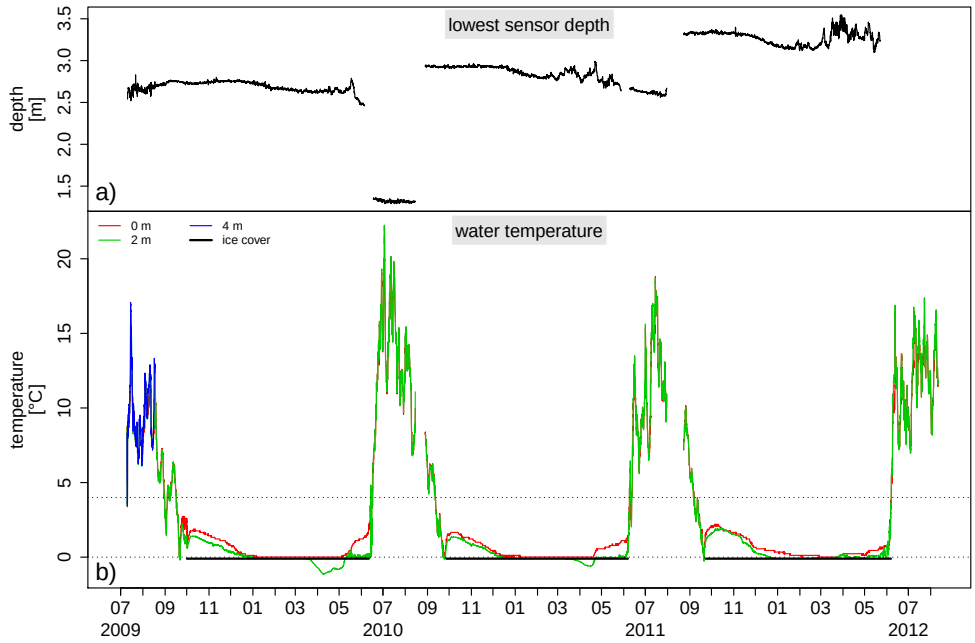

Figure A7. Hourly lake temperatures and lowest sensor depth (indicating water level changes) for Sa_Lake_3, from July 2009 to August 2012. Thick black lines indicate ice-covered periods.

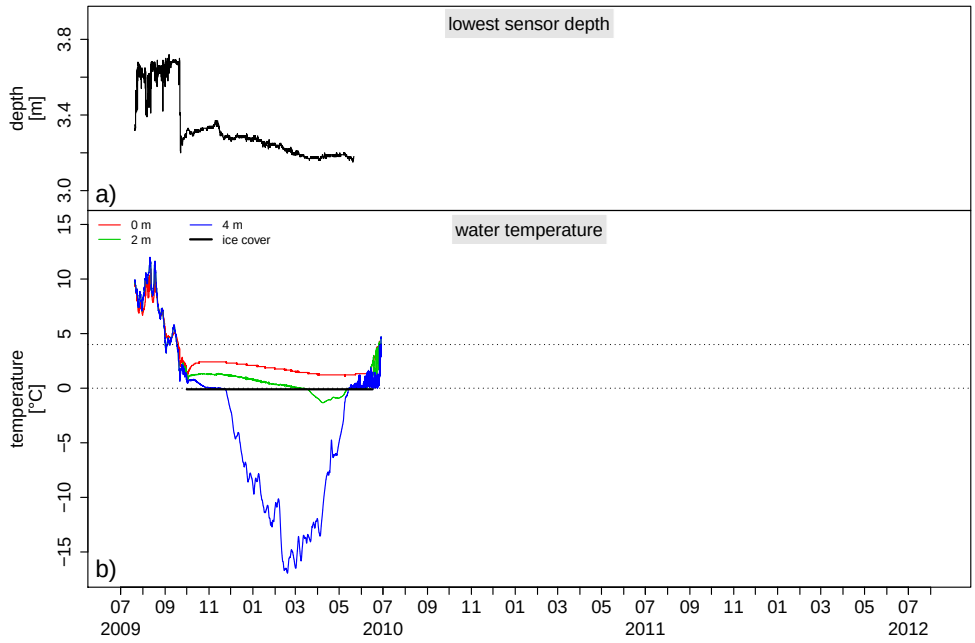

Figure A8. Hourly lake temperatures and lowest sensor depth (indicating water level changes) for Ku_Lake_1, from July 2009 to August 2010. Thick black lines indicate ice-covered periods.

Information about the supplement

- Model data input (Samoylov); air temperature, air humidity, wind speed; radiation components Samoylov_2009_2012.dat
- Model validation data: hourly lake temperatures and sensor depth (lake water level) data, where measured

  Sa_Lake_1_2009_2012.dat
  Sa_Lake_2_2009_2012.dat
  Sa_Lake_3_2009_2012.dat
  Sa_Lake_4_2009_2012.dat
  Ku_Lake_1_2009_2010.dat
  LenaRiver_2009_2010.dat
- Animation (movie) of temperatures in Sa_Lake_1 using daily average temperatures at depth and interpolated between depths using cubic interpolation. Daily temperature plots were added to produce the animation of temperatures Sa_Lake_1_2010-daily-color-.2s.gif
- Summary table of mean monthly air and bottom lake temperatures: meanlake_air_temp.txt

The Supplement related to this article is available online at doi:10.5194/bg-12-5941-2015-supplement.

Author contributions. J. Boike designed the research and led the discussions, supported by G. Kirilin and M. Langer. The FLake modeling was carried out by G. Kirilin and C. Georgi. The paper was written by J. Boike, with comments from all authors.

Acknowledgements. The logistical support provided by the Russian Research station on Samoylov Island is gratefully acknowledged. Field support, including data collection, was provided by Grigoriy Soloviev, Waldemar Schneider, Günther Stoof, and Karoline Wischnewski. Elizabeth Miller, Max Heikenfeld, Wil Lieberman-Cribbin and Stephan Lange assisted with the data analysis and helpful discussions. The authors acknowledge the financial support provided through the European Union's FP7-ENV PAGE21 project under contract number GA282700, and through the Feodor Lynen grant from the Alexander-von-Humboldt Foundation awarded to Moritz Langer. The research was carried out under the Russian government's Program of Competitive Growth, Kazan Federal University.

Edited by: V. Brovkin

References

Abnizova, A., Siemens, J., Langer, M., and Boike, J.: Small ponds with major impact: The relevance of ponds and lakes in permafrost landscapes to carbon dioxide emissions, Global Biogeochem. Cy., 26, GB2041, doi:10.1029/2011gb004237, 2012.

Alekseevsky, N. I. (Ed.): Geoecological state of Russian Arctic coast and their safety of nature management, GEOS Publ., Moscow, Russia, 586 pp., 2007 (in Russian).

Alerstam, T., Gudmundsson, G. A., Green, M., and Hedenström, A.: Migration along orthodromic sun compass routes by arctic birds, Science, 291, 300–303, 2001.

Are F. E.: Thermal regime of small thermokarst lakes in the Siberian Taiga zone (for example of Central Yakutia), Collection of papers "Lakes of Cryolithozone of Siberia", edited by: Are F. E., Nauka, Siberian brunch, 98–116, 1974 (in Russian).

Arp, C. D., Jones, B. M., Whitman, M., Larsen, A., and Urban, F. E.: Lake Temperature and Ice Cover Regimes in the Alaskan Subarctic and Arctic: Integrated Monitoring, Remote Sensing, and Modeling, J. Am. Water Resour. Ass., 46, 777–791, doi:10.1111/j.1752-1688.2010.00451.x, 2010.

Arp, C. D., Jones, B. M., Lu, Z., and Whitman, M. S.: Shifting balance of thermokarst lake ice regimes across the Arctic Coastal Plain of northern Alaska, Geophys. Res. Lett., 39, L16503, doi:10.1029/2012gl052518, 2012.

Boike, J., Wille, C., and Abnizova, A.: Climatology and summer energy and water balance of polygonal tundra in the Lena River Delta, Siberia, J. Geophys. Res., 113, G03025, doi:10.1029/2007JG000540, 2008.

Boike, J., Kattenstroth, B., Abramova, K., Bornemann, N., Chetverova, A., Fedorova, I., Fröb, K., Grigoriev, M., Grüber, M., Kutzbach, L., Langer, M., Minke, M., Muster, S., Piel, K., Pfeiffer, E.-M., Stoof, G., Westermann, S., Wischnewski, K., Wille, C., and Hubberten, H.-W.: Baseline characteristics of climate, permafrost and land cover from a new permafrost observatory in the Lena River Delta, Siberia (1998–2011), Biogeosciences, 10, 2105–2128, doi:10.5194/bg-10-2105-2013, 2013.

Burn, C. R.: Tundra Lakes and Permafrost, Richards Island, Western Arctic Coast, Canada, Can. J. Earth Sci., 39, 1281–1298, doi:10.1139/E02-035, 2002.

Burn, C. R.: Lake-bottom Thermal Regimes, Western Arctic Coast, Canada, Permafrost Periglac., 16, 355–367, doi:10.1002/PPP.542, 2005.

Brewer, M. C.: The thermal regime of an arctic lake, EOS Transactions, American Geophysical Union, 39, 2, 278–284, doi:10.1029/TR039i002p00278, 1958.

Costard, F. and Gautier, E.: The Lena River: Hydromorphodynamic Features in a Deep Permafrost Zone, in: Large Rivers: Geomorphology and Management, edited by: Gupta, A., John Wiley & Sons, Ltd, West Sussex, England, 225–233, 2007.

Chetverova, A., Fedorova, I., Potapova, T., and Boike, J.: Hydrological and geochemical features of lakes of Samoylov Island of the Lena River Delta, Proceedings of AARI, no. 1, 97–110, 2013 (in Russian).

Ensom, T. P., Burn, C. R., and Kokelj, S. V.: Lake- and channel-bottom temperatures in the Mackenzie Delta, Northwest Territories, Can. J. Earth Sci., 49, 963–978, doi:10.1139/e2012-001, 2012.

Fedorova, I., Chetverova, A., Bolshiyanov, D., Makarov, A., Boike, J., Heim, B., Morgenstern, A., Overduin, P. P., Wegner, C., Kashina, V., Eulenburg, A., Dobrotina, E., and Sidorina, I.: Lena Delta hydrology and geochemistry: long-term hydrological data and recent field observations, Biogeosciences, 12, 345–363, doi:10.5194/bg-12-345-2015, 2015.

Golosov, S. and Kirillin, G.: A parameterized model of heat storage by lake sediments, Environ. Modell. Software, 25, 793–801, doi:10.1016/j.envsoft.2010.01.002, 2010.

Golosov, S., Terzhevik, A., Zverev, I., Kirillin, G., and Engelhardt, C.: Climate change impact on thermal and oxygen regime of shallow lakes, Tellus A, 64, 17264, doi:10.3402/tellusa.v64i0.17264, 2012.

Gordeev, V. V. and Sidorov, I. S.: Concentrations of major elements and their outflow into the Laptev Sea by the Lena River, Mar. Chem., 43, 33–45, 1993.

Grigoriev, M.: Cryomorphogenesis of the Lena River mouth area, Siberian Branch, USSR Academy of Sciences, Yakutsk, 176 pp., 1993 (in Russian).

Grigoriev, N. F.: The temperature of permafrost in the Lena delta basin–deposit conditions and properties of the permafrost in Yakutia, Yakutsk, 2, 97–101, 1960 (in Russian).

Grigoriev, N. F. Perennially frozen rocks of the maritime lowlands of Yakutia, Moscow, Nauka, 80 pp., 1966 (in Russian).

Grosse, G., Jones, B., and Arp, C. D.: Thermokarst Lakes, Drainage, and Drained Basins, in: Treatise on Geomorphology, edited by: Giardino, R. and Harbor, J., 8, Glacial and Periglacial Geomorphology, 29, 325–353, Academic Press, San Diego, CA, doi:10.1016/B978-0-12-374739-6.00216-5, 2013.

Harris, S. A.: Causes and consequences of rapid thermokarst development in permafrost or glacial terrain, Permafrost Periglac., 13, 237–242, doi:10.1002/ppp.419, 2002.

Hinkel, K. M., Lenters, J. D., Sheng, Y., Lyons, E. A., Beck, R. A., Eisner, W. R., Maurer, E. F., Wang, J., and Potter, B. L.: Thermokarst Lakes on the Arctic Coastal Plain of Alaska: Spatial and Temporal Variability in Summer Water Temperature, Permafrost Periglac., 23, 207–217, doi:10.1002/ppp.1743, 2012.

Hobbie, J. E. and Kling, G. W.: Alaska's changing Arctic: Ecological consequences for tundra, streams, and lakes, Oxford University Press, Oxford, New York, 352 pp., 2014.

Jeffries, M. O., Zhang, T., Frey, K., and Kozlenko, N.: Estimating Late-Winter Heat Flow to the Atmosphere from the Lake-Dominated Alaskan North Slope, J. Glaciol., 45, 315–347, 1999.

Jorgenson, M. T., Romanovsky, V., Harden, J., Shur, Y., O'Donnell, J., Schuur, E. A. G., Kanevskiy, M., and Marchenko, S.: Resilience and vulnerability of permafrost to climate change, Can. J. Forest Res., 40, 1219–1236, doi:10.1139/x10-060, 2010.

Kalnay, E., Kanamitsu, M., Kistler, R., Collins, W., Deaven, D., Gandin, L., Iredell, M., Saha, S., White, G., Woollen, J., Zhu, Y., Leetmaa, A., Reynolds, R., Chelliah, M., Ebisuzaki, W., Higgins, W., Janowiak, J., Mo, K. C., Ropelewski, C., Wang, J., Jenne, R., and Joseph, D.: The NCEP/NCAR 40-Year Reanalysis Project, B. Am. Meteorol. Soc., 77, 437–471, 1996.

Keatley, B. E., Douglas, M. S. V., and Smol, J. P.: Physical and chemical limnological characteristics of lakes and ponds across environmental gradients on Melville Island, Nunavut/N.W.T., High Arctic Canada, Fund. Appl. Limnol., 168, 355–376, doi:10.1127/1863-9135/2007/0168-0355, 2007.

Kirillin, G.: Modeling the impact of global warming on water temperature and seasonal mixing regimes in small temperate lakes, Boreal Environ. Res., 15, 279–293, 2010.

Kirillin, G., Leppäranta, M., Terzhevik, A., Granin, N., Bernhardt, J., Engelhardt, C., Efremova, T., Golosov, S., Palshin, N., and Sherstyankin, P.: Physics of seasonally ice-covered lakes: a review, Aquat. Sci., 74, 659–682, 2012.

Lachenbruch, A. H.: Mechanics of thermal contraction cracks and ice-wedge polygons in permafrost, Special papers, 70, Geological Society of America, New York, 69 pp., 1962.

Langer, M., Westermann, S., Muster, S., Piel, K., and Boike, J.: The surface energy balance of a polygonal tundra site in northern Siberia – Part 1: Spring to fall, The Cryosphere, 5, 151–171, doi:10.5194/tc-5-151-2011, 2011a.

Langer, M., Westermann, S., Muster, S., Piel, K., and Boike, J.: The surface energy balance of a polygonal tundra site in northern Siberia – Part 2: Winter, The Cryosphere, 5, 509–524, doi:10.5194/tc-5-509-2011, 2011b.

Langer, M., Westermann, S., Heikenfeld, M., Dorn, W., and Boike, J.: Satellite-based modeling of permafrost temperatures in a tundra lowland landscape, Remote Sens. Environ., 135, 12–24, doi:10.1016/j.rse.2013.03.011, 2013.

Langer, M., Westermann, S., Walter Anthony, K., Wischnewski, K., and Boike, J.: Frozen ponds: production and storage of methane during the Arctic winter in a lowland tundra landscape in northern Siberia, Lena River delta, Biogeosciences, 12, 977–990, doi:10.5194/bg-12-977-2015, 2015.

Laurion, I., Vincent, W. F., Retamal, L., Dupont, C., Francus, P., MacIntyre, S., and Pienitz, R.: Variability in greenhouse gas emissions from permafrost thaw ponds, Limnol. Oceanogr., 55, 115–133, 2010.

Lehner, B. and Döll, P.: Development and validation of a global database of lakes, reservoirs and wetlands, J. Hydrol., 296, 1–22, 2004.

Ling, F. and Zhang, T.: Numerical simulation of permafrost thermal regime and talik development under shallow thaw lakes on the Alaskan Arctic Coastal Plain, J. Geophys. Res., 108, 4511, doi:10.1029/2002JD003014, 2003.

Luecke, C., Giblin, A. E., Bettez, N. D., Burkart, G. A., Crump, B. C., Evans, M. A., Gettel, G., McIntyre, S., O'Brien, W. J., Rublee, P. A., and King, G. W.: The response of lakes near the Arctic LTER to environmental change, in: Alaska's changing Arctic: ecological consequences for tundra, streams, and lakes, edited by: Hobbie, J. and Kling, G. W., Oxford University Press, New York, 238–286, 2014.

Martynov, A., Sushama, L., and Laprise, R.: Simulation of temperate freezing lakes by one-dimensional lake models: performance assessment for interactive coupling with regional climate models, Boreal Environ. Res., 15, 143–164, 2010.

Martynov, A., Sushama, L., Laprise, R., Winger, K., and Dugas, B.: Interactive lakes in the Canadian Regional Climate Model, version 5: the role of lakes in the regional climate of North America, Tellus A, 64, 16226, doi:10.3402/tellusa.v64i0.16226, 2012.

Mironov, D. V.: Parameterization of lakes in numerical weather prediction. Description of a lake model, COSMO technical report, Technical Report No. 11, August 2008, http://www.cosmo-model.org/content/model/documentation/techReports/ (last access: 6 July 2015), 2008.

Mironov, D. V., Terzhevik, A., Kirillin, G., Jonas, T., Malm, J., and Farmer, D.: Radiatively driven convection in ice-covered lakes: Observations, scaling, and a mixed layer model, J. Geophys. Res.-Oceans, 107, 1–16, doi:10.1029/2001JC000892, 2002.

Mironov, D., Ritter, B., Schulz, J.-P., Buchhold, M., Lange, M., and Machulskaya, E.: Parameterization of sea and lake ice in numerical weather prediction models of the German Weather Service, Tellus A, 64, 17330, doi:10.3402/tellusa.v64i0.17330, 2012.

Morgenstern, A., Grosse, G., Günther, F., Fedorova, I., and Schirrmeister, L.: Spatial analyses of thermokarst lakes and basins in Yedoma landscapes of the Lena Delta, The Cryosphere, 5, 849–867, 10, http://www.the-cryosphere-discuss.net/5/849/10/.5194/tc-5-849-2011, 2011.

Morgenstern, A., Ulrich, M., Günther, F., Roessler, S., Fedorova, I. V., Rudaya, N. A., Wetterich, S., Boike, J., and Schirrmeister, L.: Evolution of thermokarst in East Siberian ice-rich permafrost: A case study, Geomorphology, 201, 363–379, doi:10.1016/j.geomorph.2013.07.011, 2013.

Mortimer, C. and Mackereth, F: Convection and its consequences in ice-covered lakes, Verh. Int. Ver. Limnol., 13, 923–932, 1958.

Muster, S., Langer, M., Heim, B., Westermann, S., and Boike, J.: Subpixel heterogeneity of ice-wedge polygonal tundra: a multi-scale analysis of land cover and evapotranspiration in the Lena River Delta, Siberia, Tellus B, 64, 17301, doi:10.3402/tellusb.v64i0.17301, 2012.

Nolan, M. and Brigham-Grette, J.: Basic hydrology, limnology, and meteorology of modern Lake El'gygytgyn, Siberia, J. Paleolimnol., 37, 17–35, doi:10.1007/s10933-006-9020-y, 2006.

Oveisy, A. and Boegman, L.: One-dimensional simulation of lake and ice dynamics during winter, J. Limnol., 73, 441–453, doi:10.4081/jlimnol.2014.903, 2014.

Pavlov, A. V. and Tishin, M. I.: Heat balance of a large lake and surrounding area in central Yakutia, Collection of papers "Structure and thermal regime of frozen rocks", edited by: Katasonova, E. G., Pavlov, A. V., Nauka, Siberian branch, 53–62, 1981 (in Russian).

Pienitz, R., Smol, J. P., and Lean, D. R. S.: Physical and Chemical limnology of 59 lakes located between the southern Yukon and the Tuktoyaktuk Peninsula, Northwest Territories (Canada), Can. J. Fish. Aquat. Sci., 54, 330–346, 1997.

Rawlins, M. A., Serreze, M. C., Schroeder, R., Zhang, X., and McDonald, K. C.: Diagnosis of the record discharge of Arctic-draining Eurasian rivers in 2007, Environ. Res. Lett., 4, 1–8, 2009.

Read, J. S., Hamilton, D. P., Jones, I. D., Muraoka, K., Winslow, L. A., Kroiss, R., Wu, C. H., and Gaiser, E.: Derivation of lake mixing and stratification indices from high-resolution lake buoy data, Environ. Modell. Soft., 26, 1325–1336, doi:10.1016/j.envsoft.2011.05.006, 2011.

Rizk, W., Kirillin, G., and Leppäranta, M.: Basin-scale circulation and heat fluxes in ice-covered lakes, Limnol. Oceanogr., 59, 445–464, 2014.

Sepulveda-Jauregui, A., Walter Anthony, K. M., Martinez-Cruz, K., Greene, S., and Thalasso, F.: Methane and carbon dioxide emissions from 40 lakes along a north-south latitudinal transect in Alaska, Biogeosciences, 12, 3197–3223, doi:10.5194/bg-12-3197-2015, 2015.

Schertzer, W. M.: Freshwater Lakes, in: Surface climates of Canada, edited by: Bailey, W. G., Oke, T. R., and Rouse, W. R., McGill-Queens University Press, Montreal, 124–148, 1997.

Schneider von Deimling, T., Grosse, G., Strauss, J., Schirrmeister, L., Morgenstern, A., Schaphoff, S., Meinshausen, M., and Boike, J.: Observation-based modelling of permafrost carbon fluxes with accounting for deep carbon deposits and thermokarst activity, Biogeosciences, 12, 3469–3488, doi:10.5194/bg-12-3469-2015, 2015.

Schwamborn, G., Rachold, V., and Grigoriev, M. N.: Late Quaternary sedimentation history of the Lena Delta, Quatern. Int., 89, 119–134, doi:10.1016/S1040-6182(01)00084-2, 2002.

Sobiech, J., Boike, J., and Dierking, W.: Observation of melt onset in an Arctic Tundra landscape using high resolution TerraSAR-X and RADARSAT-2 data, IGARSS, Munich, Germany, 3552–3555, 2012.

Spigel, R. H. and Imberger, J. The classification of mixed-layer dynamics of lakes of small to medium size, J. Phys. Oceanogr., 10, 1104–1121, 1980.

Stepanenko, V. M., Goyette, S., Martynov, A., Perroud, M., Fang, X., and Mironov, D.: First steps of a lake model intercomparison Project: LakeMIP, Boreal. Environ. Res., 15, 191–202, 2010.

Thiery, W., Stepanenko, V. M., Fang, X., Jöhnk, K. D., Li, Z., Martynov, A., Perroud, M., Subin, Z. M., Darchambeau, F., Mironov, D., and van Lipzig, N. P. M.: LakeMIP Kivu: evaluating the representation of a large, deep tropical lake by a set of one-dimensional lake models, 66, 21390, doi:10.3402/tellusa.v66.21390, 2014.

Vincent, A. C., Mueller, D. R., and Vincent, W. F.: Simulated heat storage in a perennially ice-covered high Arctic lake: Sensitivity to climate change, J. Geophys. Res., 113, C04036, doi:10.1029/2007JC004360, 2008.

Vincent, W. F., Pienitz, R., Laurion, I., and Walter Anthony, K.: Climate impacts on Arctic lakes, in: Climatic Change and Global Warming of Inland Waters: Impacts and Mitigation for Ecosystems and Societies, edited by: Goldman, C. R., Kumagai, M., and Robarts, R. D., John Wiley & Sons, Ltd, Chichester, UK, 27–42, 2013.

Vtyurina, E. A.: Temperature regime of the Lake Glubokoe, Trudy institute merzlotovedeniya im, V.A. Obrucheva, Academia Nauk SSSR, Moscow, 132–140, 1960 (in Russian).

Walsh, S. E., Vavrus, S. J., Foley, J. A., Fisher, V. A., Wynne, R. H., and Lenters, J. D.: Global Patterns of Lake Ice Phenology and Climate: Model Simulation and Observation, J. Geophys. Res., 103, 825–828, 1998.

Walter, K. M., Zimov, S. A., Chanton, J. P., Verbyla, D., and Chapin III, F. S.: Methane bubbling from Siberian thaw lakes as a positive feedback to climate warming, Nature, 443, 71–75, doi:10.1038/nature05040, 2006.

Welch, H. E. and Bergmann, M. A.: Water circulation in small arctic lakes in winter, Can. J. Fish. Aquat. Sci., 42, 506–520, 1985.

Wetterich, S., Schirrmeister, L., Meyer, H., Andreas, F. A., and Mackensen, A.: Arctic freshwater ostracods from modern periglacial environments in the Lena River Delta (Siberian Arctic, Russia): geochemical applications for palaeoenvironmental reconstructions, J. Paleolimnol., 39, 427–449, doi:10.1007/s10933-007-9122-1, 2008.

Wetzel, R. G.: Limnology: lake and river ecosystems, 3rd Edn., Gulf Professional Publishing, Orlando, 1006 pp., 2001.

Yi, S., Wischnewski, K., Langer, M., Muster, S., and Boike, J.: Freeze/thaw processes in complex permafrost landscapes of northern Siberia simulated using the TEM ecosystem model: impact of thermokarst ponds and lakes, Geosci. Model Dev., 7, 1671–1689, doi:10.5194/gmd-7-1671-2014, 2014.